UCSF
UC San Francisco Electronic Theses and Dissertations

Title
Linking cortical inhibitory circuit dysfunction and psychiatric disease

Permalink
https://escholarship.org/uc/item/88s8894f

Author
Cunniff, Margaret

Publication Date
2019

Peer reviewed|Thesis/dissertation

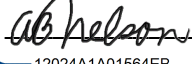Linking cortical inhibitory circuit dysfunction and psychiatric disease

by
Margaret Cunniff

DISSERTATION
Submitted in partial satisfaction of the requirements for degree of
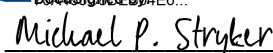DOCTOR OF PHILOSOPHY

in

Neuroscience

in the

GRADUATE DIVISION
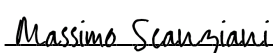of the
UNIVERSITY OF CALIFORNIA, SAN FRANCISCO

Approved:

Alexandra Nelson
_____
Chair

Vikaas Sohal
_____

Michael P. Stryker
_____

Massimo Scanziani
_____

_____
Committee Members

Dedication

To all my teachers

Acknowledgements

This work could not have happened without my mentor, Vikaas Sohal. Thank you for your endless support and positivity. It has been an honor and pleasure to learn from you over the course of this PhD. Thank you, also, to all members of the Sohal lab, past and present, for their support and guidance throughout this project.

Thank you to my friends and colleagues in the UCSF Neuroscience community for your professional and personal support throughout my time in San Francisco. I am so lucky to have wonderful classmates, especially Yelena Kulik, Rachel Care, Ally Girasole, Jiggy Athilingam, and Alex Clemente. I couldn't have done it without you all.

Thank you to my family, particularly my parents, Anne and Dave Cunniff, for their endless support wherever life took me.

Thank you to the Toast and the wonderful community it brought into my life. My life is so much better – and I am a better person – for having you all in it. Your support was immeasurable. Special thanks to the Bay Area community for welcoming me with open arms.

Contributions

All sections were primarily written by MC with input from VS.

Chapter 1 has been prepared in the following manuscript:

Cunniff, M.M., Markenscoff-Papadimitriou, E., Ostrowski, J., State, M., Rubenstein, J.R., and Sohal, V.S. (2019) Altered hippocampal-prefrontal communication during anxiety-related avoidance in mice deficient for the autism-associated gene *PogZ. In preparation.*

MC and VS designed experiments with input from EMP and JR. EMP generated the mouse model.

JO performed the PCA/ICA analysis with input from MC and VS.

Chapter 2 is unpublished data. MC and VS designed all experiments.

Chapter 3 is modified from the following:

Lee, A. T., Cunniff, M.M., See, J.Z., Wilke, S.A., Luongo, F.J., Ellwood, I.T., Ponnavolu, S., and Sohal, V.S. (2019). VIP Interneurons Contribute to Avoidance Behavior by Regulating Information Flow across Hippocampal-Prefrontal Networks. Neuron, 102(6), 1223-1234.e4.

AL, VS, and MC designed experiments. Data for figures 3.1-3.4 were collected and analyzed by AL; these sections have been condensed from the original text. Data for figure 3.5 was collected and analyzed by MC.

Linking cortical inhibitory circuit dysfunction and psychiatric disease

Margaret Mary Cunniff

Abstract

Inhibitory interneurons make up approximately 10% of all cortical neurons, but they are critical for normal circuit functioning, as evidenced by presence of inhibitory dysfunction in a number of neurological and psychiatric diseases. In this dissertation, I show multiple examples of inhibitory perturbations causing circuit dysfunction and abnormal behavior in models of psychiatric disease. In Chapter 1, I characterize behavioral abnormalities in a loss of function model of a high confidence autism gene, link these to changes in long-range communication between the prefrontal cortex and ventral hippocampus, and show deficits in inhibitory signaling related to these long-range deficits. In Chapter 2, I characterize the response of VIP interneurons to cholinergic stimulation and show this is altered in both genetic and environmental models of autism. In Chapter 3, I demonstrate how VIP interneuron signaling regulates prefrontal cortex-ventral hippocampal synchrony in order to properly regulate anxiety behavior. Together, these studies show how critical proper inhibitory signaling is to normal prefrontal cortex processing, and how disruptions in this signaling can give rise to disease states.

Table of Contents

List of Figures

List of Tables

Chapter 1: Altered hippocampal-prefrontal communication during anxiety-related avoidance in mice deficient for the autism-associated gene *PogZ*

SUMMARY

Great progress has been made in identifying genes associated with autism. However, it remains unclear what long-term changes in neural circuitry result from disruptions in these genes, and how these circuit changes might contribute to abnormal behaviors. To address these questions, we studied behavior and physiology in mice heterozygous for *PogZ*, a high confidence autism gene. *PogZ*$^{+/-}$ mice exhibit reduced anxiety-related avoidance in the elevated plus maze (EPM). Theta-frequency communication between the ventral hippocampus (vHPC) and medial prefrontal cortex (mPFC) is known to be necessary for normal avoidance in the EPM. We found deficient theta-frequency synchronization between the vHPC and mPFC *in vivo*. Furthermore, this involves a specific loss of excitatory synaptic drive from the vHPC onto prefrontal GABAergic interneurons. These findings illustrate how inhibitory circuit dysfunction can impair long-range communication in the context of abnormal behavioral resulting from the loss of a high confidence autism gene.

INTRODUCTION

Mutations in *PogZ* have been identified in over forty patients with autism spectrum disorder (ASD) (Devlin et al., 2012; Fukai et al., 2015; Hashimoto et al., 2016; Iossifov et al., 2014, 2012; Stessman et al., 2016; Zhao et al., 2019), intellectual disability (Dentici et al., 2017; Fitzgerald et al., 2015; Gilissen et al., 2014; Tan et al., 2016; White et al., 2016; Ye et al., 2015), and schizophrenia (Fromer et al., 2014; Gulsuner et al., 2013). Most of these are *de novo* mutations

presumed to cause loss of function. Such *de novo* loss of function mutations are exceedingly rare in controls, ranking *PogZ* among the highest confidence genes for ASD (FDR < 0.01) (Sanders et al., 2015). *PogZ* is known to play a role in chromatin regulation, mitotic progression, and chromosome segregation (Nozawa et al., 2010). ASD associated mutations have been shown to disrupt *PogZ*'s DNA-binding activity (Matsumura et al., 2016) and reduce neurite outgrowth *in vitro* (Hashimoto et al., 2016; Zhao et al., 2019).

Among the highest confidence ASD associated genes, there is a striking enrichment for genes which, like *PogZ*, are involved in chromatin remodeling (Cotney et al., 2015; De Rubeis et al., 2014; Krumm, O'Roak, Shendure, & Eichler, 2014; Sanders et al., 2015). One hypothesis is that this enrichment reflects the developmental complexity of the nervous system, which renders the brain more vulnerable than other systems to regulatory disruptions (Ronan, Wu, & Crabtree, 2013; Suliman, Ben-David, & Shifman, 2014). This hypothesis is supported by the convergent expression of genes associated with neurodevelopmental disease at specific developmental timepoints (Gulsuner et al., 2013; Willsey et al., 2013). Despite this progress in identifying ASD associated genes and their convergence onto specific developmental processes, we do not yet understand how these genetic disruptions cause behavioral phenotypes, nor what mechanisms in the developed brain might be targeted to normalize behavior. This is because it remains unclear what long-term changes in neural circuitry result from these genetic disruptions, and how they might contribute to the abnormal functioning of the developed brain.

In order to further understand the nature of neural network dysfunction that results from genetic disruptions and altered development, we characterized behavior and physiology in adult *PogZ* heterozygous loss of function (*PogZ*^{+/-}) mice. We found that these mice exhibit altered behavior in a well-studied assay of anxiety-related avoidance, the elevated plus maze (EPM). We

then studied communication between the ventral hippocampus (vHPC) and medial prefrontal cortex (mPFC), which is known to be necessary for normal anxiety-related avoidance in the EPM. We found that theta-frequency synchronization between the vHPC and mPFC is decreased *in vivo*. Furthermore, this involves a specific loss of excitatory synaptic drive from the vHPC onto prefrontal GABAergic interneurons.

Two major hypotheses about the pathophysiology of ASD are that developmental disruptions can lead to 1) persistent dysfunction of cortical GABAergic circuits (Nelson & Valakh, 2015), and 2) impairments in long-range communication (Kana, Uddin, Kenet, Chugani, & Müller, 2014). Our findings illustrate a case in which these two mechanisms may be linked following the heterozygous loss of a high confidence ASD gene – specifically, impaired inhibitory circuits can contribute to deficient long-range communication.

RESULTS

PogZ^{+/-} mice have decreased anxiety-related avoidance in the EPM

To characterize their behavioral phenotypes, we tested *PogZ^{+/-}* mice using a battery of standard behavioral assays. We found a reduction in anxiety-related avoidance in the elevated plus maze (EPM) (Fig 1.1A,B). Rodents typically avoid the center and open arms of the EPM, because they are exposed, brightly lit, and raised off the ground, and instead spend the bulk of their time in the closed arms. However, *PogZ^{+/-}* mice spent significantly more time exploring the open arms and center region of the elevated plus maze compared to their wildtype littermates (Fig 1.1C,E; ratio of open vs. closed arm time: p = 0.003; open time: p = 0.001, center time: p = 0.02). The total distance traveled during the assay was not different between genotypes, suggesting that this increase in open arm exploration is not simply an artefact related to changes in overall exploratory

behavior (Fig 1.1D, p = 0.35). *PogZ* heterozygotes also made more head-dips in the EPM than their wildtype littermates, consistent with the interpretation that their phenotype reflects a decrease in anxiety-related behavior and a corresponding increase in active exploration (Fig 1.1F, p = 0.03). There was no difference in the number of open arm entries between genotypes, but individual open arms visits were longer in duration in *PogZ*$^{+/-}$ mice (Fig 1.1G,H; number of entries: p = 0.32; duration of entries: p = 0.047). The performance of *PogZ* heterozygotes did not differ from that of wild-type mice on cognitive tests including an odor-texture rule shifting task (Cho et al., 2015; Ellwood et al., 2017) and a T-maze based delayed nonmatch-to-sample task (Spellman et al., 2015; Tamura, Spellman, Rosen, Gogos, & Gordon, 2017). This indicates that their altered behavior in the EPM was not related to nonspecific impairments in spatial cognition or learning (Fig S1.1).

PogZ+/- mice have reduced hippocampal-prefrontal theta synchrony

Many studies, including work from our lab, have shown that communication between the ventral hippocampus (vHPC) and medial prefrontal cortex (mPFC), is necessary for anxiety-related avoidance in the EPM, and that theta-frequency synchronization between these structures can serve as a biomarker for this communication (Adhikari, Topiwala, & Gordon, 2010, 2011; Jacinto, Cerqueira, & Sousa, 2016; Kjaerby, Athilingam, Robinson, Iafrati, & Sohal, 2016; Lee et al., 2019; Padilla-Coreano et al., 2016, 2019). Based on this, we recorded local field potentials from the mPFC and vHPC to assess hippocampal-prefrontal theta synchrony in *PogZ*$^{+/-}$ mice (Fig 1.2A). At rest, *PogZ* heterozygotes had a reduction in theta-frequency neural activity that was synchronized across the vHPC and mPFC, as measured by the weighted phase locking index (WPLI) (Vinck, Oostenveld, Van Wingerden, Battaglia, & Pennartz, 2011) (Fig 1.2B; p = 0.03). Previous work has shown that vHPC-mPFC theta synchrony is dynamically modulated in different compartments of the EPM (Adhikari et al., 2010; Jacinto et al., 2016). Consistent with these earlier findings, in wild-

type mice, vHPC-mPFC theta synchrony increased as mice approached the center of the EPM. This has previously been interpreted to reflect movement from a less-anxiogenic to more anxiogenic location, as well as the approach to a choice point where mice must decide whether to avoid or explore the open arms (Adhikari et al., 2010; Jacinto et al., 2016). This increase in theta synchrony, which normally occurs as mice approach the center of the EPM, was conspicuously absent in *PogZ* heterozygous mice, (Fig 1.2C; difference in theta synchrony at the time of center approach: p = 0.001). *PogZ*$^{+/-}$ mice also had overall reduced vHPC-mPFC theta synchrony while in the EPM, as compared to wild-type littermates (Fig 1.2D; 2-way ANOVA with genotype and open vs. closed arms as factors, significant effect of genotype, p = 0.03). There were no differences in power in the vHPC or mPFC between *PogZ*$^{+/-}$ mice and wildtypes, suggesting that this change in synchrony reflects altered communication between these brain regions, not just reduced activity in one or both structures (Fig S1.2).

An unbiased, data-driven approach to examine the significance of vHPC-mPFC theta synchrony for normal behavior and PogZ$^{+/-}$ mice

As noted above, many studies have focused on vHPC-mPFC theta synchrony as a potential biomarker for vHPC-mPFC communication that is relevant to anxiety-related behaviors. As described above, we found deficits in vHPC-mPFC theta synchrony that correlate with deficits in anxiety-related avoidance behaviors in *PogZ*$^{+/-}$ mice. However, perhaps this is simply a case of the streetlight effect. I.e., perhaps there are alternative patterns of activity within the hippocampal-prefrontal circuit that are also engaged during EPM exploration, but which remain largely intact in *PogZ*$^{+/-}$ mice. In this context, multiple studies from the Dzirasa laboratory and one from ours have shown that data-driven approaches can uncover patterns of rhythmic activity across limbic networks ('electomes' or 'intrinsic coherence networks') which correlate with, and potentially

5

predict, aspects of emotional behaviors (Hultman et al., 2016, 2018; Kirkby et al., 2018). Can this kind of data-driven approach identify hippocampal-prefrontal networks that are engaged by EPM exploration, and if so, would these be intact or deficient in *PogZ*$^{+/-}$ mice?

To address this question, we took a data-driven approach to identify salient features within LFP recordings, relate these to EPM behavior, and assess them in *PogZ*$^{+/-}$ mice. A combination of principal components analysis (PCA) and independent components analysis (ICA) was applied (Methods) to a broad list of potential LFP features for all mice (Table 1.1). These features comprise power (within each region), synchrony (between regions), and cross-frequency coupling (within or between regions), across multiple frequency bands. Each independent component (IC) discovered in this way was defined by a set of weights for each feature (Fig 3A; 80 total ICs derived from 15 mice). To identify similar ICs that were conserved across mice and thus likely to be biologically meaningful, we calculated the correlation coefficient between all pairs of ICs (Fig 3B), then applied a threshold to this pairwise correlation matrix to identify pairs of highly similar ICs (Fig 3C). We then performed clustering on this dataset (Methods) to identify characteristic ICs that appear repeatedly across mice (Fig 3D). One such cluster was characterized by strong weights for cross-frequency (phase-amplitude) coupling between hippocampal theta and higher frequency activity in either the ventral hippocampus or mPFC (Fig 3E). In other words, this cluster corresponds to a "network" that is conserved across mice. When activity in this network goes up, it means that the hippocampal theta rhythm more strongly modulates the amplitude of beta and gamma-frequency activity in both the hippocampus and prefrontal cortex.

For each mouse, we could calculate the time-varying activity of this IC by convolving the weights of this IC (averaged across mice) with the time series of each feature. When mice approach the center of the elevated plus maze, the activity of this IC shows the same pattern we previously

observed for vHPC-mPFC theta synchrony. Specifically, in wild-type mice, the activity of this IC increased as mice approached more anxiogenic regions (e.g., the center zone). Strikingly, this modulation was once again absent in *PogZ* heterozygotes (Fig 1.3F). Thus, this unbiased approach validated the general finding we made earlier, when we focused on a specific measure of vHPC-mPFC theta synchrony. Theta-frequency synchronization across the hippocampal-prefrontal circuit (measured by the modulation of higher frequency activity) normally correlates with entries into more anxiogenic regions of the EPM, but this relationship is abolished in *PogZ* heterozygotes.

vHPC excitation of mPFC interneurons is deficient in PogZ$^{+/-}$ mice

Impaired synchrony suggests a deficit in the transmission of neural activity from the vHPC to mPFC. This could reflect local deficits within these structures, and/or altered synaptic connections between them. To explore potential factors underlying this impaired synchrony, we made patch clamp recordings from neurons in the prefrontal cortex. The resting membrane potential, input resistance, and action potential properties of pyramidal cells and interneurons were not grossly different between *PogZ$^{+/-}$* mice and wild-type littermates (Fig S1.3). To assess synaptic communication between the vHPC and mPFC, we injected virus encoding CamKII-ChR2-EYFP into the vHPC, then, after waiting 8 weeks for viral expression, recorded optically evoked responses in the mPFC. We recorded both excitatory currents (Fig 1.4A,B) and optically evoked spikes (Fig 1.4C,D).

Fast-spiking interneurons (FSINs) in *PogZ* heterozygotes showed a marked reduction in excitatory synaptic input from vHPC projections, including a ~50% reduction in total charge (Fig 1.4E, p = 0.006). Short term plasticity of these excitatory synapses onto FSINs also exhibited a shift towards greater depression as evidenced by a decrease in the paired-pulse ratio (PPR) (Fig 1.4F, p = 0.03). In current clamp recordings, these FSINs exhibited a much longer latency to spike

following each light flash (Fig 1.4G, p = 0.01). There was a trend towards an overall reduction in spiking which did not reach statistical significance (Fig 1.4H, p = 0.08). Notably, all of these changes were specific to FSINs. In recordings from pyramidal neurons, we did not observe any changes in the size or PPR of optogenetically evoked synaptic currents, nor in the latency or number of optogenetically evoked spikes (Fig 1.5).

Deficient FSIN excitation impairs information transmission across vHPC-mPFC circuits

Excitatory and inhibitory postsynaptic currents are major contributors to LFPs (Buzsáki, Anastassiou, & Koch, 2012). Thus, a major deficit in synaptic currents evoked by hippocampal inputs could explain the reductions in synchronization between vHPC and mPFC LFPs that we observed. But how might this synaptic deficit in *PogZ*^{+/-} mice explain their decreased avoidance of the open arms in the EPM? As discussed above, the transmission of information from the vHPC to mPFC is necessary for open arm avoidance. We hypothesized that a decrease in excitatory drive onto FSINs could impair the PFC's ability to appropriately filter information, reducing the transmission of information from the vHPC to mPFC, and resulting in the decreased open arm avoidance seen in *PogZ* heterozygotes. Specifically, we hypothesized that because ventral hippocampal input to the mPFC is rhythmically modulated, feedforward inhibition might preferentially suppress the responses of prefrontal neurons to out-of-phase "noise" while sparing hippocampally-driven responses.

To test the plausibility of this hypothesis, we constructed a simple computational model composed of 2 integrate-and-fire neurons – a FSIN and an output neuron (i.e. a pyramidal cell). Both cells received the same two sources of synaptic input – "noise," generated by a Poisson process with constant rate, and "hippocampal input," which was modeled as a Poisson process whose rate varied according to the theta rhythm, i.e., was modulated at 8 Hz (Fig 1.6A). Both cells had the

same thresholds and membrane time constants, and we set the time constants of decay for EPSPs and IPSPs to 8 and 20 msec, respectively, to reflect the typically longer timescales for synaptic inhibition. The rate of hippocampal inputs varied sinusoidally between 0 and 100 Hz, and the rate of noise inputs was constant at the midpoint of this distribution (50 Hz). Pyramidal neuron spiking ranged from ~0-50 Hz, whereas FSIN spiking ranged from ~0-150 Hz. Finally, we explored how varying the strength of excitatory input from both hippocampal and noise inputs onto FSINs affected the transmission of information from the vHPC to mPFC. Specifically we quantified the correlation between hippocampal input and mPFC output spikes, as well as between the noise input and mPFC output spikes, while varying a single parameter which represents the EPSP amplitude that each hippocampal or noise spike elicits in the FSIN.

As expected, as excitatory drive to the FSIN decreases, the rate of FSIN spiking falls while that of the pyramidal cell goes up (Fig 1.6C). When we examined the correlation between pyramidal cell spikes and either noise or hippocampal input, we found that decreasing FSIN excitatory drive decreases the correlation between pyramidal cell output and hippocampal input (Fig 1.6B), causing a drop in the signal-to-noise ratio (Fig 1.6D). This occurs because as the strength of FSIN excitation increases, feedforward inhibition preferentially filters noise inputs, while hippocampal inputs are spared (due to their rhythmicity) (Fig. 1.6B). Thus, when FSIN excitation is weak, there is minimal FSIN spiking and minimal pyramidal cell inhibition. Under these conditions, weak input is sufficient to excite the pyramidal cell, and the circuit fails to filter between the rhythmically occurring hippocampal signal and the (nonrhythmic) noise. As the level of FSIN excitation increases, it reaches an optimal level at which FSINs generate excitation that suffices to filter out weak inputs. As a result, isolated noise inputs fail to elicit pyramidal cell spikes, whereas rhythmic bursts of hippocampal input provide a strong drive that allows them to be

reliably transmitted via pyramidal cell spiking. Finally we note that while an extensive exploration of all possible inhibitory-disinhibitory circuit motifs is beyond the scope of this study, adding a simple form of disinhibition, in which a simulated VIP interneurons receives feedforward excitation and inhibits other interneurons, does not change our basic finding that there is an optimal level of feedforward excitation onto interneurons, below which the transmission of hippocampal input is degraded (Fig S1.5).

DISCUSSION

We identified a specific behavioral deficit in mice with heterozygous loss of function of a high confidence ASD gene, then found associated deficits in biomarkers and pathways that we and others have previous linked to this behavior. *PogZ*$^{+/-}$ mice show reduced anxiety-related avoidance in the EPM. Communication between the vHPC and mPFC is known to be necessary for this avoidance (Kjaerby et al., 2016; Padilla-Coreano et al., 2016), theta synchrony between LFPs recorded from the vHPC and mPFC is a biomarker for this communication (Padilla-Coreano et al., 2016), and vHPC-mPFC theta synchrony normally increases when mice approach the center of the EPM (Adhikari et al., 2010; Lee et al., 2019). In *PogZ*$^{+/-}$ mice, both baseline vHPC-mPFC theta synchrony and its task-dependent modulation in the EPM are reduced. Notably, we confirmed this specific deficit in behaviorally-modulated theta-frequency vHPC-mPFC communication using an unbiased, data-driven approach. Furthermore, by directly examining vHPC-mPFC connections in brain slices, we found reduced excitatory drive from vHPC onto fast-spiking interneurons. This synaptic abnormality could plausibly contribute to the abnormalities we found in both avoidance behavior and LFP synchrony. Specifically, synaptic potentials are a

major driver of LFP signals, and in a computational model we found that weakening feedforward excitation of inhibitory interneurons impairs the transmission of signals from the vHPC to mPFC.

vHPC-mPFC communication and anxiety

A growing body of work shows that vHPC-prefrontal communication is important for anxiety-related behavior. The vHPC, unlike other portions of the hippocampus, projects directly to prefrontal cortex (Parent, Wang, Su, Netoff, & Yuan, 2010), and both structures are necessary for normal anxiety-related behavior (Kjelstrup et al., 2002; Shah & Treit, 2003). Theta-frequency synchronization between activity in the ventral hippocampus and mPFC increases in anxiety-provoking environments such as the EPM (Adhikari et al., 2010). Furthermore, single units in the mPFC that encode anxiety-related information phase-lock to the hippocampal theta rhythm more strongly than other mPFC units (Adhikari et al., 2011). This suggests that these anxiety-encoding prefrontal units preferentially receive theta-modulated hippocampal input. Optogenetically manipulating vHPC-mPFC projections can also bidirectionally modulate anxiety-related avoidance (Padilla-Coreano et al., 2016, 2019). In particular, suppressing vHPC input to the mPFC reduces both vHPC-mPFC theta synchrony, avoidance behavior, and the encoding of anxiety-related information by mPFC neurons. In previous work, we similarly found that pharmacologically suppressing vHPC-mPFC connections reduces open arm avoidance in the EPM (Kjaerby et al., 2016). Our present results build on and extend these prior findings. Two key new aspects are, 1) that abnormal vHPC-mPFC communication can be secondary to loss of function of an autism-associated gene, and 2) that this communication can be disrupted by weakening vHPC synapses onto prefrontal inhibitory interneurons (rather than onto excitatory projection neurons).

Excitatory-inhibitory (E-I) balance and autism

Another recently published study from our laboratory showed that inhibiting vasoactive intestinal polypeptide (VIP)-expressing interneurons in the mPFC causes a similar behavioral phenotype, i.e., reduced open arm avoidance in the EPM (Lee et al., 2019). That study found VIP interneurons normally facilitate the transmission of anxiety-related information from the vHPC to mPFC by disinhibiting prefrontal responses to vHPC input. As a result, when VIP interneurons are inhibited, information about anxiety is not transmitted properly, causing mice to spend more time exploring the open arms. Since VIP interneurons inhibit other GABAergic interneurons, the effect of inhibiting VIP interneurons is to *increase* feedforward inhibition. In this context, it may seem paradoxical that the present study finds a similar phenotype (increased open arm exploration) in *PogZ*$^{+/-}$ mice when mPFC inhibition evoked by vHPC input is *impaired*. Together, these two studies underscore the importance of properly *balanced* cortical circuit inhibition.

In the context of approach-avoidance behaviors, the PFC is believed to play a key role by *evaluating* information from multiple sources in order to make a decision about whether to approach or avoid a potentially anxiogenic region (Calhoon & Tye, 2015). As illustrated by Fig. 1.6, circuit inhibition is critical for this process. When levels of inhibition are too low, the firing of simulated mPFC output neurons is driven mainly by noise, i.e., inputs unrelated to anxiety signals. This could prevent the mPFC from properly representing anxiety-related information, and/or cause the inappropriate transmission of signals related to exploratory behavior. Only when circuit inhibition is appropriately balanced is responsiveness to hippocampal input optimized, potentially facilitating the transmission of anxiety-related information across hippocampal-prefrontal circuits. In this way, appropriately balanced inhibition may be indispensable for proper action selection related to approach and avoidance behavior.

Disruptions in the balance between cortical excitation and inhibition (E-I balance) have long been hypothesized to play a role in ASD (Rubenstein & Merzenich, 2003). Numerous studies have identified examples of altered E-I balance related to autism. These reflect changes in the relative levels of synaptic excitation and inhibition and can be secondary to a variety of different factors, including alterations in synaptic plasticity, homeostasis, and regulatory feedback loops (Bourgeron, 2015; Mullins, Fishell, & Tsien, 2016; Nelson & Valakh, 2015; Sohal & Rubenstein, 2019; Toro et al., 2010; Wondolowski & Dickman, 2013).

Deficits in long-range communication in autism

In addition to the hypothesis that E-I balance is disturbed in autism, another hypothesis is that autism (and altered E-I balance) may reflect changes in long-range connectivity (Just, Keller, Malave, Kana, & Varma, 2012). While early work focused mainly on a theory of under-connectivity in autism (Just, Cherkassky, Keller, & Minshew, 2004), evidence for both hypo- and hyper-connectivity has been identified using a range of methods, including functional magnetic resonance imaging (fMRI) (Müller et al., 2011; Redcay et al., 2013), electroencephalography (EEG) (Coben, Mohammad-Rezazadeh, & Cannon, 2014; Zeng et al., 2017), magnetoencephalography (MEG) (Buard, Rogers, Hepburn, Kronberg, & Rojas, 2013), and structural imaging (Mueller et al., 2013; Nair, Treiber, Shukla, Shih, & Müller, 2013). Changes in long-range connectivity have been identified in a number of other disorders, including schizophrenia (Guo et al., 2014; X. Wang et al., 2014), generalized anxiety disorder (Andreescu, Sheu, Tudorascu, Walker, & Aizenstein, 2014; Xing et al., 2017), and bipolar disorder (Kam, Bolbecker, O'Donnell, Hetrick, & Brenner, 2013; Y. Wang et al., 2017), suggesting that altered connectivity may be common to a range of neurodevelopmental and psychiatric disorders. Here we find disturbed long-range connectivity that appears to occur because of a deficiency in the excitation of inhibitory interneurons. This

reveals a specific mechanism that could potentially link together two prominent hypotheses about the neurobiology of autism in a way that could contribute to behavioral abnormalities.

It should be noted that the changes we observed are not necessarily static. Connectivity abnormalities in ASD have been shown to be age-(Keehn, Wagner, Tager-Flusberg, & Nelson, 2013; Padmanabhan, Lynn, Foran, Luna, & O'Hearn, 2013) and state-dependent (You et al., 2013). Our study focuses on the outcome of developmental disruptions in the adult brain but does not establish a direct mechanism tracing changes in *PogZ* expression to network level changes. It is possible that these changes in connectivity would be different in juvenile mice, and/or that the changes we see reflect a compensatory response to changes at an earlier timepoint.

Clinical and therapeutic implications

While our findings illustrate how loss of function of an autism-associated gene can cause circuit and behavioral abnormalities, it is not clear that the particular phenotype we observed is relevant to human autism. Even assuming that the circuit and behavioral abnormalities we found in *PogZ*$^{+/-}$ mice are relevant, it is not immediately obvious how one would translate our findings into new treatments. Some ASD studies have found that very generalized restoration of inhibition, such as by treatment with benzodiazepines, is sufficient to rescue behavior (Gogolla, Takesian, Feng, Fagiolini, & Hensch, 2014; Han, Tai, Jones, Scheuer, & Catterall, 2014; Han et al., 2012; Jung et al., 2017). Other studies have normalized social behaviors by specifically targeting prefrontal parvalbumin (PV) interneurons (Selimbeyoglu et al., 2017; Yizhar et al., 2011). However, a recent study found that to increase open arm avoidance, it was necessary to activate vHPC-mPFC projections using a very specific, sinusoidally-varying, and theta-frequency, pattern of optogenetic stimulation (Padilla-Coreano et al., 2019). In this study, stimulation using other waveforms and frequencies was ineffective. In this context, follow up studies could explore whether nonspecifically

enhancing inhibition (e.g. with subanxiolytic doses of benzodiazepines), specifically targeting prefrontal interneurons, and/or delivering rhythmic inhibition that is synchronized to the hippocampal theta rhythm might normalize behavior in $PogZ^{+/-}$ mice.

One intriguing finding is that abnormalities in long-range synapses in $PogZ^{+/-}$ mice are associated with disruptions in long-range synchronization, both at baseline and during a specific task. This raises the possibility that in some forms of ASD, it may be possible to detect underlying alterations, e.g., in E-I balance, by assaying patterns of synchronization within EEG signals. Such changes could potentially be used as biomarkers to aide in diagnosis and identifying appropriate therapeutic interventions.

CONCLUSIONS

We characterized behavior and network-level physiology in mice with heterozygous loss of function in $PogZ$, a high confidence autism gene. $PogZ^{+/-}$ mice show reduced avoidance behavior in the EPM and altered vHPC-PFC synchrony, consistent with recent work characterizing the role of the vHPC-mPFC circuit in anxiety behavior. Additionally, in slice experiments, we found reduced excitatory drive from the hippocampus to prefrontal fast-spiking interneurons, suggesting an impairment in ability to properly filter incoming hippocampal input. This work elucidates the nature of a network level phenotype linking genetic and developmental perturbations with specific behavioral and physiological changes in the adult brain.

MATERIALS AND METHODS

Subjects and behavioral assays

All experiments were conducted in accordance with procedures established by the Administrative Panels on Laboratory Animal Care at the University of California, San Francisco.

15

Male and female mice >4 weeks old were used in all experiments. All mice were *PogZ* heterozygotes or wild-type littermates. Gene expression changes in this mice have been extensively characterized in a related publication. Briefly, these mice were generated by CRISPR-Cas9 and sgRNAs targeting exons 1 and 6, a 10kb span, which generated a premature stop codon. Reduced POGZ expression in *PogZ*^{+/-} cortex at P28 was verified by Western blot.

Unless otherwise noted, experiments were performed under ambient light and mice were group housed with littermates. Mice were habituated to the behavioral testing area for >30 minutes at the beginning of all sessions. For LFP experiments, mice were habituated to the head tether in their home cage for 15 minutes daily for 3 days. ANY-maze (Stoelting) was used to track the position of the mouse during assays using a USB webcam. Experimenter was blinded to each mouse's genotype during behavioral assessment.

Elevated Plus Maze: Mice were exposed to the elevated plus maze for a single 15-minute session. All mice were placed in the center of the maze facing an open arm. Time spent in zones, distance traveled, and number of entries were scored with ANY-maze; head-dips were manually scored by a blinded observer.

Social/Novel Assay: Mice were exposed to a conspecific juvenile followed by a novel object in their home cage for 10 minutes each. Active interaction time was scored by a blinded observer.

Marble Burying: Marble burying was performed as previously described (Angoa-Pérez, Kane, Briggs, Francescutti, & Kuhn, 2013). Mice were placed in a larger housing cage for 20 minutes with 20 marbles arranged in a 4x5 grid. After 20 minutes, the number of fully buried marbles was counted.

Cognitive Tasks: Mice were singly housed and placed on a reverse light-dark cycle for the duration of testing. Mice received 3 days of restricted food intake to reach a goal weight of ~80%

free-feeding weight in order to sufficiently motivate them. In each task, this period was used to habituate mice to testing apparatus and basic task mechanics (location of food reward, trial structure, etc.). Water was freely available during the entire period. All testing was done under red light.

Rule Shifting: An odor/texture rule shifting task was performed as previously described (Cho et al., 2015; Ellwood et al., 2017). Briefly, mice were presented with two bowls containing either sand (Mosser Lee White Sand) or bicarbonate-free cat x (1% by volume) with either ground coriander (McCormick) or garlic powder (McCormick), as well as finely chopped peanut butter chips to mask scent of food reward. Each trial contained one of two possible sets of media: sand and garlic paired with litter and coriander or sand and coriander paired with litter and garlic. In the initial association phase of the task, mice had to learn that a single texture (e.g. sand) signaled the location of a reward. Once mice learned this rule (8 out of 10 previous trials correct), there was an un-cued extradimensional rule shift such that a texture (e.g. garlic) now signaled the reward.

Delayed Match to Sample Task: A delayed match to sample T-maze task was performed as previously described (Spellman et al., 2015; Tamura et al., 2017). Briefly, mice were placed at the base of a T-shaped maze at the start of each trial. During the sample phase, one of the two choice arms of the T was blocked off such that mice were forced to one arm. After reaching the end of the arm, mice then had to return to the start point, where a sliding door held them for a variable delay phase (all data presented here from a 4s delay). Following the delay was a choice phase – the door was removed, allowing the mice to run down the arms and choose which to enter. Mice had to learn to go to the opposite arm from the sample phase (e.g. if they entered the right arm during the sample phase, a food reward would be present in the left arm).

Local Field Potential Recordings

All surgeries were done under isofluorane anesthesia in a stereotaxic frame (Kopf). Standard-tip 0.5 MΩ-impedance stainless steel electrodes (Microprobes, SS30030.5A10) were inserted into the vHPC and mPFC. The coordinates for vHPC and mPFC were as follows: vHPC, -3.25 (AP), 3.1(ML), -4.1 (DV); mPFC, 1.7 (AP), 0.3 (ML), -2.75 (DV). A common reference screw was implanted into the cerebellum (500 m posterior to lambda) and a silver ground wire was placed underneath the left lateral scalp. After affixing the electrodes in place using Metabond, connections were made to the headstage of a multi-channel recording system (Pinnacle). All channels shared a common reference (cerebellum). Data was collected at 2000 Hz and band-pass filtered 1-200Hz at the pre-amp. Electrode placement was verified histologically. We also examined the power spectra from all electrodes; only animals with vHPC power spectra that exhibited a visible peak in the theta frequency range were used for further analysis.

Analysis of LFP data was facilitated using custom MATLAB code. The LFP signals were FIR-filtered (filter length 3x period corresponding to minimum frequency of frequency band) and Hilbert transformed to yield the instantaneous amplitudes (magnitude) and phases (angle). Bulk measures were calculated using data from the entire recording period; dynamic measures were calculated using a 2.5 second window, at 1.5 sec intervals from 7.5 seconds before to 7.5 seconds after the animal entered the center of the elevated plus maze.

Power was quantified using Welch's power spectral density estimate with nonoverlapping segments. Synchrony between vHPC and mPFC was measured by taking the Hilbert transform of band-passed data and either comparing the instantaneous phase using the weighted phase locking index (Vinck et al., 2011) or instantaneous amplitude using amplitude covariation. These measures

were computed across four frequency bands: theta (4-12 Hz), beta (13-30 Hz), low gamma (30-55 Hz), and high gamma (65-100 Hz).

Cross-frequency coupling was calculated by comparing the instantaneous phase in a high frequency band with the instantaneous amplitude in a low frequency band. Low frequency bands were theta (4-8 Hz) and alpha (8-12 Hz). High frequency bands were beta (13-30 Hz), low gamma (30-55 Hz), and high gamma (65-100 Hz). Cross frequency coupling was calculated for all possible combinations of a single low and single high frequency band in all combinations of brain regions (PFC low/HPC high, HPC high/PFC low, PFC low/PFC high, HPC low/HPC high).

These features (Table 1) were all used as input for the independent components analysis based on methods outlined in previous work (Kirkby et al., 2018). First, all features were calculated for each subject and principal components analysis was performed for dimensionality reduction and orthogonalization and the number of significant components was calculated using the threshold set by the Marchenko-Pastur Law (Lopes-dos-Santos, Ribeiro, & Tort, 2013). Independent components analysis (ICA) was used on the significant PCs to separate the signal mixtures into independent sources using the *fastICA* algorithm (Hyvärinen & Oja, 2000). Similarity of ICs across mice was calculated using the Pearson correlation coefficient. Significant clusters were isolated by selecting for ICs that had a correlation coefficient of >0.7 with at least one other IC and using MATLAB's *graph* function to identify groups of highly similar ICs. Characteristic ICs were found by averaging groups of ICs with members from at least 3 different animals. The projection of these characteristic ICs onto behavior was found by multiplying the vector of Z-scored features in each point in time by the weight in the characteristic IC and summing all values.

Whole cell patch clamp recordings

Mice were injected with 750nL of AAV5-CaMKIIa-hChR2(H134R)-EYFP (UNC Vector Core) into the vHPC (DV: -4, AP: -3.3, ML: -3.2) to label excitatory projections from the vHPC to the mPFC. A subset of mice were also injected with 500nL AAV-DlxI12b-mCherry in the mPFC (DV: -2.75, AP: 1.7, ML: 0.3) to label MGE-derived interneurons (Potter et al., 2009). We waited ~8 weeks from virus injection to slice experiments. Whole cell patch recordings were obtained from 250μm coronal slices. Cells were identified using differential contrast video microscopy on an upright microscope (BX51W1, Olympus) and recordings were made using a Multiclamp 700A (Molecular Devices). Data was collected using pClamp (Molecular Devices) software and analyzed using custom MATLAB code. Patch electrodes were filled with the following (in mM): 130 K-gluconate, 10 KCl, 10 HEPES, 10 EGTA, 2 MgCl, 2 MgATP, and 0.3 NaGTP (pH adjusted to 7.3 with KOH). All recordings were at 32.0±1°C. Series resistance was usually 10–20 MΩ, and experiments were discontinued above 25 MΩ. For voltage clamp recordings, cells were held at -70mV and +10mV to isolate EPSCs and IPSCs, respectively. An LED engine (Lumencor) was used for optogenetic stimulation of terminals from vHPC projections. We used ~1-3mW of 470nm light in 5ms pulses to stimulate ChR2-infected fibers. The light was delivered to the slice via a 40x objective (Olympus) which illuminated the full field.

Computational model of the role of feedforward inhibition

The effects of changing the strength of excitatory drive onto interneurons was modeled using two integrate and fire neurons – an output cell, representing a pyramidal cell, and an interneuron that targeted the output cell, representing a fast-spiking interneuron. Each cell received noise input and theta-patterned "hippocampal" input. Initial values were selected such

that the inhibitory neuron would spike at ~20 Hz and the output neuron would spike at ~25 Hz and ~50 Hz in the presence and absence of inhibition. All values were held constant except for the strength of excitatory input onto the output-targeting interneuron, adjusting either just the hippocampal strength or adjusting the hippocampal and noise strength in parallel. Input spikes were modeled as a Poisson process. Correlation between the input sources was calculated by comparing binned spike times for input spikes (from the Poisson train) and output spikes (when the output cell's membrane potential cleared a threshold). The relative contributions of the two input sources was calculated by comparing the ratio of the correlation between the output spikes and the noise input or hippocampal input. Correlation values were based on 1000 iterations of a 1 second spike train.

Statistics and data analysis

Unless otherwise specified, non-parametric tests were used for all statistical comparisons and all tests are two-sided. Statistics were calculated using MATLAB or Python's SciPy package.

FIGURES
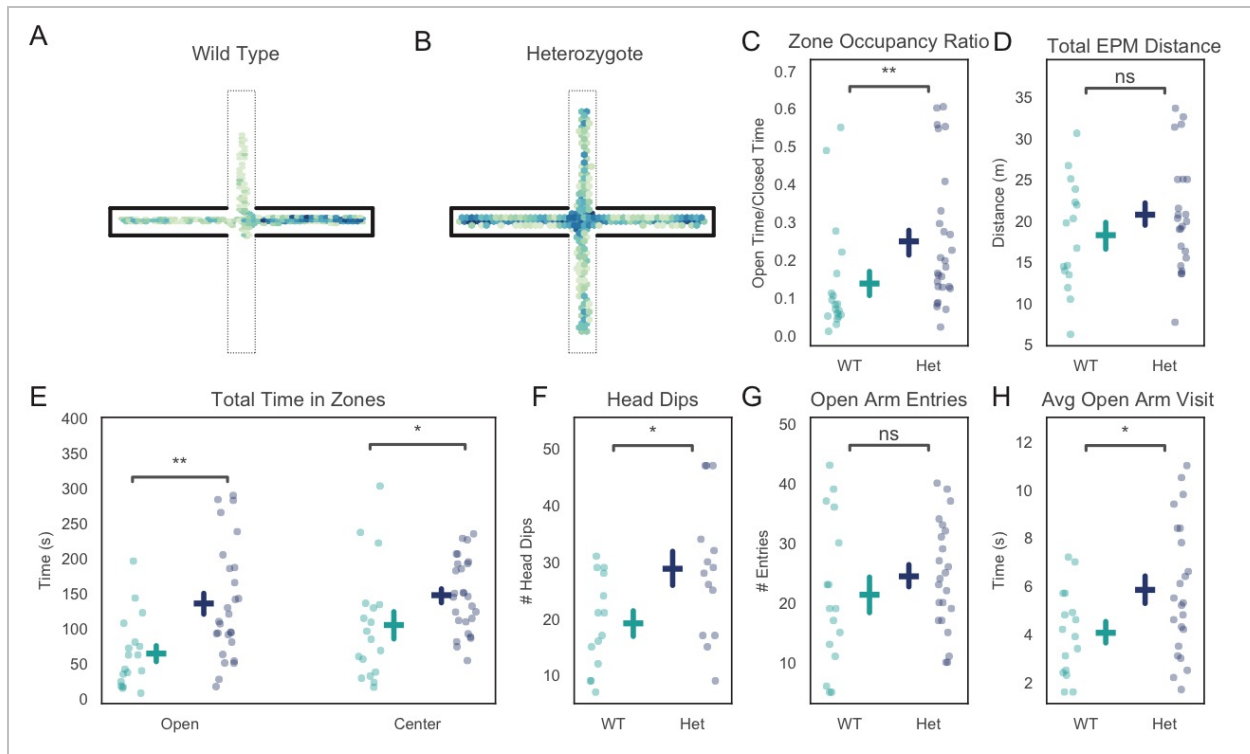
Figure 1.1: *PogZ*^{+/-} mice exhibit reduced avoidance in the elevated plus maze.

(A) Occupancy plot for a 15 minute elevated plus maze session for a representative wildtype mouse.

(B) Occupancy plot for a *PogZ*^{+/-} mouse.

(C) Ratio of time spent in open vs. closed arms of the elevated plus maze, p = 0.003.

(D) Total distance traveled during elevated plus maze sessions, p = 0.35.

(E) Total time spent in exposed areas of elevated plus maze, open arms: p = 0.001, center: p = 0.02.

(F) Total number of head dips for each mouse, p = 0.03.

(G) Number of open arm entries, p = 0.32.

(H) Average duration of each open arm visit, p = 0.047.
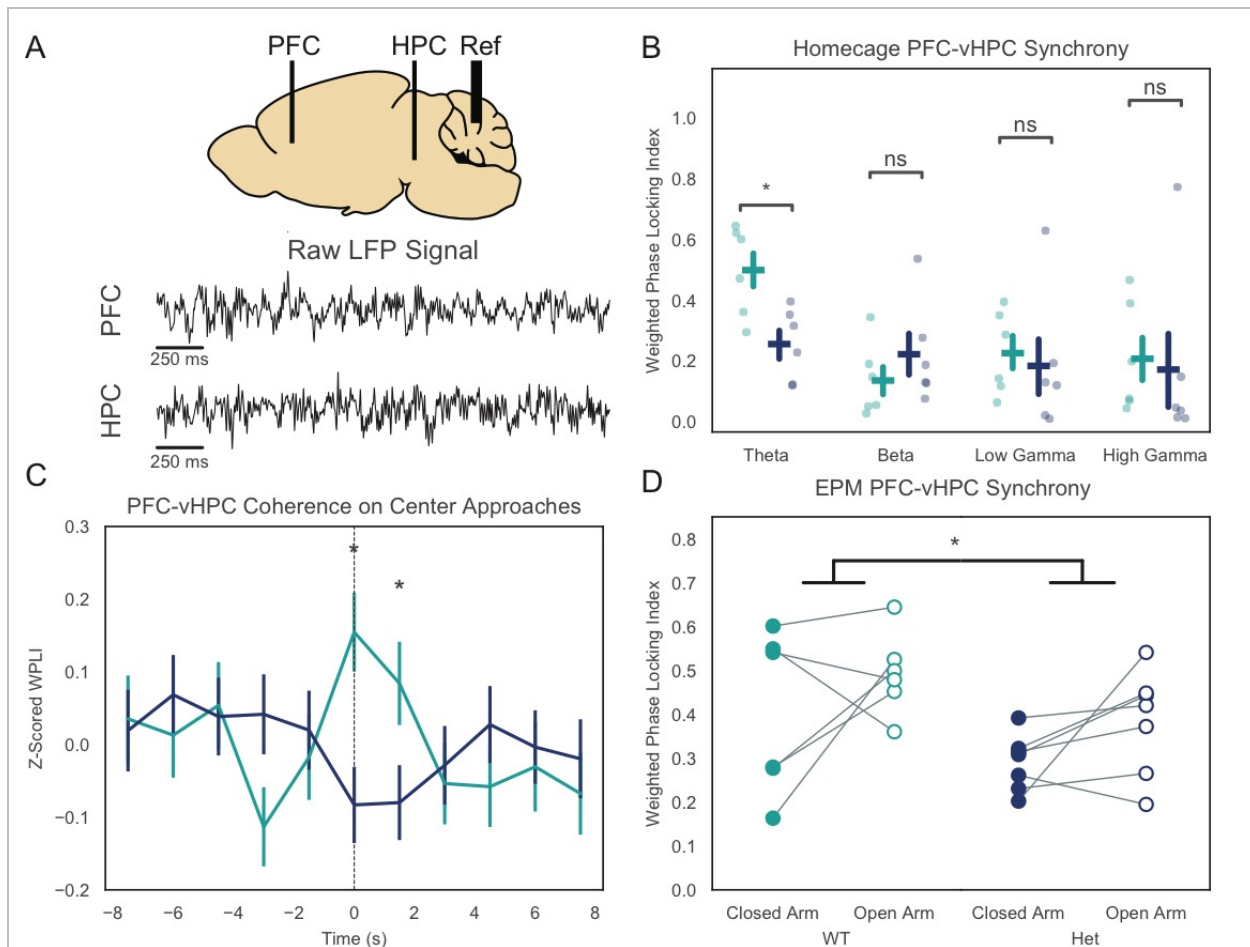
Figure 1.2: *PogZ*+/- mice have reduced vHPC-PFC theta synchrony both at baseline and in the elevated plus maze.

(A) Recording schematic and examples of raw local field potential traces.

(B) Comparison of the weighted-phase locking index (WPLI), measuring synchrony in various frequency bands, for mice in their homecages. Theta (4-12 Hz): p = 0.031, Beta (13-30 Hz): p = 0.38, Low Gamma (30-55 Hz): p = 0.47, High Gamma (65-100 Hz): p = 0.23.

(C) Z-scored theta band WPLI as mice approach the center of the elevated plus maze. t = 0: p = 0.0007; t = 1.5: p = 0.043.

(D) Average theta band WPLI in the open vs. closed arms of the EPM. Two-way ANOVA including arm and genotype as factors - significant effect of genotype: p = 0.03.

Figure 1.3: An unbiased, data-driven approach confirms that theta-frequency vHPC-mPFC communication is behaviorally-relevant and deficient in _PogZ+/-_ mice.

(A) Example weight vectors showing how various LFP features (x-axis) contribute to different independent components (ICs) in one mouse. The y-axis shows the weight of each feature.

(B) Correlation matrix showing the similarity of weight vectors corresponding to different ICs, from all mice.

(C) Binarized version of the correlation matrix showing pairs of ICs that have a correlation coefficient >0.7.

(D) Clusters of ICs that are strongly correlated with ICs from at least 3 other animals.

(E) Example weights vectors (light, colored traces) for ICs from one cluster. This cluster is characterized by strong weights for cross-frequency coupling between vHPC theta activity and higher frequency activity in either vHPC or mPFC. The bold black trace shows the average of these weight vector.

(F) The projection of network activity onto the characteristic (averaged) weight vector (from E) as a function of time during approaches to the center of the EPM, for wild-type or _PogZ+/-_ mice. As mice approach the center, activity in this characteristic IC rises sharply and reaches a in WT mice, but this is absent in _PogZ+/-_ mice (p = 0.007). This is similar to what Fig 2C shows for theta synchrony.

24

Figure 1.4: Excitatory hippocampal input to prefrontal fast-spiking interneurons is reduced in PogZ mutants.

(A, B) Representative examples of optically evoked excitatory post-synaptic currents (oEPSCs) recorded from prefrontal fast-spiking interneurons (FSINs) in wildtype **(A)** or *PogZ⁺/⁻* mice **(B)**.

(C, D) Representative traces of optically-evoked excitatory post-synaptic potentials (oEPSPs) and action potentials recorded from FSINs in wildtype **(C)** or *PogZ⁺/⁻* mice**(D)**.

(E) The total oEPSC charge in FSINs is reduced in *PogZ⁺/⁻* mice, p = 0.006.

(F) The paired pulse ratio (PPR) for oEPSCs is reduced in *PogZ⁺/⁻* FSINs, p = 0.03.

(G) The latency of the first optically evoked action potential is increased in *PogZ⁺/⁻* FSINs, p = 0.013.

(H) The number of action potentials elicited by oEPSPs is non-significantly altered, p = 0.08.
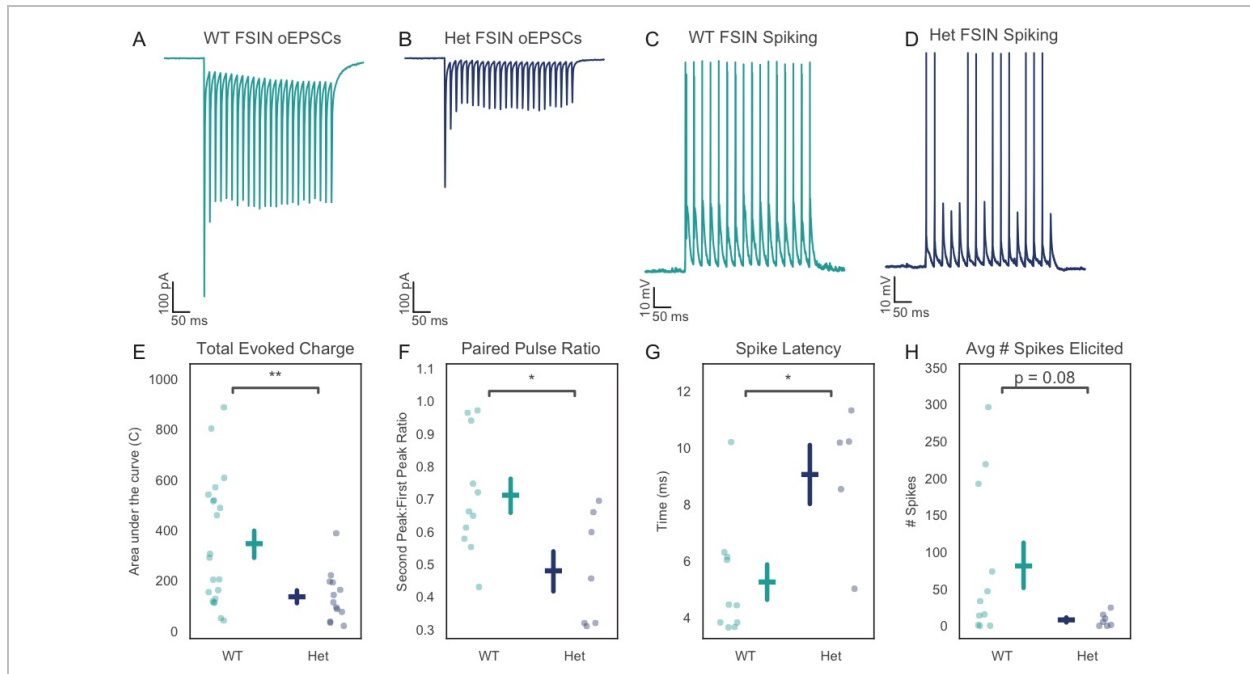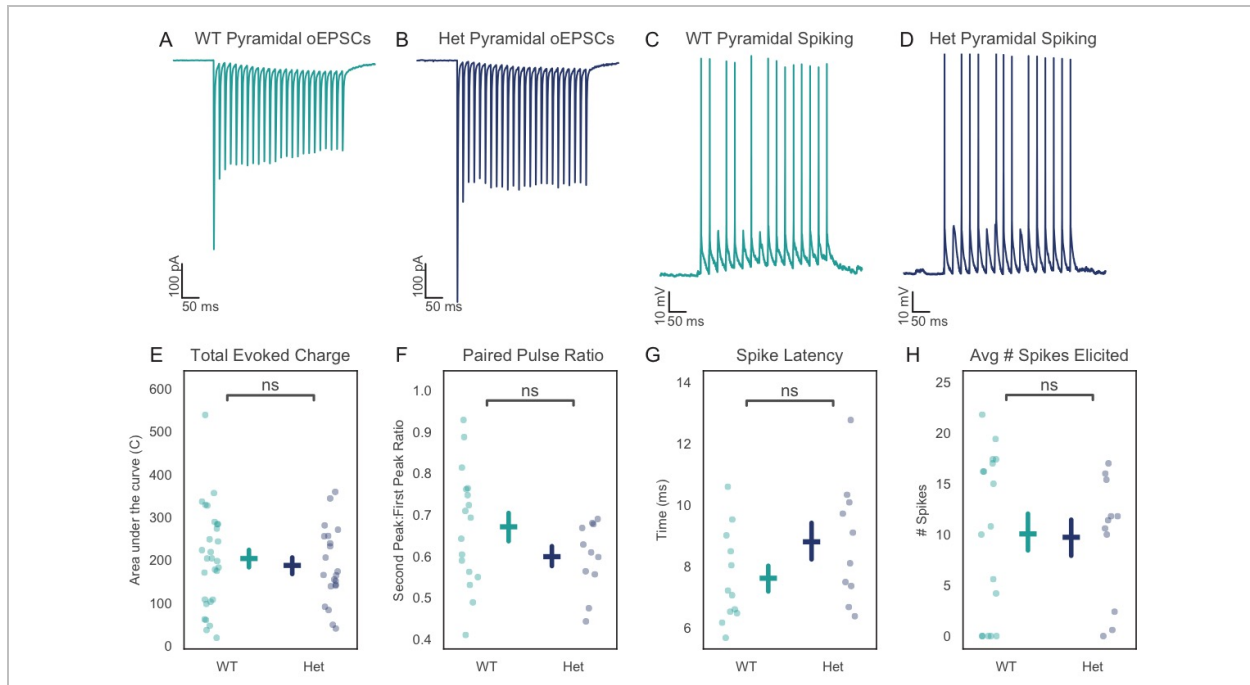
Figure 1.5: Excitatory hippocampal input to prefrontal pyramidal neurons is not changed in *PogZ* mutants.

(A, B) Representative examples of optically evoked excitatory post-synaptic currents (oEPSCs) recorded from prefrontal pyramidal neurons in wildtype **(A)** or *PogZ*⁺/⁻ mice **(B)**.

(C, D) Optically evoked excitatory post-synaptic potentials (oEPSPs) and action potentials in wildtype **(C)** or *PogZ*⁺/⁻ **(D)** pyramidal neurons.

(E) Total oEPSC charge in pyramidal neurons, p = 0.28.

(F) Paired pulse ratio for oEPSCs in pyramidal neurons, p = 0.15

(G) Latency to first optically evoked action potential in pyramidal neurons, p = 0.76.

(H) Number of action potentials elicited by oEPSPs in pyramidal neurons, p = 0.78.
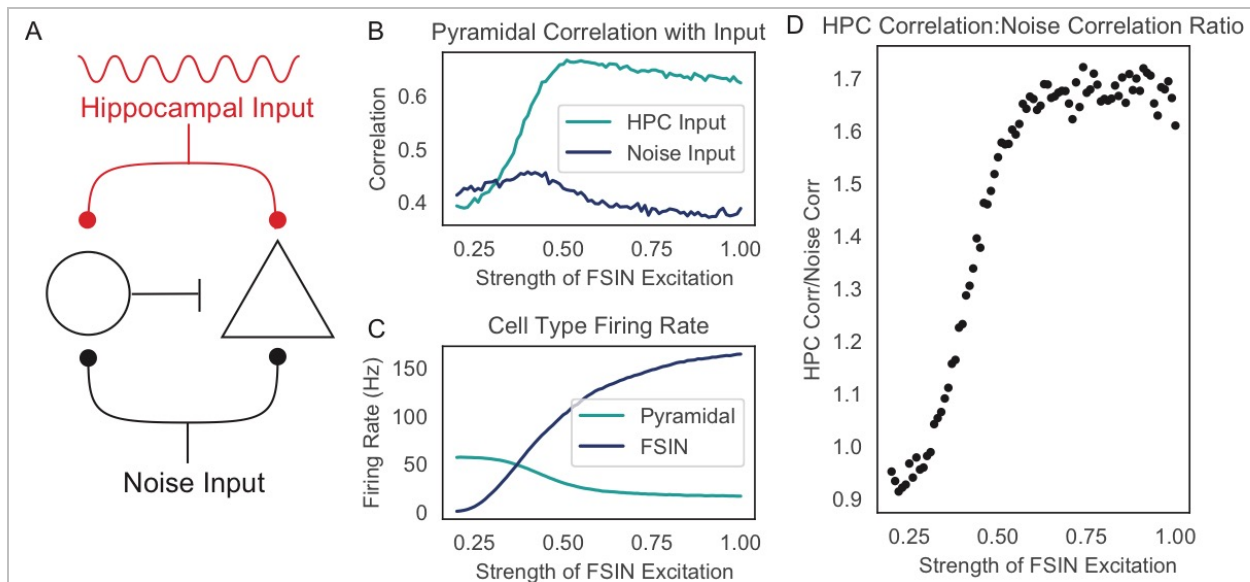
Figure 1.6: Reducing the excitatory drive onto prefrontal FSINs impairs the transmission of hippocampal inputs.

(A) Computational model schematic. Both a model pyramidal neuron (triangle) and a model FSIN (circle) receive simulated hippocampal input (which is rhythmically modulated at 8 Hz), and additional input which represents noise.

(B) The correlation between the pyramidal neuron output spike rate and the rate of either noise inputs (dark blue) or hippocampal spikes (turquoise), as functions of a single parameter which represents how strongly hippocampal and noise inputs excite the model FSIN.

(C) The spike rate of the model pyramidal neuron (turquoise) and FSIN (dark blue) as functions of a single parameter representing how strongly hippocampal and noise inputs excite the model FSIN.

(D) The ratio of the correlation between pyramidal neuron output spikes and either hippocampal input or noise input.

27

Table 1: LFP measures used as features in PCA/ICA analysis.

| Measure	Region	Frequencies
Power	HPC	Theta (4-12 Hz)
		Beta (13-30 Hz)
		Low Gamma (30-55 Hz)
		High Gamma (65-100 Hz)
	PFC	Theta (4-12 Hz)
		Beta (13-30 Hz)
		Low Gamma (30-55 Hz)
		High Gamma (65-100 Hz)
Amplitude Covariation	HPC-PFC	Theta (4-12 Hz)
		Beta (13-30 Hz)
		Low Gamma (30-55 Hz)
		High Gamma (65-100 Hz)
Weighted Phase Locking	HPC-PFC	Theta (4-12 Hz)
		Beta (13-30 Hz)
		Low Gamma (30-55 Hz)
		High Gamma (65-100 Hz)
Cross-Frequency Coupling	HPC (low) → PFC (high)	Theta (2-6 Hz) → Beta (13-30 Hz)
		Theta (2-6 Hz) → Low Gamma (30-55 Hz)
		Theta (2-6 Hz) → High Gamma (65-100 Hz)
		Alpha (6-10 Hz) → Beta (13-30 Hz)
		Alpha (6-10 Hz) → Low Gamma (30-55 Hz)
		Alpha (6-10 Hz) → High Gamma (65-100 Hz)
	PFC (low) → HPC (high)	Theta (2-6 Hz) → Beta (13-30 Hz)
		Theta (2-6 Hz) → Low Gamma (30-55 Hz)
		Theta (2-6 Hz) → High Gamma (65-100 Hz)
		Alpha (6-10 Hz) → Beta (13-30 Hz)
		Alpha (6-10 Hz) → Low Gamma (30-55 Hz)
		Alpha (6-10 Hz) → High Gamma (65-100 Hz)
	HPC (low) → HPC (high)	Theta (2-6 Hz) → Beta (13-30 Hz)
		Theta (2-6 Hz) → Low Gamma (30-55 Hz)
		Theta (2-6 Hz) → High Gamma (65-100 Hz)
		Alpha (6-10 Hz) → Beta (13-30 Hz)
		Alpha (6-10 Hz) → Low Gamma (30-55 Hz)
		Alpha (6-10 Hz) → High Gamma (65-100 Hz)
	PFC (low) → PFC (high)	Theta (2-6 Hz) → Beta (13-30 Hz)
		Theta (2-6 Hz) → Low Gamma (30-55 Hz)
		Theta (2-6 Hz) → High Gamma (65-100 Hz)
		Alpha (6-10 Hz) → Beta (13-30 Hz)
		Alpha (6-10 Hz) → Low Gamma (30-55 Hz)
		Alpha (6-10 Hz) → High Gamma (65-100 Hz)
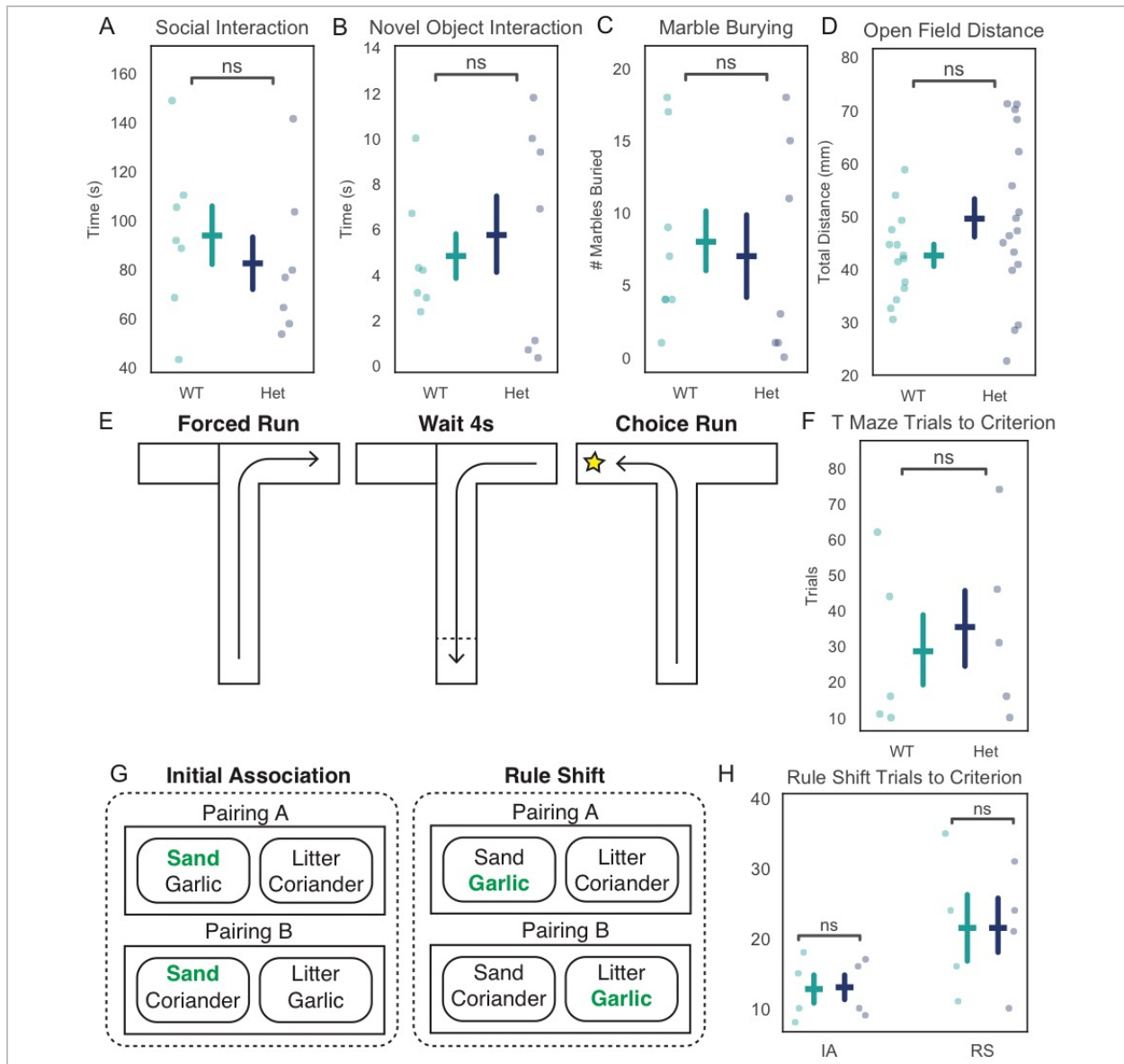
Figure S1.1: Other behavioral assays in *PogZ*⁺/⁻ mice.

(A) Time that *PogZ*⁺/⁻ mice or wild-type littermates spend interacting with a novel juvenile conspecific, p = 0.34.

(B) Time that *PogZ*⁺/⁻ mice or wild-type littermates spend interacting with a novel object, p = 0.95.

(C) Number of marbles buried *PogZ*⁺/⁻ mice or wild-type littermates during 20 min, p = 0.45.

(D) Distance traveled in an open field by *PogZ*⁺/⁻ mice or wild-type littermates, p = 0.15.

(E) Schematic of the T-maze delayed match to sample task. Mice must recall the direction of the forced run during the sample phase in order to successfully obtain reward from the opposite arm during the choice phase.

(F) Number of trials *PogZ*⁺/⁻ mice or wild-type littermates need to reach a learning criterion (80% accuracy) in the T-maze task, p = 0.60.

(G) Schematic of the odor-texture rule shift task. Mice must initially learn that a texture cue signals the location of a hidden food reward. Once they learn this initial rule, there is an extra-dimensional rule shift such that an odor now signals the reward location.

(H) Number of trials *PogZ*⁺/⁻ mice or wild-type littermates need to reach a learning criterion (80% accuracy) during the initial association or rule shift, IA: p = 0.89; RS: p = 0.89.
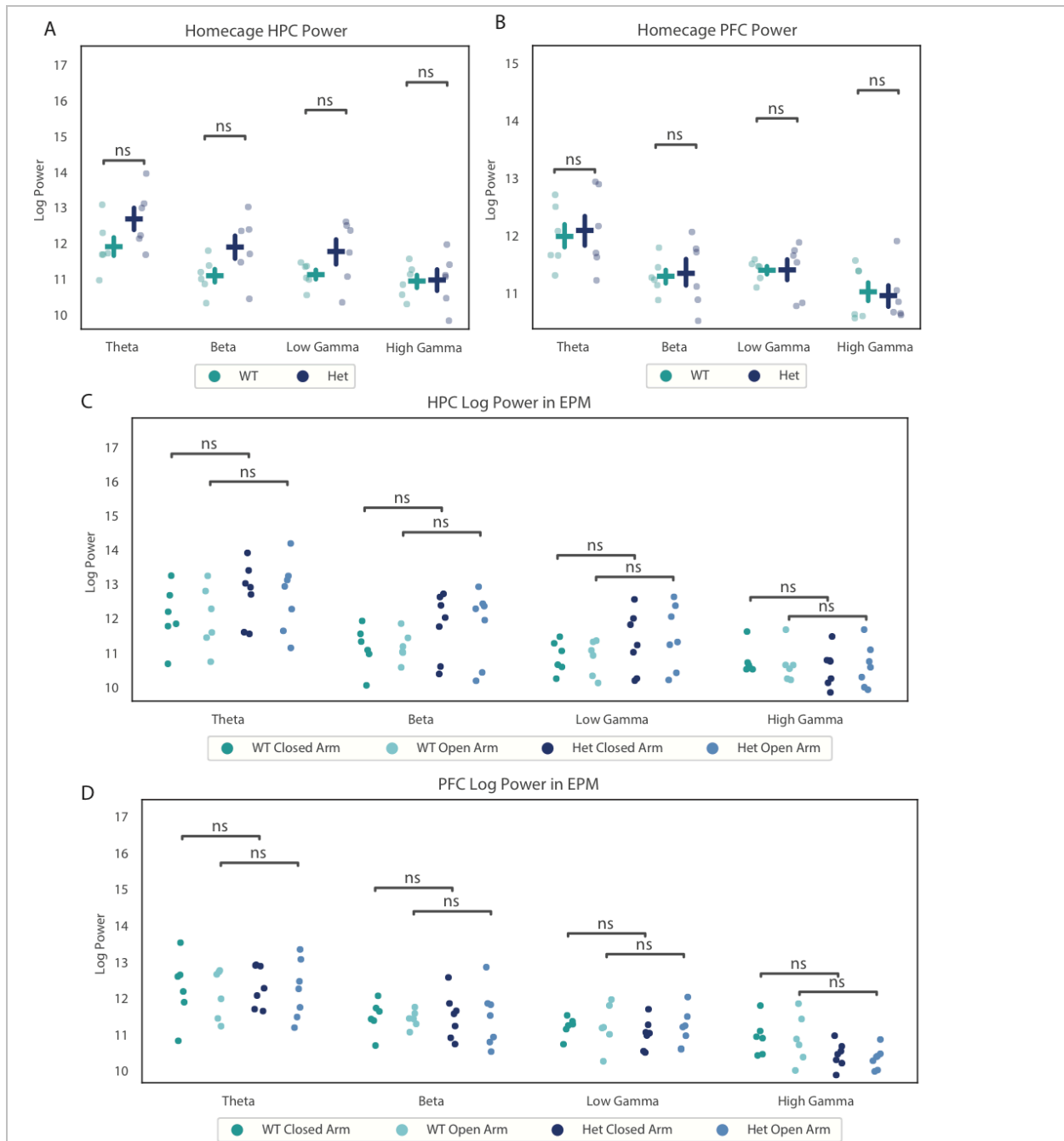
Figure S1.2: LFP power in various frequency bands in the vHPC and mPFC is not changed in *PogZ*^{+/-} mice.

(A) vHPC LFP power in the home cage: θ (4-12 Hz), p = 0.23; β (12-30 Hz), p = 0.093; low γ (30-55 Hz), p = 0.17; high γ (65-100 Hz), p = 0.94.

(B) mPFC LFP power in home cage: θ, p = 0.81; β, p = 0.94; low γ, p = 0.47; high γ, p = 0.8.

(C) vHPC LFP power in EPM: θ closed arm, p = 0.25, open arm, p = 0.32; β closed arm, p = 0.15, open arm, p = 0.20; low γ closed arm, p = 0.48, open arm, p = 0.25; high γ closed arm, p = 0.89, open arm, p = 1.0.

(D) mPFC LFP power in EPM: θ closed arm, p = 0.88, open arm, p = 0.89; β closed arm, p = 1.0, open arm, p = 0.89; low γ closed arm, p = 0.20, open arm, p = 1.0; high γ closed arm, p = 0.10, open arm, p = 0.15.
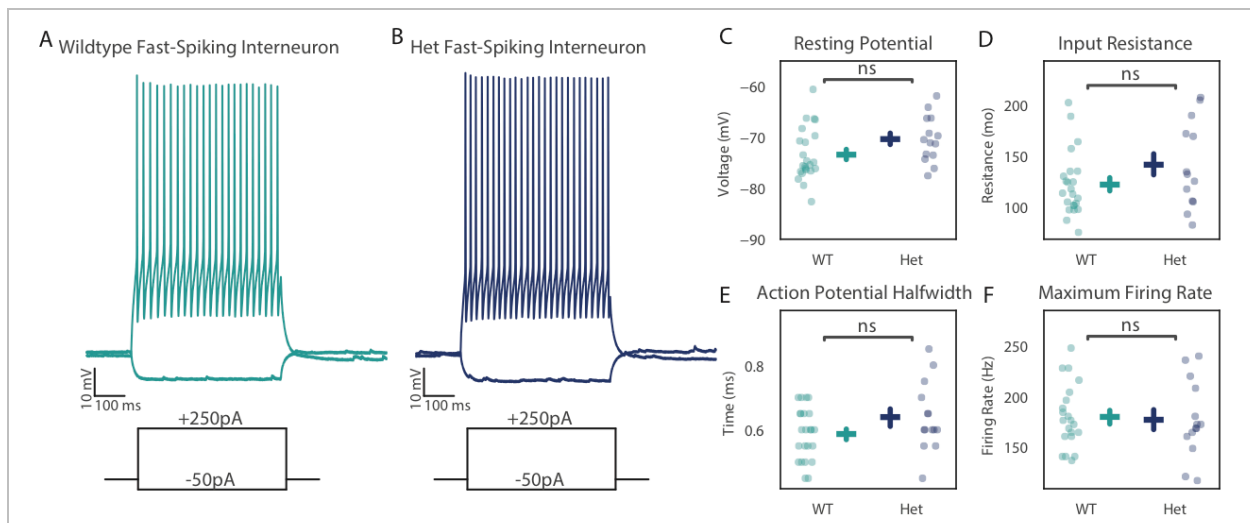
Figure S1.3: Intrinsic properties of prefrontal FSIN are not changed in *PogZ*+/- mice.

(A, B) Representative examples of FSIN responses to current injection in WT (left) or *PogZ*+/- (right) mice.

(C) Membrane resting potential, p = 0.053.

(D) Input resistance, p = 0.09.

(E) Action potential halfwidth, p = 0.18.

(F) Maximum firing rate, p = 0.50.

Figure S1.4: Pyramidal cell properties are not changed in *PogZ*^{+/-} mice.

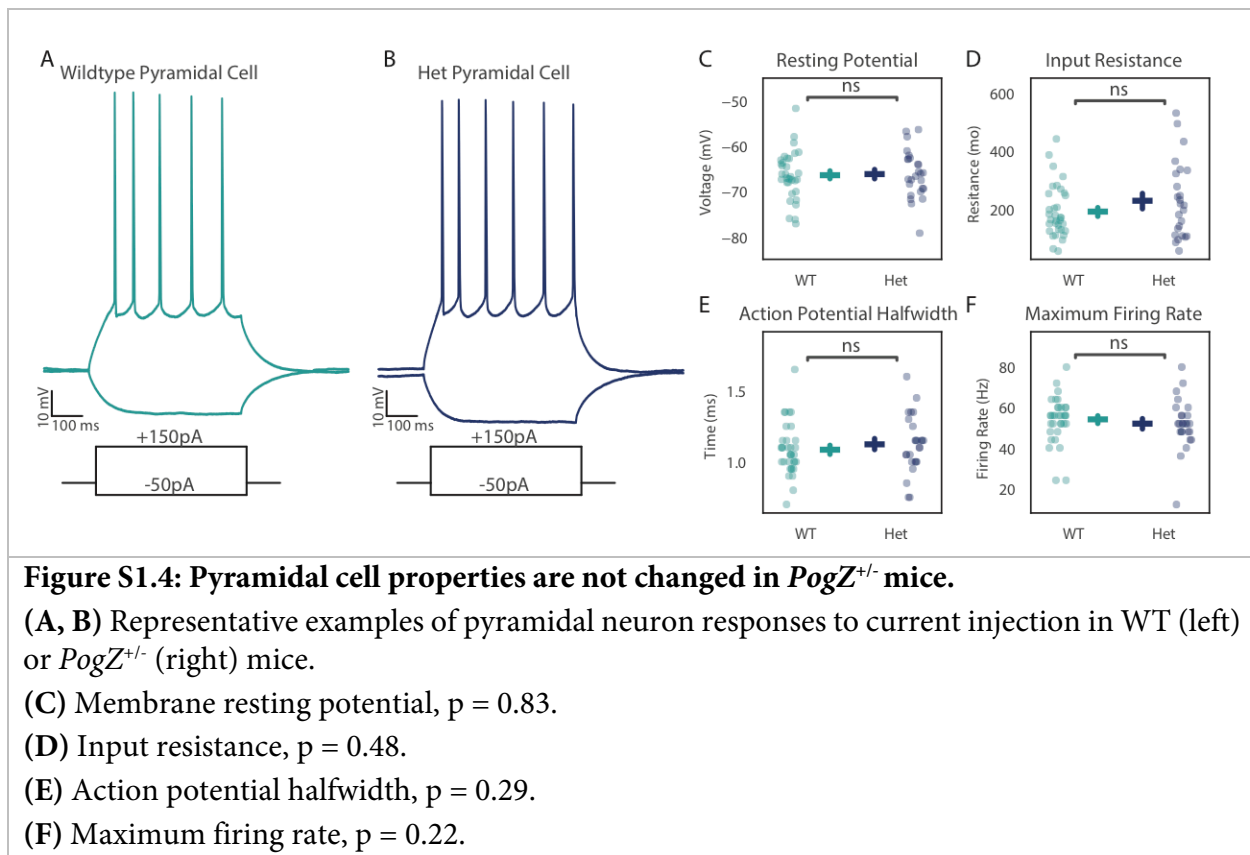**(A, B)** Representative examples of pyramidal neuron responses to current injection in WT (left) or *PogZ*^{+/-} (right) mice.

(C) Membrane resting potential, p = 0.83.

(D) Input resistance, p = 0.48.

(E) Action potential halfwidth, p = 0.29.

(F) Maximum firing rate, p = 0.22.
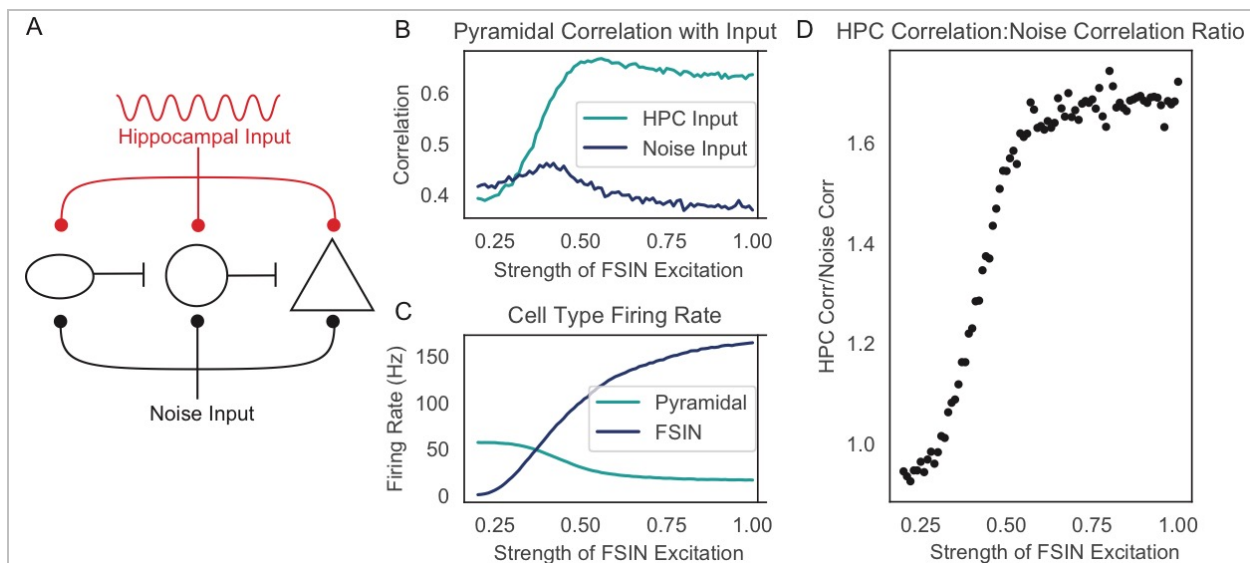
Figure S1.5: Adding feedforward disinhibition does not change the relationship between inhibitory strength and hippocampal correlation.

(A) Schematic of the computational model including cells and input sources. In comparison to the original model (Fig 6), this model includes an additional interneuron (ellipse) which receives feedforward excitation representing noise or hippocampal input. This new interneuron inhibits the first interneuron (circle), providing disinhibition.

(B) The correlation between the pyramidal neuron output spike rate and the rate of either noise inputs (dark blue) or hippocampal spikes (turquoise), as functions of a single parameter which represents how strongly hippocampal and noise inputs excite the model FSIN.

(C) The spike rate of the model pyramidal neuron (turquoise) and FSIN (dark blue) as functions of a single parameter representing how strongly hippocampal and noise inputs excite the model FSIN.

(D) The ratio of the correlation between pyramidal neuron output spikes and either hippocampal input or noise input.

Chapter 2: Cholinergic modulation of VIP interneurons in the prefrontal cortex

INTRODUCTION

Though VIP cells only make up approximately 15% of cortical interneurons (Rudy, Fishell, Lee, & Jens, 2011), recent work has shown they are positioned to provide very powerful regulation of circuit activity. VIP cells selectively target other interneuron subtypes, primarily somatostatin expressing interneurons. This creates a disinhibitory circuit, whereby activation of VIP cells serves to inhibit other interneurons and lift inhibition on excitatory pyramidal cells (Fu et al., 2014; Pfeffer, Xue, He, Huang, & Scanziani, 2013; Pi et al., 2013).

Disinhibitory circuits allow control of the balance between excitation and inhibition in microcircuits, which is critical for proper circuit functioning and hypothesized to be abnormal in autism (Nelson & Valakh, 2015; Rubenstein & Merzenich, 2003). Disinhibitory circuits can control gain in the circuit and provide a mechanism primed for detection of salient stimuli. Gain control allows circuits change the strength of inputs, by amplifying or suppressing the strength of a signal in a network. This is key for attention and directing behavior to novel and relevant stimuli. Cholinergic modulation from the basal forebrain plays a major role in arousal and attention (Hasselmo & Sarter, 2011). Acetylcholine has been shown to play a role in decorrelation and disinhibition of neural circuits, suggesting a mechanism through which cholinergic modulation regulates attention (Letzkus et al., 2011; Runfeldt, Sadovsky, & N, 2014).

The role of VIP cells is critical in the prefrontal cortex (PFC), which controls higher order behavior and executive control. PFC driven behavior involves integrating information from multiple brain regions and distinguishing between relevant and irrelevant stimuli. The ability of

VIP cells and the disinhibitory circuit they create to suppress or enhance inputs is crucial for proper information flow and gating of signals.

There is increasing evidence that VIP cells and acetylcholine may be working in conjunction to regulate neural circuit activity (Alitto & Dan, 2012; Fu, Kaneko, Tang, Arturo, & Stryker, 2015; Porter et al., 1998). Despite the fact that VIP cells are extraordinarily influential in regulating circuit activity, particularly in states of arousal and high attentional demand, the details of how acetylcholine regulates VIP on a cellular and microcircuit level is still poorly defined.

Sensory processing disorders and executive function deficits are common features of autism, both of which may involve the cholinergic system (Kern, 2006; Russo et al., 2007). Postmortem analysis of brain tissue from human ASD patients shows decreased expression of both nicotinic and muscarinic receptors (Perry et al., 2001). Mouse models of autism have shown attentional problems, as well as decreased brain measurements of acetylcholine (M, Neal, Lin, Hughes, & Smith, 2013). Additionally, increasing available acetylcholine in the synaptic cleft by treating autistic mice with acetylcholinesterase inhibitors can ameliorate impairments in social behavior (Karvat & Kimchi, 2013).

Earlier work from the Sohal lab has shown that acetylcholine normally decorrelates neural circuits, but this normal decorrelation fails to occur in multiple models of autism (F. Luongo, Horn, & Sohal, 2015). Importantly, these differences in correlations are not simply due to differences in the amount of activity but rather reflect a difference in the way activity is organized. Because a growing body of work suggests that VIP cells mediate many important effects of acetylcholine on cortical circuits, abnormalities in the responses of VIP cells to cholinergic modulation represent an attractive candidate mechanism for the failure of acetylcholine to decorrelate circuits in autism models. Therefore, we sought to characterize the response of VIP

cells to cholinergic modulation in wildtype mice and autism models, as well as examining links between VIP cell activity and PFC-dependent behaviors.

RESULTS

Acetylcholine causes widened halfwidth and increased excitability in VIP cells

To assess the effect of acetylcholine on VIP cell properties, we used two forms of cholinergic stimulation: washing on carbachol, a broad cholinergic agonist, and optically stimulating native cholinergic release using ChAT-ChR2 animals. In both cases, we saw an increased spike halfwidth (Fig 2.1A-C) and decreased ability to fire repeatedly in response to sustained stimulation (Fig 2.1D-F). Despite this decrease in maximum firing frequency, we found that VIP cells were actually more excitable after cholinergic stimulation, particularly to weak stimuli. VIP cells responded more robustly to brief current pulses following carbachol application (Fig 2.2A-C) and spiked more in response to simulated excitatory postsynaptic currents (EPSCs) when ChAT fibers were simultaneously activated (Fig 2.2D,E). In the ChAT-ChR2 experiments, spiking increased during cholinergic stimulation but fell to near-baseline levels shortly after the cessation of stimulation, indicating that this is a rapid and local effect.

Characterizing components of VIP cell acetylcholine response

In order to more fully understand this effect, we sought to isolate its components using pharmacological methods. First, we looked at separating out contributions from the two classes of cholinergic receptors: muscarinic and nicotinic receptors. We used atropine, a muscarinic antagonist, to isolate nicotinic effects, and mecamylamine, a nicotinic antagonist, to isolate muscarinic effects. Atropine blocked the increase in halfwidth, while it was preserved in mecamylamine, suggesting the halfwidth change is a muscarinic effect (Fig 2.3A). In terms of

excitability, atropine alone causes an increase in spiking with no further effect after washing on carbachol, while there is no increase in spiking in mecamylamine alone or after carbachol (Fig 2.3B). This suggests that that carbachol induced increase in excitability is a nicotinic effect, though manipulating muscarinic receptors may also affect cell excitability. These changes in excitability are likely mechanistically different, as nicotinic receptors are ionotropic and likely affect excitability through direct opening of cationic channels, while muscarinic receptors are metabotropic, with changes in excitability due to the action of secondary messengers (Brown, 2010; Christophe et al., 2002; Dani & Bertrand, 2007; Gil, Connors, & Amitai, 1997). In combination, these results suggest that the increase in action potential halfwidth and increase in excitability in VIP cells following cholinergic stimulation are dissociable effects mediated by different receptor families.

We also attempted to isolate responsible currents and channels using a combination of current clamp, voltage clamp, and pharmacology. Using a standard K-Gluoconate internal to see all currents, we saw a decreased inward current and an increased voltage-activated outward current (Fig 2.4A). Our goal was to recapitulate this response while isolating a single current or family of currents to identify the source. Using Nickel and TTX in bath and a cesium internal to isolate potassium currents blocked all changes (Fig 2.4B), showing potassium is not sufficient for the carbachol response. Adding TEA and 4AP to isolate only passive potassium currents does preserve the reduced inward current (Fig 2.4C), suggesting this is a passive potassium effect that may have been occluded by voltage-activated potassium currents in the previous recordings. Calcium alone is also not sufficient to reproduce the effect (Fig 2.4D), suggesting that this response is likely a combinatorial effect involving multiple ion channels.

Based on these results, we thought that calcium-activated potassium channels were a strong candidate for this effect, as they fit the criteria of being both voltage-dependent and requiring multiple ions. Additionally, nicotinic acetylcholine receptors have been shown to both directly and indirectly increase intracellular calcium, through direct calcium influx and contributing to depolarization that triggers voltage-gated calcium channels (Dani & Bertrand, 2007; F & Wonnacott, 2004). We decided to investigate this further in current clamp to assess spiking properties using a variety of calcium manipulation techniques to try and block the effect, including Nickel (non-specific calcium channel antagonist), BAPTA (calcium chelator to block calcium activated currents), nimodipine (L-type calcium channel blocker), and iberiotoxin (BK channel blocker) (Brown, 2010; C Gotti, Moretti, Gaimarri, & Zanardi, 2007; Cecilia Gotti et al., 2009). Altering calcium did affect VIP cell firing, often in ways that overlapped with cholinergic manipulation, such as increased halfwidth (Fig 2.4E) and decreased maximum firing rate (Fig 2.4F), showing that changes in calcium can produce the changes we see following cholinergic stimulation, but we were unable to specifically block the carbachol effect and find a strong candidate mechanism.

VIP cells respond abnormally to acetylcholine in multiple autism models

We recorded from VIP cells in in wildtype mice and two etiologically distinct models of autism, Fragile X knockout mice and prenatal valproate exposed mice. Fragile X syndrome is the most common single gene cause of autism (Bassell & Warren, 2008). Prenatal exposure to valproate, a commonly prescribed antiepileptic drug, increases the risk of autism in humans and reproduces core features of autism in animal models (Bromley, Mawer, Briggs, & Cheyne, 2013; Schneider & Przewłocki, 2005). As the cause of autism is poorly understood, there is a great heterogeneity in mouse models. By looking for areas of convergence between two etiologically

distinct models (i.e. genetic knockout and environmental exposure), we can identify deficits that are common and more likely to be truly associated with the disease state. We found that VIP cells in both models were subtly abnormal at baseline and showed an exaggerated carbachol effect, with much wider spikes and an impaired ability to fire repeatedly (Fig 2.5A,B). Both FMR-KO and VPA mice had significantly wider halfwidths at baseline that further increased after carbachol exposure (Fig 2.5C. 2-way ANOVA, WT vs VPA: significant effect of genotype, $p = 0.000011$, and stage, $p = 0.0029$. WT vs FMR: significant effect of genotype, $p = 0.000025$, and stage, $p = 0.016$. FMR vs VPA: no effect of genotype, $p = 0.0622$, significant effect of stage, $p = 0.01$). This is consistent with previous reports of widened halfwidths in autism models (Deng et al., 2013; Guglielmi et al., 2015). They responded similarly to strong pulse stimuli at baseline, but were unable to maintain this response after carbachol exposure (Fig 2.5D).

In addition to recording the properties of VIP cells in autism models, we wanted to see whether manipulating VIP cells alone was sufficient to produce the decorrelation changes observed in our earlier work. We combined slice calcium imaging with cell-type specific DREADDs (Designer Receptors Exclusively Activated by Designer Drugs) to suppress the activity of VIP cells. Slice calcium imaging allows us to record the activity of ~50-100 neurons *in vitro* by expressing GCaMP in excitatory cells and imaging for an hour (Fig 2.6A). We used a segmentation algorithm to identify individual cells and measure their fluorescence level as a proxy for changes in calcium (Fig 2.6B) and converted this into a raster plot reflecting changes in cell activity (Fig 2.6C). To manipulate VIP cells, we used DREADDs to suppress activity. To account for changes over the course of the experiment, we compared slices imaged in standard ACSF for one hour with slices that had 30 minutes of ACSF followed by 30 minutes of ACSF with CNO. There was no difference in the correlation strength distribution (Fig 2.6D,E), total amount of activity (Fig 2.6F),

or fraction of strong correlations (Fig 2.6G). We recorded single VIP cell responses after washing on CNO and saw only a modest decrease in excitability, so it is possible that our manipulation was not sufficient to silence VIP cells enough to see an effect on circuit activity (Fig S2.1).

Optogenetically manipulating VIP cells does not affect select prefrontal-dependent behaviors

Given the strong evidence for the role of VIP cells in sensation, we were interested in how manipulating VIP cells might affect PFC-mediated behaviors. First, based on our hypothesized role for VIP cells in attention, we used a classic attention task, the five choice serial reaction time test (5CSRTT). In this task, mice are trained in an operant chamber with five ports where they can nose poke. Following a cue indicating a trial start, mice must attend to the five ports, watch for one to light up, wait a predetermined time, and then nose-poke for a reward. We looked at the role of VIP cells by implanting mice with bilateral optic fibers in the PFC and injecting halorhodopsin (NpHR) or a fluorescent control virus (EYFP) specifically into VIP cells. We saw no changes due to VIP manipulation in any measures in the test, including premature choice trials, i.e. impulsivity (Fig 2.7A), omitted trials, i.e. inattention (Fig 2.7B), or overall accuracy, i.e. ability to learn (Fig 2.7C). There were some modest changes between sessions, but these were identical between NpHR and EYFP mice, suggesting that these were likely an artefact of trial stage or non-specific light/heating effects. Because we saw changes in VIP cell physiology in both FMR-KO mice and VPA-exposed mice, we decided to look at social behavior and novel object exploration during both VIP inhibition with NpHR (Fig 2.7D,E) and excitation with ChR2 (Fig 2.7F,G) but saw no changes in either case.

DISCUSSION

We sought to characterize the response of VIP interneurons to cholinergic stimulation. Previous work had shown that VIP cells play a key role in several attention related tasks and are robustly modulated by acetylcholine *in vivo,* but the cellular mechanisms underlying these effects remained unclear. Furthermore, we wanted to examine the properties of VIP interneurons in mouse models of autism, as we thought VIP cells were a strong candidate to mediate a previous network level phenotype shown in our lab.

Using both carbachol, a non-specific cholinergic agonist, and stimulation of native cholinergic release using ChAT-ChR2 mice, we saw robust changes in VIP physiology, notably a widened action potential halfwidth and increase in excitability, particularly to weak inputs. Using antagonists for the two major classes of cholinergic receptors, nicotinic receptors and muscarinic receptors, these effects appear to be dissociable, with changes in halfwidth mediated by muscarinic receptors and changes in excitability mediated by nicotinic receptors. Voltage clamp experiments showed that these effects are mediated by a combination of currents, but we could not isolate a specific source. We hypothesized that calcium-activated potassium currents were a strong candidate, but further pharmacology focused on calcium manipulations was inconclusive.

One possible obstacle is the challenges of capturing cholinergic dynamics in slice. There is still debate in the field as to the spatial specificity of acetylcholine release, with proponents of both bulk volume release and targeted release (Sarter, Parikh, & Howe, 2009). This concern was partially mitigated by using ChAT-ChR2 mice, allowing for stimulation of native cholinergic fibers. Additionally, cholinergic signaling occurs across multiple time scales with effects occurring on timescales from milliseconds to tens of minutes (Parikh, Kozak, Martinez, & Sarter, 2007). A

common concern in slice pharmacology experiments is the effect of receptor desensitization caused by washing on drugs for a sustained period of time, resulting in effects that would not occur in the intact brain. However, in the case of acetylcholine, even this is not straightforward – some types of nicotinic acetylcholine receptors desensitize so quickly that desensitization of the receptor may actually be part of the normal response (Picciotto, Addy, Mineur, & Brunzell, 2008). Our results likely are a combination of multiple changes, as evidence by the fact that there are both nicotinic and muscarinic contributions. Therefore, it is possible that the physiological relevance of our results could vary for different components of the response. Our results clearly demonstrate that VIP cells in the prefrontal cortex are sensitive to acetylcholine and likely have both nicotinic and muscarinic receptors, but the exact effect of cholinergic stimulation *in vivo* remains unclear.

Reducing VIP activity during slice calcium imaging did not change patterns of network imaging, and optogenetically manipulating VIP cells during social behavior or an attention task did not change behavior. Given previous work showing the large impact of VIP cells on dynamics in sensory cortices, we were somewhat surprised by these results. One possibility is that VIP cells have a critical but very local domain of action *in vivo* (Karnani et al., 2016), such that recording slice network activity or manipulating the entire population using opsins is unable to accurately recapitulate their behavior in the intact system and any population level manipulation occludes local effects. It is also possible our manipulations were not able to effectively silence VIP activity.

METHODS

Animals

All experiments were conducted in accordance with procedures established by the Administrative Panels on Laboratory Animal Care at the University of California, San Francisco. Unless otherwise

noted, experiments were performed under ambient light and mice were group housed with littermates. All experiments were done in mice >8 weeks of age. The following transgenic mouse lines were used: *Fmr-KO* (Jax Stock #003025), ChAT-ChR2 (Jax Stock #014546), VIP-Cre (Jax Stock # 031628), and Ai14 (Jax Stock # 007914). FMR and ChAT-ChR2 mice were crossed with VIP-Cre mice to facilitate identification and targeting of VIP cells. For valproic-acid experiments, C57Bl6 dams were housed with male VIP-Cre mice for a limited time to establish a pregnancy timeline. Dams were then injected intraperitoneally at E10.5 with either 500mg/kg valproic acid in saline or saline as a control. Mice of both sexes were used for all experiments except Fmr-KO experiments, as Fmr1 is an X-linked gene so all null animals are male.

Surgical Procedures

All surgeries were performed under isoflurane anesthesia using standard mouse stereotactic technique. Unless otherwise noted, all injections used PFC coordinates of AP +1.7, ML +/- 0.3, and DV -2.75. The following viruses were used: AAV5-EF1α-DIO-mCherry, AAV5-EF1α-DIO-EYFP, AAV5-EF1α-DIO-ChR2-EYFP, AAV5-EF1α-DIO-eNpHR3.0-EYFP, AAV5-hSyn-DIO-hM3D(Gi)-mCherry, and AAV5-Syn-GCaMP6s. Slice experiments used unilateral injections, while behavior experiments used bilateral injections followed by implantation of optic fibers above the injection site which were secured to the skull using metabond.

Whole-cell patch clamp

All whole-cell patch clamp experiments were done in 250μm coronal slices including the PFC. Slicing solution was chilled to 4°C and contained the following (in mM): 234 sucrose, 26 NaHCO$_3$, 11 glucose, 10 MgSO$_4$, 2.5 KCl, 1.25 NaH$_2$PO$_4$, 0.5 CaCl$_2$, bubbled with 5% CO$_2$/95% O$_2$. Slices were incubated in ACSF at 32°C for 30 min and then at room temperature until recording.

Standard ACSF contained (in mM) the following: 123 NaCl, 26 NaHCO$_3$, 11 glucose, 3 KCl, 2 CaCl$_2$, 1.25 NaH$_2$PO$_4$, 1 MgCl$_2$, also bubbled with 5% CO$_2$/95% O$_2$. For some voltage clamp experiments, a low sodium ACSF with TEA was used, containing the following (in mM): 2.5 KCl, 10 Glucose, 96 NaCL, 1.25 NaH$_2$PO$_4$, 1 MgCl$_2$, 2 CaCl$_2$, 30 TEA. Neurons were visualized using differential interference contrast or DODT contrast microscopy on an upright microscope (Olympus). Recordings were made using a Multiclamp 700B (Molecular Devices) amplifier and acquired with pClamp. Standard patch pipettes (2–5 MΩ tip resistance) were filled with the following (in mM): 130 K-gluconate, 10 KCl, 10 HEPES, 10 EGTA, 2 MgCl$_2$, 2 MgATP, and 0.3 Na$_3$GTP. For some voltage clamp experiments, cesium internal was used, containing the following (in mM): 130 CsCH$_4$O$_3$S, 4 NaCl, 2 MgCl$_2$, 10 EGTA, 10 HEPES, 5 TEA, 5 QX-314-Cl, 2 MgATP, and 0.5 Na$_3$GTP. All recordings were made at 30°C–32°C. Series resistance was compensated in all current-clamp experiments and monitored throughout recordings. Recordings were discarded if Rs changed by >25%.

VIP cells were visually identified using fluorescence, either using tdTomato in VIP-Ai14 mice or an injection of DIO-mCherry in VIP-Cre mice. For all pharmacology experiments, drugs were water before being diluted in ACSF and allowed to wash on for 10 minutes following initial recordings. For experiments using both carbachol and antagonists, the antagonist was applied before carbachol. The following concentrations were used: 2μM carbachol, 1μM CNO, 100μM nickel, 100nM iberiotoxin, 1μM TTX, 1μM atropine, 20μM mecamylamine, 10μM nimodipine, 100μM APV, 100μM 4AP, 10μM BAPTA

Slice calcium imaging

Slice calcium imaging experiments were performed as previously described by our lab (F. J. Luongo, Horn, & Sohal, 2016). Preparation was similar to the patch clamp preparation with two exceptions: experiments were done in 350μm coronal slices and immediately after slicing, they were transferred to an N-methyl-D-glucamine (NMDG)-based recovery solution for 10 minutes before being transferred to standard ACSF for the remainder of their recovery (S. Zhao et al., 2011). The NMDG-based solution was maintained at 32°C and consisted of the following (in mmol/L): 93 NMDG, 93 hydrogen chloride, 2.5 potassium chloride (KCl), 1.2 sodium dihydrogen phosphate, 30 sodium bicarbonate, 25 glucose, 20 HEPES, 5 NA-ascorbate, 5 Na-pyruvate, 2 thiourea, 10 magnesium sulfate, and .5 calcium chloride (CaCl). Both changes were made to maximize the number of intact, healthy cells in the tissue to facilitate network analysis.

Imaging was performed on an Olympus BX51 upright microscope with a 20× 1.0NA water immersion lens, .5× reducer (Olympus, Tokyo, Japan), and ORCA-ER CCD Camera (Hamamatsu Photonics, Hamamatsu, Japan). Illumination was delivered using a Lambda DG4 arc lamp (Sutter Instruments, Novato, California). Light was delivered through a 472/30 excitation filter, 495 nm single-band dichroic, and 496 nm long pass emission filter (Semrock, Rochester, New York). All movies that were analyzed consisted of 36,000 frames acquired at 10 Hz (1 hour) with 4×4 sensor binning yielding a final resolution of 256×312 pixels. Light power during imaging was 100 to 500 μW/mm². The Micro Manager software suite (v1.4, National Institutes of Health, Bethesda, Maryland) was used to control all camera parameters and acquire movies. Signal extraction and analysis was performed as previously described (F. J. Luongo et al., 2016). All imaging was done in standard ACSF with 2μM carbachol added to increase spontaneous activity. At 30 minutes, slices

were switched to ACSF containing 1μM CNO or control ACSF to account for any changes caused by changing solution (minor changes in oxygenation, flow rate, etc).

Behavior

All mice used in behavior experiments were implanted with bilateral optic fibers at +/- 0.3 ML and -2.5 DV. AAV-DIO-NpHR-EYFP, AAV-DIO-ChR2-EYFP, or AAV-DIO-EYFP was injected bilaterally at +/- 0.3 ML, 1.7 AP, and -2.75 DV. For NpHR experiments, constant 532nm light was used with 2.5 mW on each side.

The five choice serial reaction time test (five choice) was performed in operant chambers (Medtronic). For the duration of testing and training, mice were singly housed, water restricted, and given free access to chow. Over the course of several weeks mice were trained in task mechanics, starting with general lever pressing, followed by sessions where the target nose-poke port was kept lit for increasingly shorter periods of time (10 min, 30s, 5s, 2s, 1s). In early training sessions, mice were not punished for incorrect nose-pokes, but later in training incorrect responses triggered a loud white noise burst. Mice were advanced to the next training level when they completed >10s in a session with >50% accuracy. Mice typically performed ~30 trials per session. Each test trail was started with an auditory cue, followed by a single nose-poke port turning on for 1s. Mice had to wait until light was off before responding. When they correctly responded, they could press a lever at the back of the chamber to receive a water reward. When mice responded prematurely or used the wrong nose-poke port, mice triggered a loud white noise burst and time-out with the lights on.

Social interaction and novel object exploration testing took place in the home cage. For social interaction, mice were exposed to a novel conspecific juvenile for 5 minutes, followed by a 5

minute break, and then 5 minutes with a novel object. All mice had two testing sessions separated by one week. Half the mice had light on in week one and off in week two, while the other half had the opposite. In each case, total interaction time was scored by a blinded observer.

Statistics and Data Analysis

Unless otherwise noted, non-parametric statistical tests were used. Data was analyzed using custom MATLAB code.
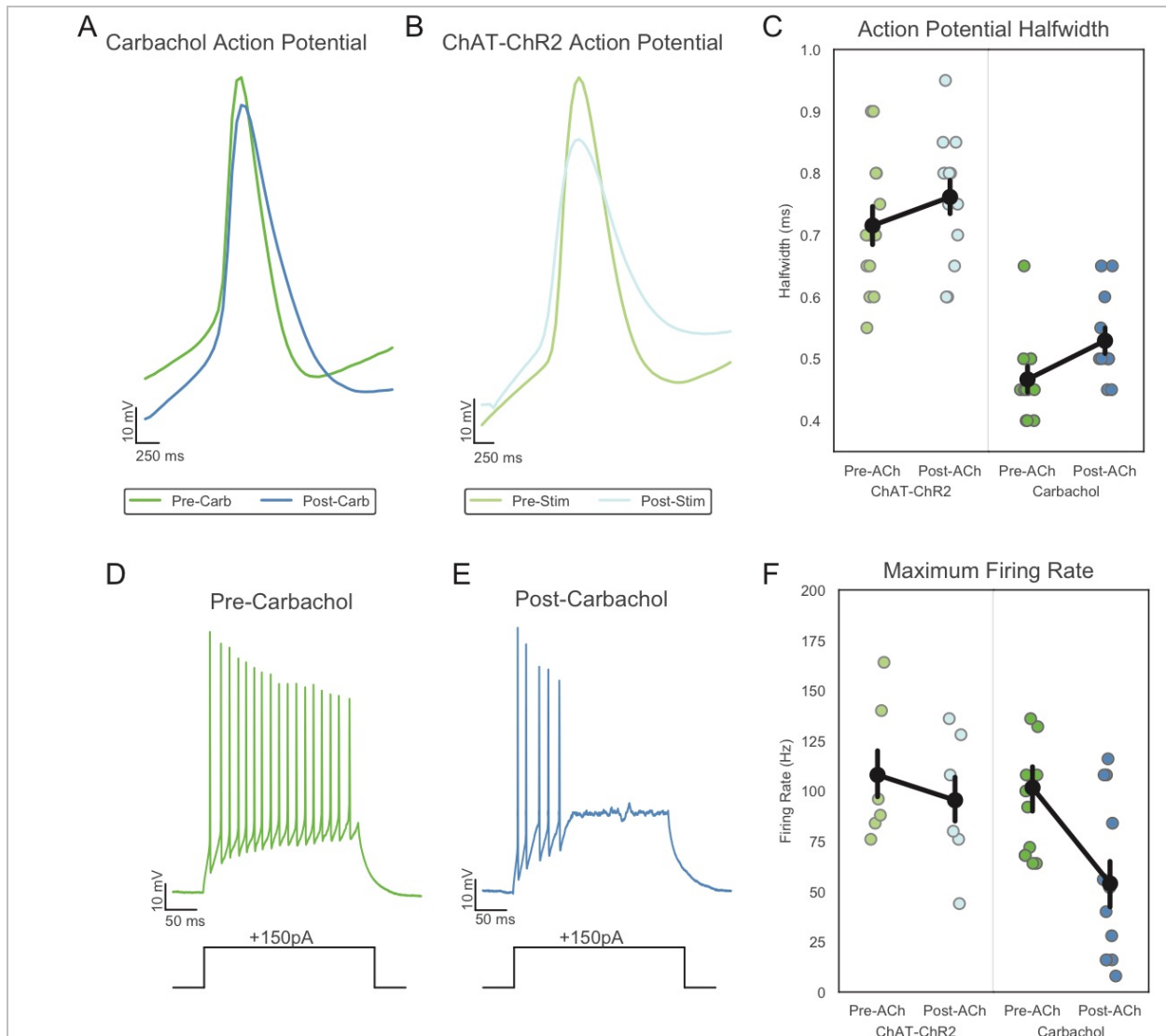
Figure 2.1: Acetylcholine increases action potential halfwidth and decreases repetitive firing in VIP interneurons. (A,B) Example action potential waveforms before and after cholinergic stimulation with either bath application of carbachol or stimulation of ChAT-ChR2 fibers. (C) Action potentials increase following ACh stimulation. ChAT-ChR2, p = 0.044; Carbachol, p = 0.011. (D,E) Example of response to a 250ms current step before and after carbachol activation. Following ACh stimulation, cells are not able to fire repeatedly and instead enter a depolarization block. (F) Depolarization block was not observed in ChAT-ChR2 mice, p = 0.67, but was robust in carbachol, p = 0.0028.
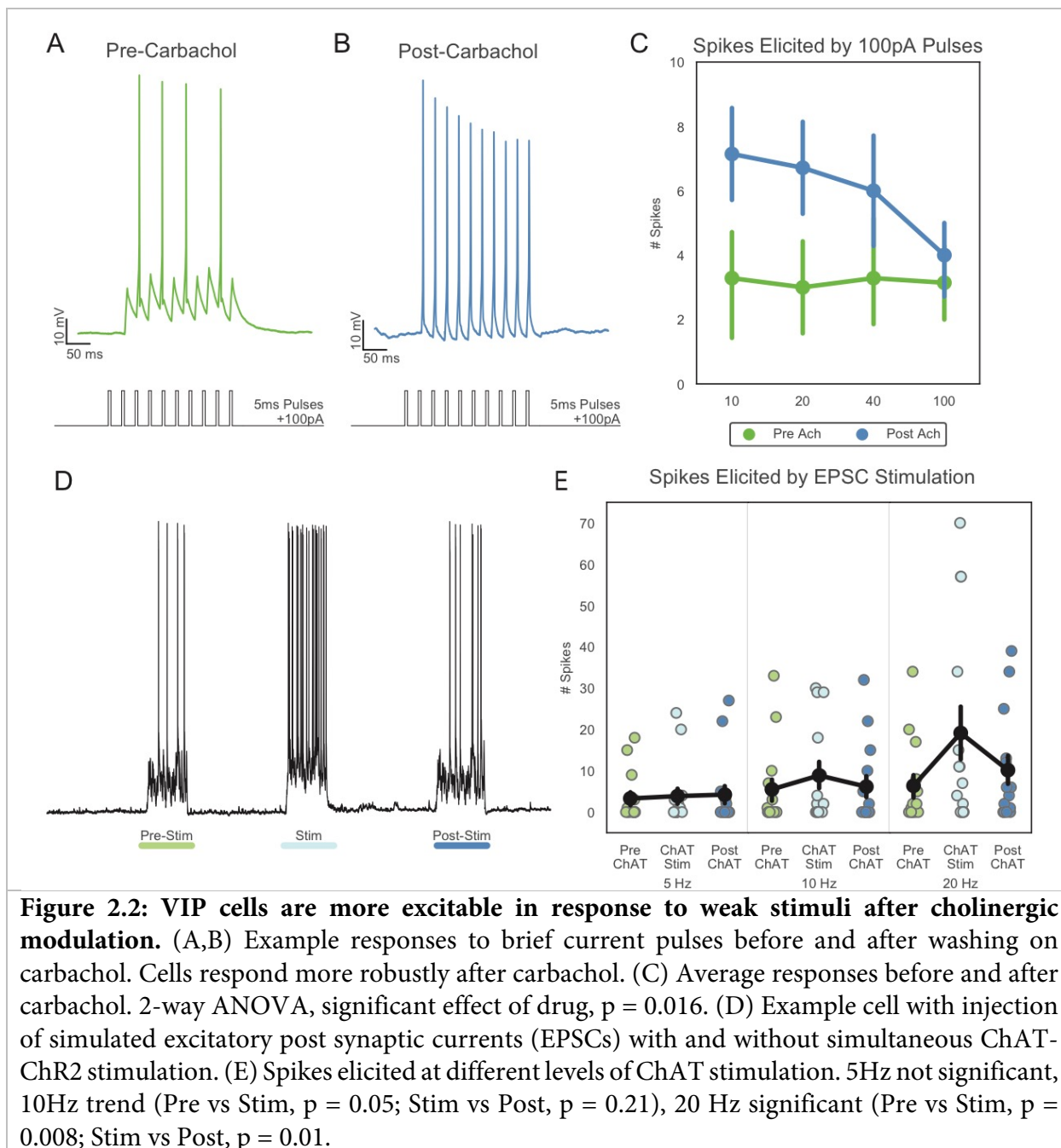
Figure 2.2: VIP cells are more excitable in response to weak stimuli after cholinergic modulation. (A,B) Example responses to brief current pulses before and after washing on carbachol. Cells respond more robustly after carbachol. (C) Average responses before and after carbachol. 2-way ANOVA, significant effect of drug, p = 0.016. (D) Example cell with injection of simulated excitatory post synaptic currents (EPSCs) with and without simultaneous ChAT-ChR2 stimulation. (E) Spikes elicited at different levels of ChAT stimulation. 5Hz not significant, 10Hz trend (Pre vs Stim, p = 0.05; Stim vs Post, p = 0.21), 20 Hz significant (Pre vs Stim, p = 0.008; Stim vs Post, p = 0.01.
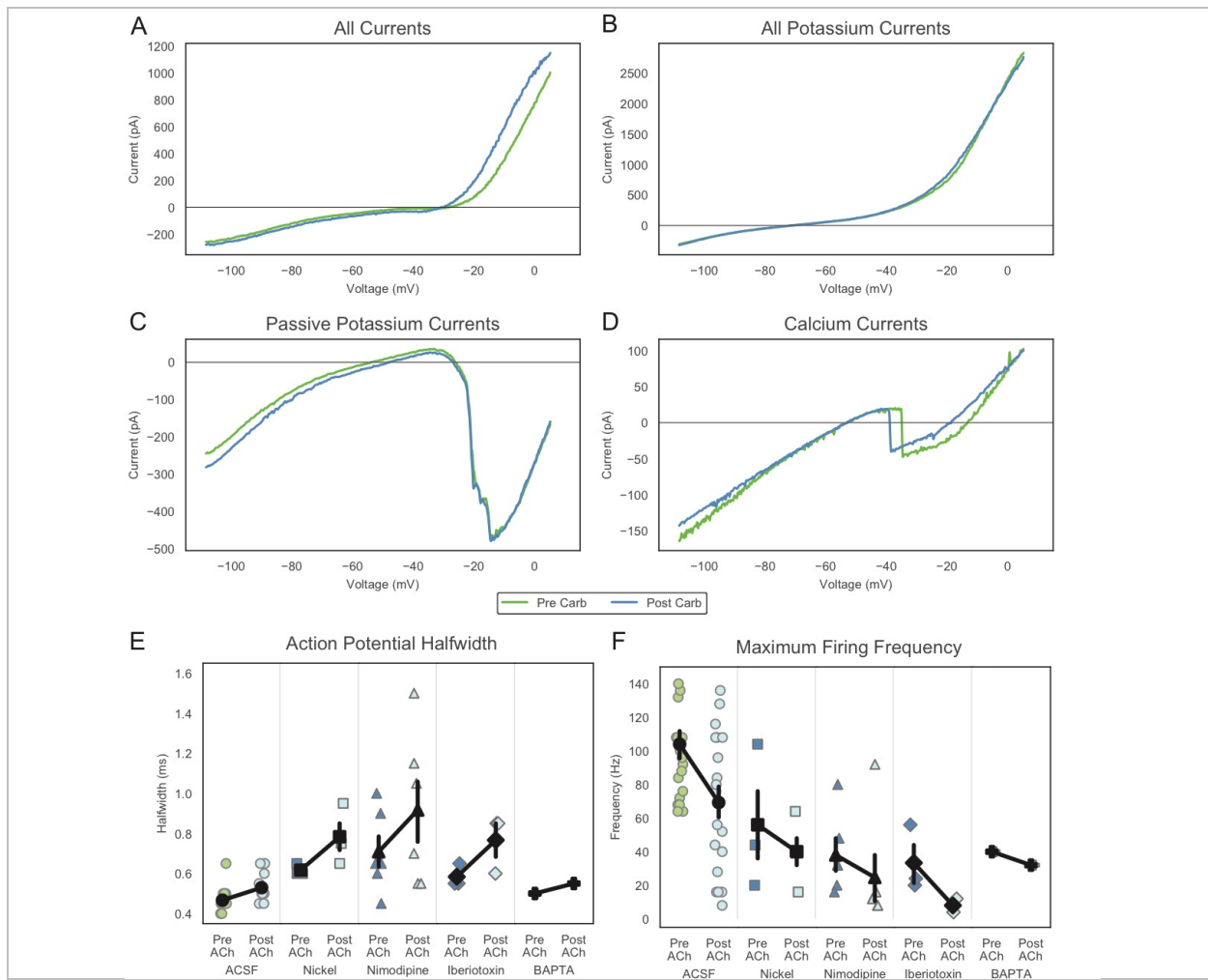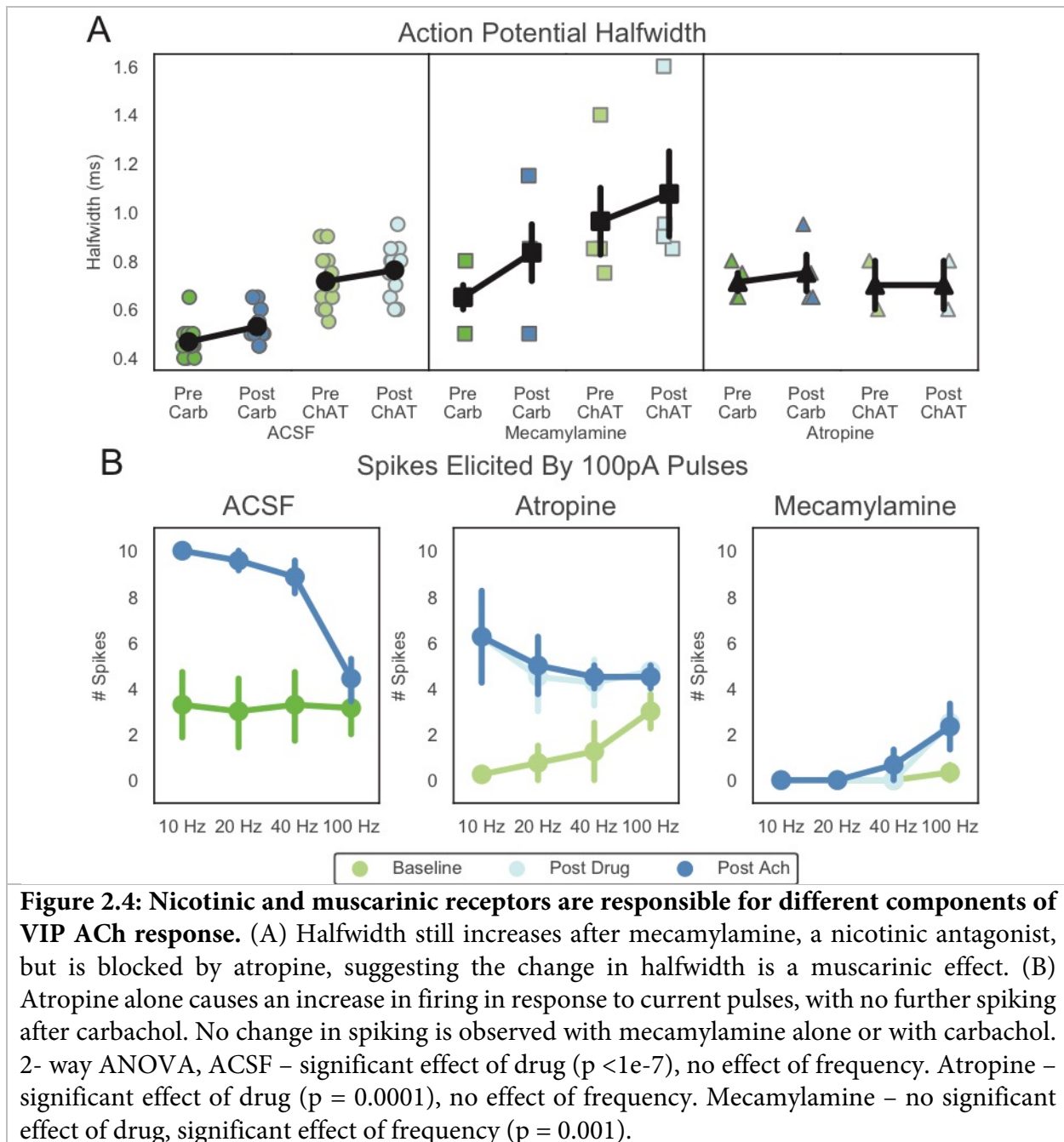
Figure 2.3: A combination of currents contribute to the cholinergic changes in VIP cells. (A) Total currents recorded after carbachol show a modest decreased outward current and large increased voltage-activated inward current. (B-D) Isolating single currents is not sufficient to recapitulate this effect, indicating it is likely combinatorial. (B) Nickel and TTX to block calcium and sodium and isolate potassium. (C) Nickel, TEA, 4AP, and TTX to block calcium, sodium, and voltage activated potassium channels and isolate passive potassium channels. (D) TEA, 4AP, and TTX to block sodium and potassium and isolate calcium. (E,F) Using a range of calcium manipulations to block the carbachol effect. (E) Action potential halfwidth is often increased by calcium manipulations alone and further increases after carbachol application. Nickel, $p = 0.11$; Nimodipine, $p = 0.06$; Iberiotoxin, $p = 0.11$. (F) Maximum firing frequency also decreased by calcium manipulations alone and further decreased by carbachol. Nickel, $p = 0.29$; Nimodipine, $p = 0.25$; Iberiotoxin, $p = 0.11$.

Figure 2.4: Nicotinic and muscarinic receptors are responsible for different components of VIP ACh response. (A) Halfwidth still increases after mecamylamine, a nicotinic antagonist, but is blocked by atropine, suggesting the change in halfwidth is a muscarinic effect. (B) Atropine alone causes an increase in firing in response to current pulses, with no further spiking after carbachol. No change in spiking is observed with mecamylamine alone or with carbachol. 2- way ANOVA, ACSF – significant effect of drug (p <1e-7), no effect of frequency. Atropine – significant effect of drug (p = 0.0001), no effect of frequency. Mecamylamine – no significant effect of drug, significant effect of frequency (p = 0.001).
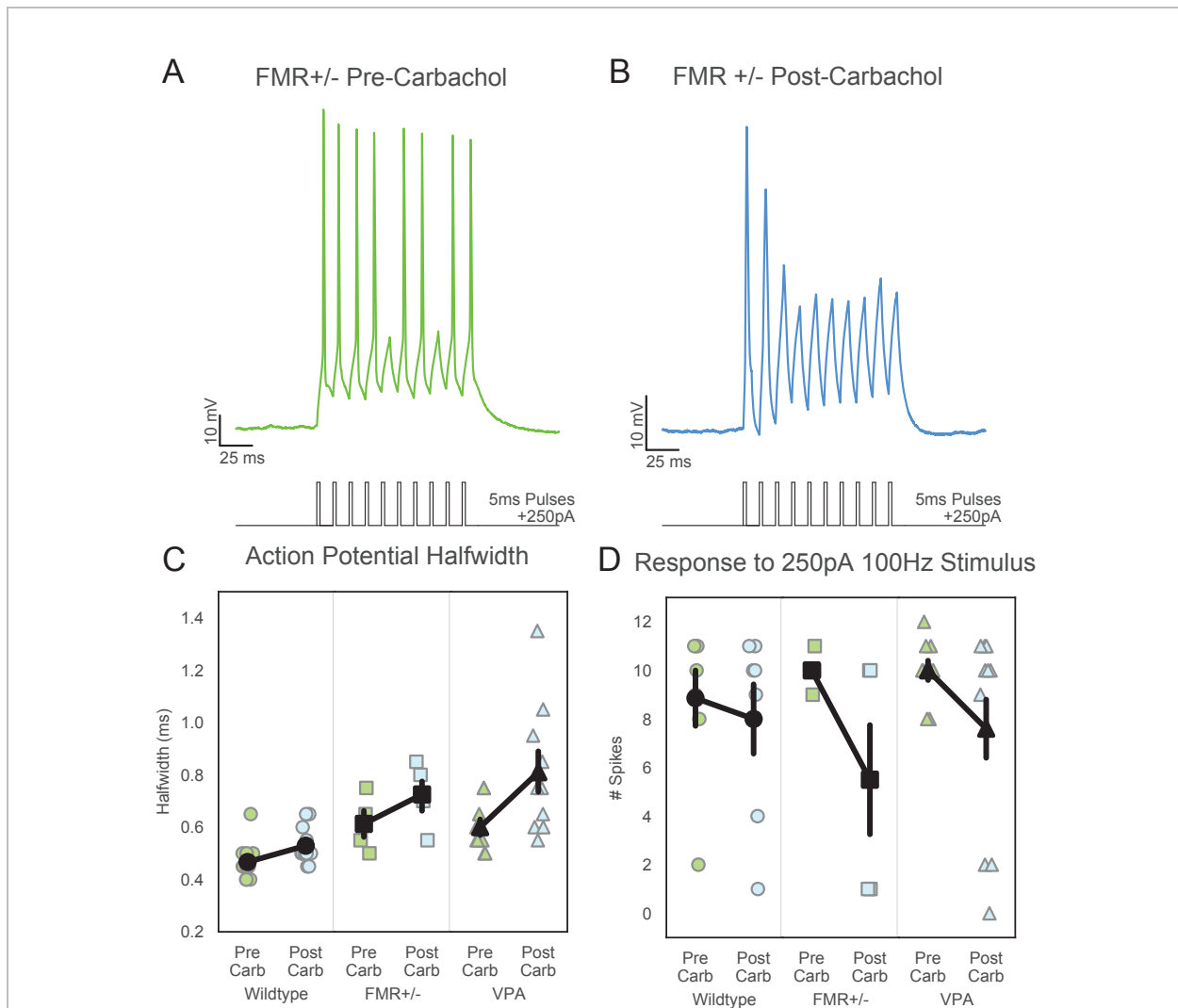
Figure 2.5: VIP cells respond abnormally to cholinergic stimulation in multiple autism models. (A,B) Example response to current pulses before and after carbachol in FMR-KO mice. Cells have a much wider halfwidth and are unable to spike repeatedly. (C) Action potential halfwidth in FMR-KO and VPA-exposed mice. Halfwidths are wider at baseline but show the same characteristic increase after carbachol exposure. 2-way ANOVA WT vs VPA, significant effect of genotype (p = 0.000011) and carbachol (p = 0.003). 2-way ANOVA WT vs FMR, significant effect of genotype (p = 0.000025) and carbachol (p = 0.016). 2-way ANOVA FMR vs VPA, no effect of genotype (p = 0.622), significant effect of carbachol (p = 0.011). (D) Response to strong pulse stimulation is similar before and after carbachol exposure in WT mice but is decreased in FMR-KO and VPA-exposed mice. WT, p = 0.59; FMR, p = 0.17; VPA, p = 0.11.
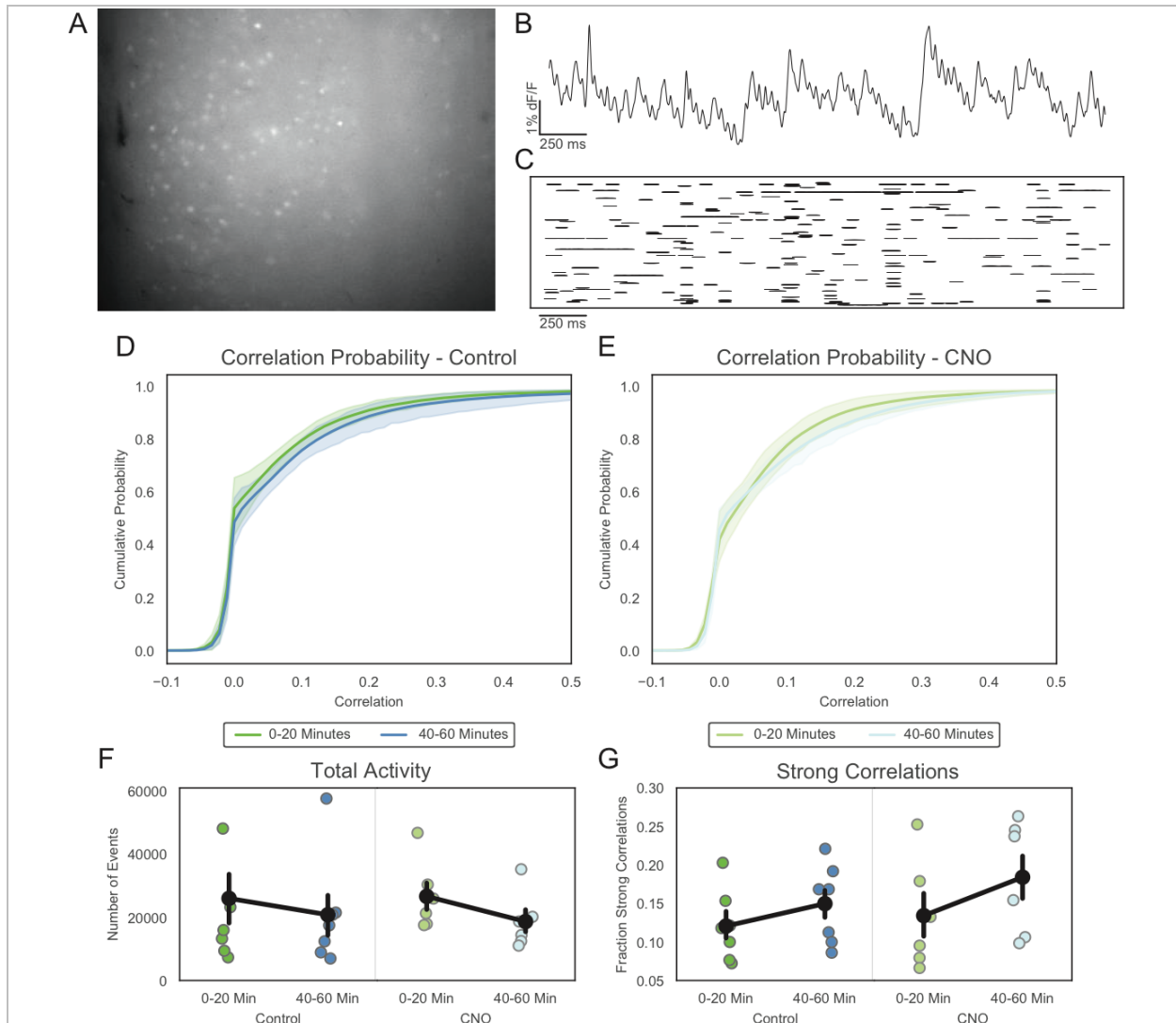
Figure 2.6: Inhibiting VIP cells does not change activity patterns in slice calcium imaging. (A) Example field of view during slice calcium imaging with GCaMP expressed in all PFC neurons. On average 50-100 neurons could be segmented and imaged simultaneously. (B) Calcium trace for a single neuron. (C) Event raster for a single recording, each row is an individual neuron. (D,E) Correlation probability distribution. There are no changes in overall correlations between control ACSF and CNO inhibiting VIP neurons. (F) Total activity. There is a minor decrease in activity over the recording session but this is unchanged between controls and CNO experiments, suggesting it is an effect of time and not VIP inhibition. 2-way ANOVA, no effect of drug ($p = 0.22$) or time ($p = 0.16$). (G) Fraction of strong correlations. 2-way ANOVA, no effect of drug ($p = 0.53$) or time ($p = 0.13$).
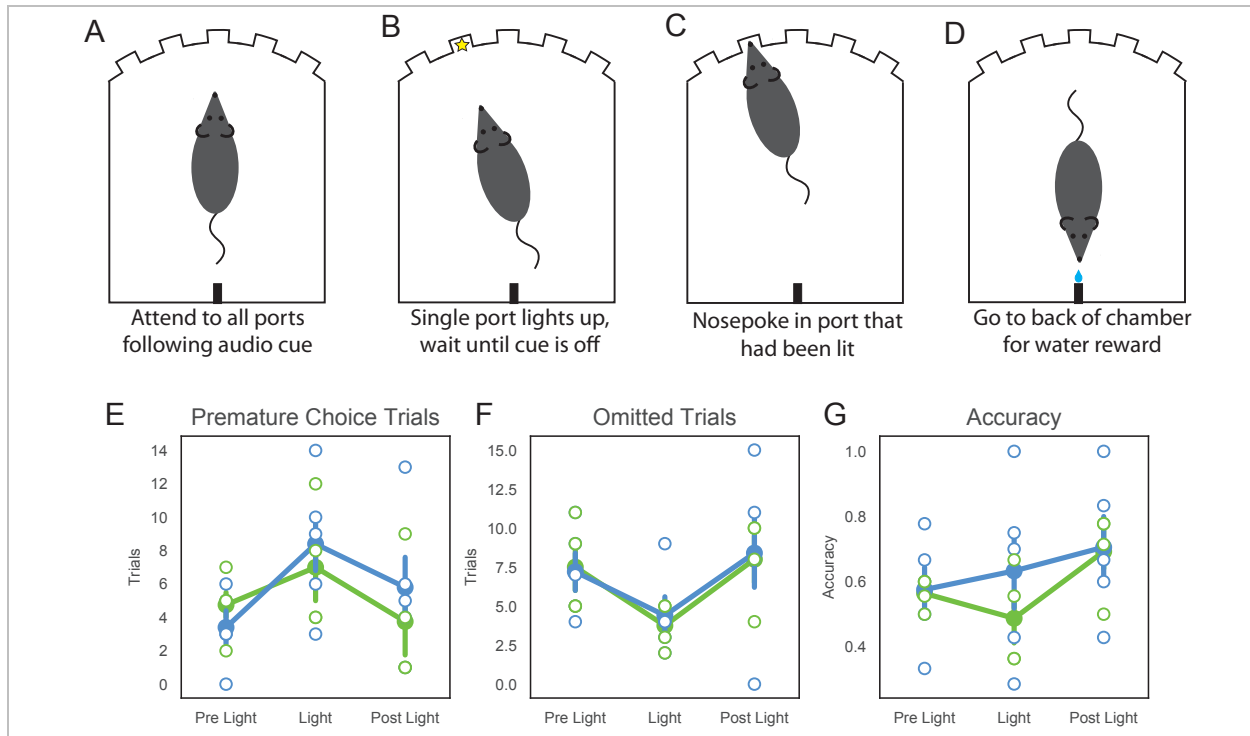
Figure 2.7: Inhibiting VIP interneurons does not affect performance on the five-choice serial reaction time test. (A-D) Schematic of 5 choice task. (A) Following an audio cue signaling beginning of trial, mice must attend to five nose-poke ports. (B) One port is briefly lit. Mice must inhibit their response and wait to respond until light is off. (C) Following waiting period, mice must nose-poke in previously lit port. (D) Following successful trial, mice receive a water reward at a spout at the back of the chamber. (E-G) Inhibiting VIP cells with NpHR during a fraction of trials does not change performance in the well-learned task. (E) Premature choice trials, where mice respond before waiting period is over. 2-way ANOVA, no effect of virus (p = 0.618) or light (p = 0.087). (F) Omitted trials, where mice fail to respond following a lit port. 2-way ANOVA, no effect of virus (p = 0.85), significant effect of light (p = 0.042). (G) Overall accuracy in choosing correct port. 2-way ANOVA, no effect of virus (p = 0.4458) or light (p = 0.26).
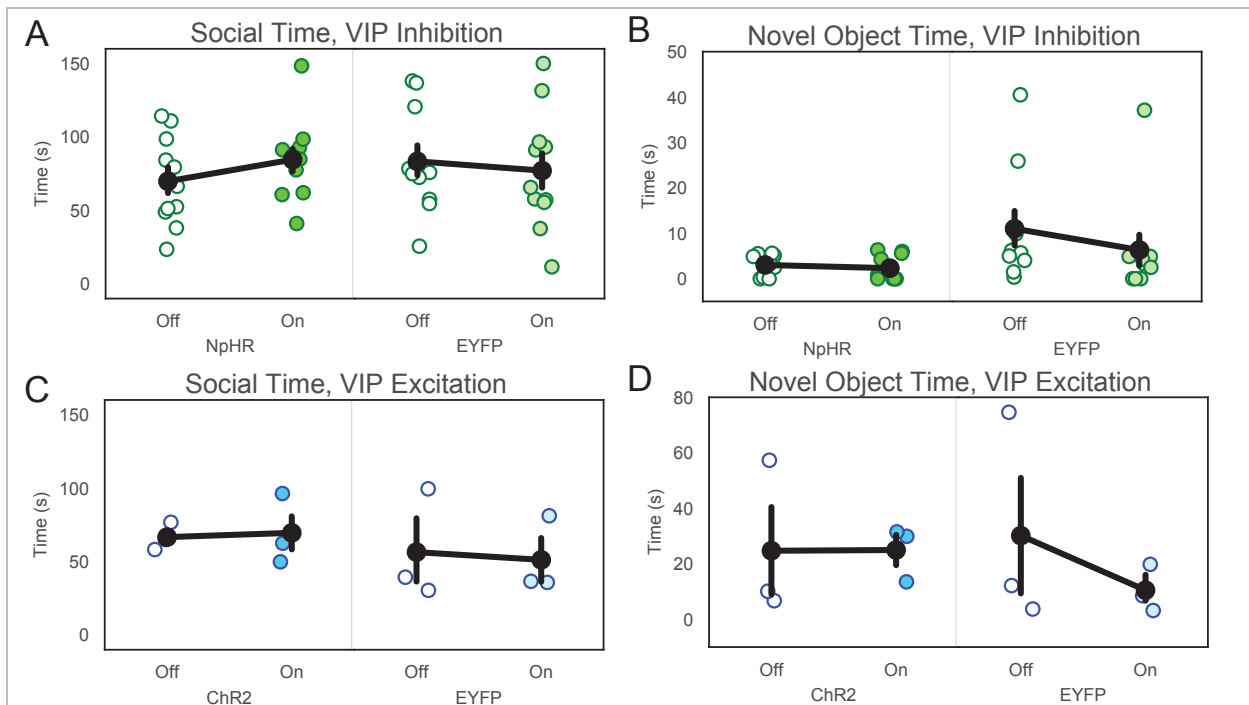
Figure 2.8: Manipulating VIP cells does not affect social interaction time or novel object exploration. (A,B) Inhibiting VIP cells with NpHR does not change interaction with a conspecific juvenile (NpHR p = 0.18, EYFP p = 0.37) (A) or novel object (NpHR p = 0.62, EYFP p = 0.11). (B). (C,D) Excitation of VIP cells with ChR2 also does not alter social (ChR2 p = 1.0, EYFP p = 0.59) (C) or novel exploratory (ChR2 p = 1.0, EYFP p = 0.11) (D) behavior.

Figure S2.1: CNO reduces excitability but does not silence VIP cells. Single cell recordings of VIP cells expressing DREADDs before and after applying CNO. (A) Resting potential. (B) Membrane resistance. (C) Spiking in response to current pulses.

Chapter 3: VIP Interneurons Contribute to Avoidance Behavior by Regulating Information Flow Across Hippocampal-Prefrontal Networks
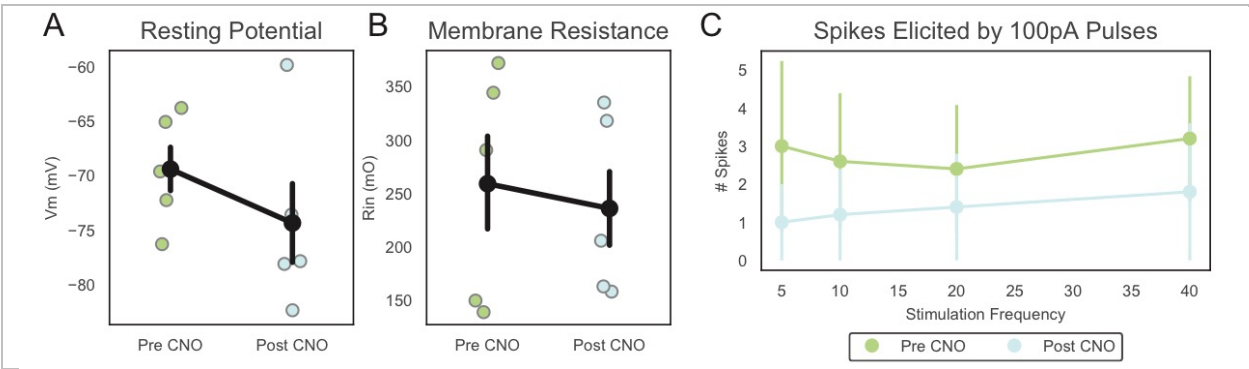
SUMMARY

Inhibitory interneurons expressing vasoactive intestinal polypeptide (VIP) are known to disinhibit cortical neurons. However, it is unclear how disinhibition, occurring at the single-cell level, interacts with network-level patterns of activity to shape complex behaviors. To address this, we examined the role of prefrontal VIP interneurons in a widely-studied mouse behavior: deciding whether to explore or avoid the open arms of an elevated plus maze. VIP interneuron activity increases in the open arms and disinhibits prefrontal responses to hippocampal inputs, which are known to transmit signals related to open arm avoidance. Indeed, inhibiting VIP interneurons disrupts network-level representations of the open arms, and decreases open arm avoidance specifically when hippocampal-prefrontal theta synchrony is strong. Thus, VIP interneurons effectively gate the ability of hippocampal input to generate prefrontal representations which drive avoidance behavior. This shows how VIP interneurons enable cortical circuits to integrate specific inputs into network-level representations that guide complex behaviors.

INTRODUCTION

Specific neuronal classes alter activity in individual downstream neurons in ways that are now beginning to be understood. However, understanding how these actions on single cells interact with network-level representations of behavioral information remains unclear. For example, in neocortex, GABAergic interneurons which express vasoactive intestinal polypeptide

(VIP) are known to mainly inhibit other classes of GABAergic interneurons (S. Lee, Kruglikov, Huang, Fishell, & Rudy, 2013; Pfeffer et al., 2013; Pi et al., 2013). Through this action, VIP interneurons disinhibit the responses of cortical excitatory neurons to various stimuli (Ayzenshtat, Karnani, Jackson, & Yuste, 2016; Fu et al., 2014; Karnani et al., 2016; Pi et al., 2013), altering both network activity and behavior (Kamigaki & Dan, 2017). However, there are many outstanding questions about the relationship between VIP interneurons, network activity, and behavior. First, can we identify specific patterns of network activity which link VIP interneurons to their behavioral effects? In particular, can we show that changes in VIP interneuron activity alter specific patterns of network activity, such that the degree of alteration predicts the magnitude of accompanying changes in behavior? Second, do the behavioral effects of manipulating VIP interneurons depend on the current state of the network and its inputs? For example, if an input is known to drive a behavior, does manipulating VIP neurons exert a consistent effect on that behavior regardless of whether that input is strong or weak? Questions like these highlight critical gaps in our current understanding of exactly how network activity mediates and modulates the behavioral effects of activity in a specific neuronal population.

To address these questions, we studied the role of VIP interneurons within the medial prefrontal cortex (mPFC) in a commonly studied behavior: open arm avoidance in the elevated plus maze (EPM). The EPM comprises two exposed open arms and two closed arms surrounded by high walls, which elicit ethologically-relevant avoidance behavior that reflects the innate preference of mice for the safety of closed spaces over open ones. We first show a role for prefrontal VIP interneurons in open arm avoidance. Then we show that VIP interneurons contribute to network-level representations of the open arms. When we inhibit prefrontal VIP interneurons, the amount by which these representations change predicts the change in open arm avoidance.

Prefrontal open arm representations are known to be driven by input from the ventral hippocampus (vHPC) (Adhikari et al., 2011; Ciocchi, Passecker, Malagon-Vina, Mikus, & Klausberger, 2015; Padilla-Coreano et al., 2016); suppressing this input disrupts these representations and open arm avoidance (Padilla-Coreano et al., 2016). We find that VIP interneurons disinhibit prefrontal responses to vHPC input, suggesting that they may contribute to prefrontal open arm representations and open arm avoidance specifically by enhancing the impact of vHPC inputs on mPFC circuits. Consistent with this model, we find that the effects of VIP interneurons on open arm avoidance change depending on the current strength of vHPC input to mPFC. Together, these results show how the recruitment of prefrontal VIP interneurons at specific times elicits synaptic actions that change network activity in ways that reshape behavior.

RESULTS

VIP interneuron activity increases in the open arms of the EPM.

To efficiently measure VIP interneuron activity during EPM exploration, we used fiber photometry (Cui et al., 2013; Gunaydin et al., 2014) in the widely studied VIP-Cre line (Batista-Brito et al., 2016; De Rubeis et al., 2014; Garcia-Junco-Clemente et al., 2017; Kamigaki & Dan, 2017; Khoshkhoo, Vogt, & Sohal, 2017; Pfeffer et al., 2013; Pi et al., 2013) VIP-Cre mice were injected with adenoassociated-virus (AAV1) encoding Cre-dependent GCaMP6s in mPFC. Two weeks after surgery, mice explored the EPM while we measured VIP-GCaMP signals. VIP-GCaMP signals were higher in the center and open arms than the closed arms (Fig3.1 A-C).

VIP interneuron activity predicts future open arm avoidance vs. exploration.

Several models could explain our finding that VIP interneuron activity is higher in the center and open arms than closed arms. One is that VIP interneuron activity drives open arm

exploration. Alternatively, VIP interneuron activity might represent an anxiety-related signal that promotes open arm avoidance. In the latter model, other signals presumably drive exploration, such that decisions to explore vs. avoid reflect a competition between these pro-exploratory signals and VIP activity-driven avoidance. In this case, exploration would occur when exploratory signals outpace increases in VIP interneuron-driven avoidance signals during approaches to the center or open arms. A final possibility is that VIP activity does not influence or predict choices to explore vs. avoid the open arms, but is simply a readout of EPM location.

First, to test whether VIP activity predicts subsequent exploration vs. avoidance, we identified all runs from a closed arm to the center, then classified each according to whether the mouse subsequently avoided or explored the open arms (closed-center-closed vs. closed-center-open runs). VIP-GCaMP signals in the center chamber were significantly lower for closed-center-open than closed-center-closed runs (Fig. 3.1D). We also looked further back in time, comparing VIP-GCaMP signals in the closed arm, prior to entry into the center. Again, lower VIP-GCaMP signals predicted subsequent open arm exploration (Fig. 3.1E).

Inhibiting VIP interneurons reduces open arm avoidance.

The preceding suggests that low vs. high VIP activity as mice approach the center chamber promotes subsequent open arm exploration vs. avoidance, respectively. We used optogenetics to directly test this hypothesized causal relationship. Bilateral fiber optics were implanted into the mPFC of VIP-Cre mice injected with Cre-dependent archaerhodopsin (AAV5-DIO-eArch3.0-eYFP; Arch) or eYFP (AAV5-DIO-eYFP). Because VIP-GCaMP signals specifically increased in the center and open arms, we delivered 532nm light to the mPFC whenever mice were within a "stimulation zone," comprising the center, open arms, and a small portion of the closed arms abutting the center. We then compared behavior during three, 3-minute-long epochs: light OFF,

60

followed by light ON (i.e., light was delivered only in the stimulation zone), and finally light OFF again (Fig. 3.2A). During the light ON epoch, there was a significant increase in relative time spent in the open arms (Fig 3.2B) and open arm entries (Fig 3.2C) for VIP-Arch mice compared to VIP-eYFP cohorts.

VIP interneurons disinhibit prefrontal responses to hippocampal input.

Given that VIP interneuron activity increases in the open arms and contributes to open arm avoidance, we decided to explore the relationship between prefrontal VIP interneurons and inputs arriving from the ventral hippocampus (vHPC). vHPC inputs to mPFC differentially encode the open vs. closed arms of the EPM (Ciocchi et al., 2015). Furthermore, mPFC neurons which encode the open vs. closed arms phase-lock to the vHPC theta rhythm suggesting they receive strong input from this source (Adhikari et al., 2011). Indeed, inhibiting vHPC-mPFC projections suppresses single-unit mPFC activity that is specific for the open vs. closed arms, and reduces open arm avoidance (Padilla-Coreano et al., 2016). Based on this, we hypothesized that mPFC VIP interneurons might be recruited by vHPC input and regulate prefrontal responses to that input. We recorded from mPFC VIP interneurons while stimulating ChR2 in vHPC terminals, and observed EPSCs in VIP interneurons in the presence of TTX (1 uM) + 4 AP (0.1 mM), which isolates monosynaptic responses (Petreanu, Mao, Sternson, & Svoboda, 2009).

To test how mPFC VIP interneurons regulate prefrontal responses to vHPC input, we recorded from layer 2/3 pyramidal neurons in acute mPFC slices from VIP-Cre mice injected with two viruses: one to drive Cre-dependent expression of halorhodopsin (VIP-eNpHR) in the mPFC, and a second to express ChR2 in vHPC projection neurons. This enabled us to stimulate ChR2 in vHPC terminals with blue light flashes (5 ms at 10 Hz), with or without concomitant optogenetic inhibition of VIP interneurons (vHPC-ChR2; Fig. 3.3A). Spiking of layer 2/3 mPFC neurons in

response to vHPC input was reduced when we simultaneously inhibited VIP interneurons (Fig. 3.4B). Repeating these experiments in voltage clamp revealed that inhibiting VIP interneurons significantly increases inhibitory synaptic currents evoked by optogenetic stimulation (Fig 3.3C) of vHPC terminals, but has no effect on excitatory currents (Fig. 3.3D). Thus, VIP interneurons normally disinhibit mPFC responses to vHPC input.

Inhibiting VIP interneurons disrupts prefrontal representations of the open arms.

Given that they disinhibit vHPC-mPFC inputs which transmit information about whether mice are in the open vs. closed arms (Adhikari et al., 2011; Ciocchi et al., 2015), we wondered whether prefrontal VIP interneurons might be necessary for prefrontal representations of the open vs. closed arms. To test this, we had to first identify patterns of prefrontal network activity which encode the open vs. closed arms, then determine how these are altered when we inhibit prefrontal VIP neurons. For this, we employed a dual-color microendoscope (nVoke, Inscopix) for combined GCaMP imaging of mPFC activity and activation of eNpHR in VIP interneurons We expressed GCaMP nonspecifically in mPFC neurons using the synapsin promoter; eNpHR expression was restricted to VIP interneurons using a Cre-dependent virus in VIP-Cre mice (Methods).

To specifically characterize *network-level* activity patterns, including potential nonlinear interactions between different neurons, we computed the (time-varying) matrix of correlations between signals from different neurons. Using this approach, we divided each dataset into 2.5 sec epochs, calculated the correlation matrix (between GCaMP signals and the derivatives of GCaMP signals) during each epoch, and classified each epoch based on whether the mouse was in the closed or open arms (Fig. 3.4A). This allowed us to determine whether patterns of prefrontal network activity, i.e., correlation matrices, correlate with EPM behavior. Indeed, every pattern of correlations observed during an open arm epoch was more similar to other patterns of correlations

observed during different open arm epochs, than to patterns observed during closed arm epochs (Fig. 3.4B).

We then evaluated how inhibiting VIP interneurons affects this encoding of the open vs. closed arms. Strikingly, *differences* in correlations between the open and closed arms were attenuated when we inhibited VIP interneurons (Fig. 3.4C), consistent with the behavioral effect of such inhibition to attenuate the preference for the closed vs. open arms. Importantly, only the magnitude of *changes* in correlations between the open vs. closed arms was altered by inhibiting VIP interneurons; the magnitude of correlations themselves was not different (p = 1 by sign-rank test). Inhibiting VIP interneurons disrupts network-level representations of the open vs. closed arms by suppressing the tendency for individual GCaMP signals to preferentially rise in either the open or closed arms.

Inhibiting VIP interneurons only reduces open arm avoidance when hippocampal-prefrontal theta synchrony is strong.

Our previous results show that inhibiting prefrontal VIP interneurons weakens mPFC responses to vHPC input, mPFC representations of the open arms, and open arm avoidance. Based on these observations, we hypothesized that VIP interneurons contribute to open arm avoidance by enhancing the transmission of open arm-related information from vHPC to mPFC. Input from the vHPC to mPFC drives mPFC activity, which differentiates between the open vs. closed arms and open arm avoidance (Adhikari et al., 2011; Ciocchi et al., 2015; Padilla-Coreano et al., 2016). Thus, one model is that inhibiting prefrontal VIP interneurons should only affect open arm avoidance when the vHPC actively transmits information to mPFC, i.e., when vHPC-mPFC communication is strong. An alternative is that prefrontal VIP interneurons make the mPFC more sensitive to weak vHPC input, such that inhibiting prefrontal VIP interneurons selectively impacts

63

open arm avoidance when vHPC-mPFC communication is weak. A third possibility is that prefrontal VIP interneurons regulate open arm avoidance independent of vHPC input to mPFC, i.e., inhibiting VIP interneurons decreases open arm avoidance regardless of whether vHPC-mPFC communication is strong vs. weak. These models are schematized in Fig. 3.5A.

To distinguish between these models and test whether the role of VIP interneurons in open arm avoidance depends on the current state of the vHPC-mPFC network, we measured vHPC-mPFC theta synchrony during periods of EPM exploration +/- inhibition of VIP interneurons. Theta-frequency synchronization is a marker for communication between vHPC and mPFC, particularly in anxiety-provoking environments such as the EPM (Adhikari et al., 2010; Jacinto et al., 2016; Padilla-Coreano et al., 2016). We implanted stainless steel electrodes within the vHPC and mPFC of VIP-Arch mice (Fig. 3.5B). In the mPFC, the implanted electrode was attached to one side of a bilateral fiber optic implant to record while stimulating Arch in VIP interneurons using the same location-based method described earlier. First, we tested whether inhibiting VIP interneurons directly alters vHPC-mPFC theta synchrony. For this we separated runs which entered the stimulation zone based on whether they exhibited dips or peaks in vHPC-mPFC theta synchrony at specific timepoints. Specifically, at each timepoint we z-scored vHPC-mPFC theta synchrony relative to the rest of the run. Then we separated runs based on whether this z-scored vHPC-mPFC theta synchrony was in the first (bottom), second, third, or fourth (top) quartile (Supplementary Table 1; Fig. 3.56C). The distribution of runs in each quartile did not differ between the light ON vs. OFF conditions at the time of stim-zone entry (t = 0) or during the next 1.5 seconds (chi-squared test, p = 0.34 and 0.35, respectively). This indicates that real-time inhibition of VIP interneurons does not trigger immediate changes in theta synchrony.

Next, we examined whether inhibiting VIP interneurons increases open arm exploration under all conditions, or only when vHPC-mPFC communication is strong or weak, i.e., when the z-scored theta synchrony is in the top or bottom quartile, respectively. For this we plotted the fraction of runs which avoid vs. explore the open arms as a function of quartile and light ON vs. OFF. When we inhibited VIP interneurons (light ON), we observed a dramatic increase in the fraction of *top quartile* runs (relatively high theta synchrony) that explored the open arms (Fig. 3.5D). In fact, the majority of such runs now explored the open arms. By contrast, there was no significant change in the fraction of runs in the *bottom quartile* – those associated with dips in theta synchrony – which explored the open arms (Fig. 3.5C). We also did not see a significant change in open arm runs for the second or third quartiles of theta synchrony. Thus, inhibiting VIP interneurons only increases open arm exploration when vHPC-mPFC theta synchrony increases, which presumably reflects the transmission of anxiety-related information from vHPC to mPFC. By contrast, when theta synchrony dips (and vHPC-mPFC input is presumably not contributing to open arm avoidance), inhibiting VIP interneurons has no effect on open arm exploration.

DISCUSSION

We have elucidated the role of prefrontal VIP interneurons in a distributed hippocampal-prefrontal network regulating open arm avoidance in the EPM. Prefrontal VIP interneurons not only encode whether mice are in the open/closed arms of the EPM, but more strikingly, predict future open arm exploration vs. avoidance. VIP interneurons receive vHPC input and disinhibit prefrontal responses to that input. Inhibiting VIP neurons disrupts the prefrontal encoding of open vs. closed arms. This specifically increases open arm exploration during periods of high vHPC-mPFC theta synchrony, which indicate the transmission of anxiety signals from vHPC to

mPFC. These observations suggest that prefrontal VIP interneurons normally disinhibit prefrontal responses to vHPC input, thereby helping to generate prefrontal representations of the open vs. closed arms, which contribute to open arm avoidance. Specifically high VIP interneurons activity in the open arms will enhance prefrontal responses to vHPC inputs during open arm exploration, producing patterns of open arm activity distinct from those observed in the closed arms, as seen in our imaging experiments. This is schematized in Fig. 6E.

These results show that VIP interneurons are recruited by, and powerfully modulate, a behavior widely studied because of its presumed relevance to anxiety. In particular, our findings that VIP activity in the EPM does not correlate with running speed, but that VIP activity in a single location (the closed arm) differs based on future behavior (whether mice explore vs. avoid the open arms when they subsequently enter the center), suggests that VIP interneurons encode behavioral state, not just sensorimotor signals. Our findings also show that VIP interneurons disinhibit cortical responses to a particular source of input, are necessary for network-level representations known to depend on that input, and elicit behavioral effects that correlate strongly with changes in these network-level representations. Together, these data connect the actions of VIP interneurons across the cellular, synaptic, microcircuit, and distributed network levels, revealing the details of a mechanism through which they can alter a specific behavior.

There are multiple possible reasons why inhibiting VIP interneurons might decrease open arm avoidance. This manipulation might make mice unable to differentiate the open vs. closed arms, reduce physiological measures of anxiety (e.g., elevated heart rate), or simply cause mice to ignore those anxiety signals as they make decisions about whether to explore vs. avoid. Notably, inhibiting VIP interneurons while mice are exploring the EPM causes an increase in open arm exploration which outlasts the period of inhibition (Fig. 3D). If inhibiting VIP interneurons simply

renders mice unaware of whether they are in the open or closed arms, then it is hard to imagine why this would lead to long-lasting changes in open arm avoidance. Future experiments could address whether inhibiting VIP interneurons reduces physiological measures of anxiety or causes mice to ignore those signals by measuring the effects of inhibiting VIP interneurons on variables such as heart rate. In addition, most of our behavioral experiments (Fig. 1-3) used male mice only. Other behavioral experiments (Fig. 5-6) used male and female mice, but in these cases, group sizes were too small to examine possible sex differences. These could be evaluated by future experiments.

Location-based, but not continuous, inhibition of VIP interneurons disrupts open arm avoidance

Inhibiting VIP interneurons disrupts open arm avoidance when inhibition is delivered selectively within a stimulation zone, but not when delivered continuously throughout a 3-minute epoch. There are many possible explanations for this. First, EPM behavior may be particularly sensitive to changes in avoidance signals, i.e., decisions about whether to explore vs. avoid may depend on the rate at which avoidance signals rise as mice enter the center zone. In this scenario, triggering inhibition as mice approach the center may be especially effective at blunting rises in VIP interneuron activity which normally promote avoidance. Alternatively, continuous inhibition may elicit circuit adaptations which reduce its effectiveness.

Inhibiting VIP interneurons only disrupts open arm avoidance when vHPC-mPFC theta synchrony is high.

The behavioral effects of inhibiting VIP interneurons depended strongly on the level of vHPC-mPFC theta synchrony. When synchrony was relatively high, inhibiting VIP interneurons increased open arm exploration by ~600%. By contrast, when synchrony was relatively low, inhibiting VIP interneurons did not alter open arm exploration. This is consistent with a model in

which VIP interneurons normally contribute to open arm avoidance specifically by enhancing the transmission of strong anxiety-related signals from hippocampus to prefrontal cortex. Theta synchrony is thought to be a biomarker for anxiety-related communication between these structures (Adhikari et al., 2010; Jacinto et al., 2016; Padilla-Coreano et al., 2016). Thus, when theta synchrony is high, a channel for anxiety-related communication between the vHPC and mPFC is effectively "open." Under these conditions, VIP interneurons can enhance prefrontal responses to the anxiety-related input coming from vHPC, thereby promoting open arm avoidance. By contrast, when theta synchrony is low, vHPC input to mPFC is either weak or unrelated to anxiety; under these conditions, the anxiety-related channel from vHPC to mPFC is effectively "closed." As a result, VIP interneurons do not contribute to open arm avoidance, and inhibiting them does not affect EPM behavior. This demonstrates that VIP interneurons do not exert a *network-autonomous* effect on prefrontal circuits, i.e., VIP interneurons do not simply enhance the output of specific set of prefrontal neurons that drive open arm avoidance. VIP interneurons also do not seem to amplify the behavioral effects of weak vHPC input – if they did, then the effects of inhibiting VIP interneurons should have been greatest when vHPC-mPFC theta synchrony is relatively low. Rather, the behavioral effects of inhibiting VIP interneurons are determined by the state of vHPC-mPFC communication, and VIP interneurons seem to specifically enhance the ability of strong hippocampal input to generate avoidance signals in prefrontal circuits.

Interestingly, we found that mice avoid the open arms, even when vHPC-mPFC theta synchrony is low (Fig. 3.5D). Under these conditions, open arm avoidance may be driven by signals which do not depend on vHPC-mPFC communication or mPFC VIP interneurons. Alternatively, when vHPC-mPFC theta synchrony is low, both exploratory and avoidance signals may be weak. As a result, inhibiting prefrontal VIP interneurons might fail to reduce open arm avoidance when

vHPC-mPFC theta synchrony is low, because exploratory signals needed to drive open arm entries are absent.

Finally, the prelimbic (PL) and infralimbic (IL) divisions of the mPFC play different roles in fear conditioning and extinction (Do-Monte, Manzano-Nieves, Quinones-Laracuente, Ramos-Medina, & Quirk, 2015; Sierra-Mercado, Padilla-Coreano, & Quirk, 2010). By contrast, studies that have used the EPM have generally not distinguished between these subregions nor described distinct functions of PL vs. IL in EPM behavior (Adhikari et al., 2010, 2011; Ciocchi et al., 2015; Jacinto et al., 2016; Kjaerby et al., 2016; Padilla-Coreano et al., 2016). We consistently implanted fiber optics near the PL/IL border and thus did not explore potential differences between the roles of PL and IL in EPM behavior, which could be addressed by future studies.

CONCLUSIONS

Previous studies of VIP interneurons have emphasized their role in disinhibition and increasing signal-to-noise at the single neuron level (Ayzenshtat et al., 2016; Fu et al., 2014; Kamigaki & Dan, 2017; Karnani et al., 2016; S. Lee et al., 2013; Pi et al., 2013). These single neuron changes can affect network representations (Ayzenshtat et al., 2016; Kamigaki & Dan, 2017). Here, we reveal two additional features about how VIP interneurons act at the network level to influence behavior (Fig. 6E). First, the degree to which manipulating VIP interneuron activity disrupts network-level representations of behaviorally-relevant information, predicts the extent to which behavior changes as a result of this manipulation ($R2 \sim 0.9$). This is a key piece of evidence that the specific changes in network activity we identified may link changes in VIP interneuron activity with changes in behavior – at the very least, these patterns of network activity represent a highly informative biomarker for changes in behavior. Second, the behavioral effects of inhibiting VIP

interneurons depend critically on the current state of the network. This shows that VIP interneurons do not simply excite or inhibit cells which drive open arm avoidance. Rather, VIP interneurons enable cortical circuits to integrate specific sources of input into emergent network-level representations that guide complex behaviors.

METHODS

Experimental Model and Subject Details

All experiments were conducted in accordance with procedures established by the Administrative Panels on Laboratory Animal Care at the University of California, San Francisco.

The following mouse lines (> 4 wks old) were used for behavior or photometry experiments: Vip<tm1(cre)Zjh>/J (line 010908; www.jax.org), Sst<tm2.1(cre)Zjh>/J (line 013044; www.jax.org), and B6;129P2-Pvalb<tm1(cre)Arbr>/J (line 008069; www.jax.org). Experiments using fiber photometry or optogenetic inhibition only were done with male mice only. For experiments which combined optogenetic inhibition + microendoscopic GCaMP imaging (n = 6 mice) or optogenetic inhibition + multisite LFP recording (n = 4 mice), we used both male and female mice but did not analyze the effects of sex due to the limited group size, which precluded population-level analyses in these experiments.

Behavioral assays

Mice were housed in reversed 12-h light/dark cycles, and all experiments were performed during the dark portion of the cycle. After sufficient time for surgical recovery and viral expression, mice underwent multiple rounds of habituation. The testing room was illuminated at 150 lux, and mice were first habituated to the behavioral testing area for 30 minutes prior to the beginning of any further handling each day. Mice were then habituated to touch with at least 3 days of handling for

~5 min each day, followed by 1-2 days of habituation to the optical tether in their home cage for 10 min. Next, mice were placed into a larger housing cage for 1-2 days for 10 min where they habituated to the tether as they explored the novel environment.

Elevated plus maze: After habituation, behavior was assessed using the elevated plus maze (EPM). EPM sessions lasted 9 minutes, with the laser stimulation delivered during the second three-minute epoch to activate Arch (532nm, 6-8mW total). eYFP-expressing mice served as controls, i.e., they also received continuous 532nm light when in the stimulation zone. Real-time light delivery was based on the location in the EPM apparatus, with the stimulation zones demarcated as the open arms, center zone, and the closed arm zone proximal (within one quarter-length) to the center zone.

Surgery and analysis of LFP experiments

Following virus injection, standard-tip 0.5 MΩ-impedance stainless steel electrodes (Microprobes, SS30030.5A10) were inserted into the mPFC, vHPC, and BLA. For the mPFC location, an optrode (optical fiber + electrode) was custom-made by affixing the electrode to the right optical fiber of a dual-fiber cannula. The tip of the electrode protruded beyond the fiber tip by 200-500μm. The coordinates for vHPC and BLA were as follows: vHPC, -3.25 (AP), 3.1(ML), -4.1 (DV); BLA, -1.34 (AP), 3.12 (ML), -4.74 (DV). A common reference screw was implanted into the cerebellum (500 μm posterior to lambda) and a silver ground wire was placed underneath the left lateral scalp. After affixing the electrodes in place using Metabond, connections were made to the headstage of a multi-channel recording system (Pinnacle). All channels shared a common reference (cerebellum). Data was collected at 2000 Hz and band-pass filtered 1-200Hz at the pre-amp. Electrode placement was verified histologically. We also examined the power spectra from

all electrodes; only animals with vHPC power spectra that exhibited a visible peak in the theta frequency range were used for further analysis. (Note for one mouse, we were not able to verify the localization of the vHPC electrode because the brain was blocked too far rostrally during histology; however, we did not exclude this mouse from analysis because its vHPC electrode exhibited a clear theta peak).

Analysis of LFP data was facilitated using custom MATLAB code. The LFP signals were FIR-filtered (filter length 3x period corresponding to minimum frequency of frequency band) and Hilbert transformed to yield the instantaneous amplitudes (magnitude) and phases (angle). The amplitude covariation between regions in a particular frequency band was calculated by the maximum normalized cross correlation of the instantaneous band-pass filtered amplitudes of each electrode. Amplitude covariation in the theta, beta, and gamma bands was calculated using a 2.5 second window, at 1.5 sec intervals from 7.5 seconds before to 7.5 seconds after the animal entered the stimulation zone of the EPM. For the delta band, amplitude covariation was calculated using a 10 second window (in order to sample a similar number of cycles). Amplitude covariation was individually z-scored for each stim-zone entry, i.e., each run. Each run is an approach to the center starting from a closed arm. A run was defined as an open run if mice proceeded into the open arms and closed run if they either crossed through the center directly to the other closed arm or retreated back into the starting arm. Z-scored amplitude covariation values were classified into quartiles by pooling z-scores from all mice and all conditions.
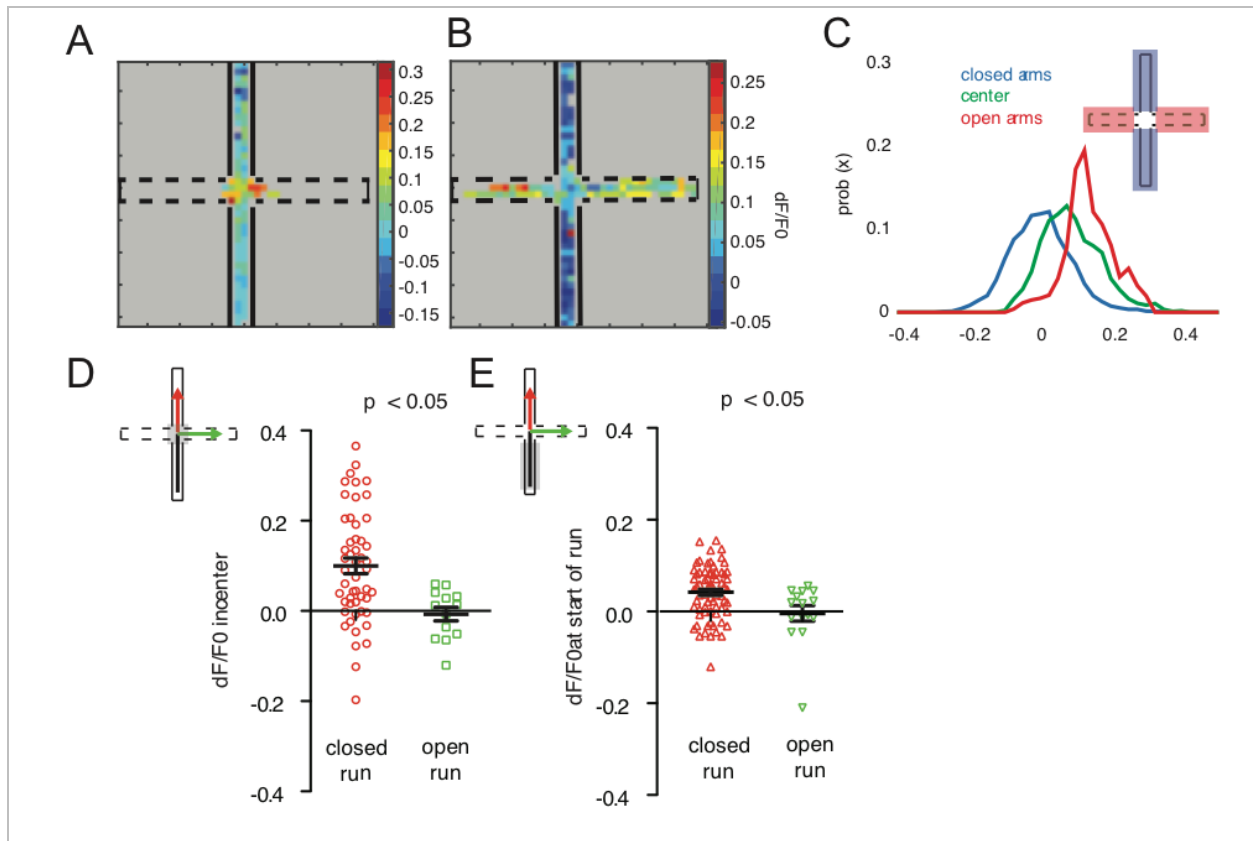
FIGURES

Figure 3.1. Prefrontal VIP neuron activity reflects elevated plus maze behavior and predicts future behavior. (A,B) Heatmaps showing the average GCaMP signal from VIP neurons in two individual mice as a function of EPM location. VIP GCaMP signals were highest in the center for a mouse that did not explore the open arms (A); for a mouse that did explore the open arms, VIP GCaMP signals were highest in the open arms (B). (C) Distributions of VIP-GCaMP signals (dF/F0) in different EPM zones: the closed arms (blue), center zone (green), or open arms (red) (n = 5 mice). (D) Average VIP-GCaMP signals in the center zone were lower just prior to runs into the open arms than before runs into the closed arms (ANOVA using mouse and run type as factors; run type: $F_{1,77}$ = 6.18, p = 0.015; n = 8 mice). (E) Average VIP-GCaMP signals were lower during runs on which mice subsequently entered the open arms compared to those on which mice subsequently entered closed arms (ANOVA using mouse and run type as factors; run type: $F_{1,77}$ = 4.1, p = 0.046; n = 8 mice).
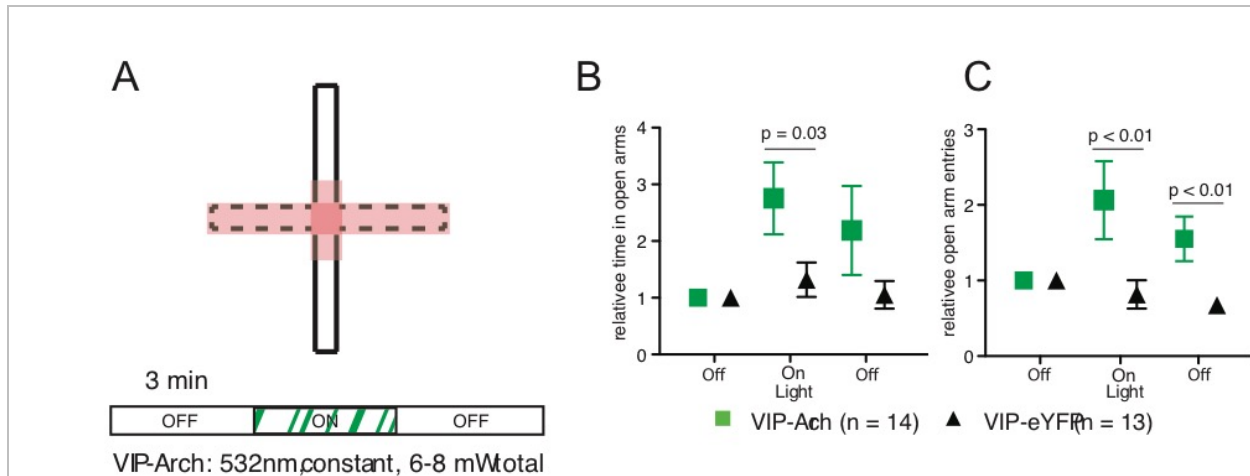
Figure 3.2. Inhibiting prefrontal VIP neurons increases open arm exploration. (A) Protocol for "location based" optogenetic stimulation in the EPM. Stimulation (532nm light to activate Arch) was delivered when the mouse entered the stimulation zone (red) during the second 3-minute epoch of EPM exploration. (B,C) Inhibiting VIP neurons (green) increased relative open arm time (B) and open arm entries (C) compared to control mice (open arm time: Z = 2.16, *p = 0.03, rank-sum test; open arm entries: Z = 2.69, **p < 0.01, rank-sum test). Open arm time and entries were normalized to the first 3-minute epoch of EPM exploration.
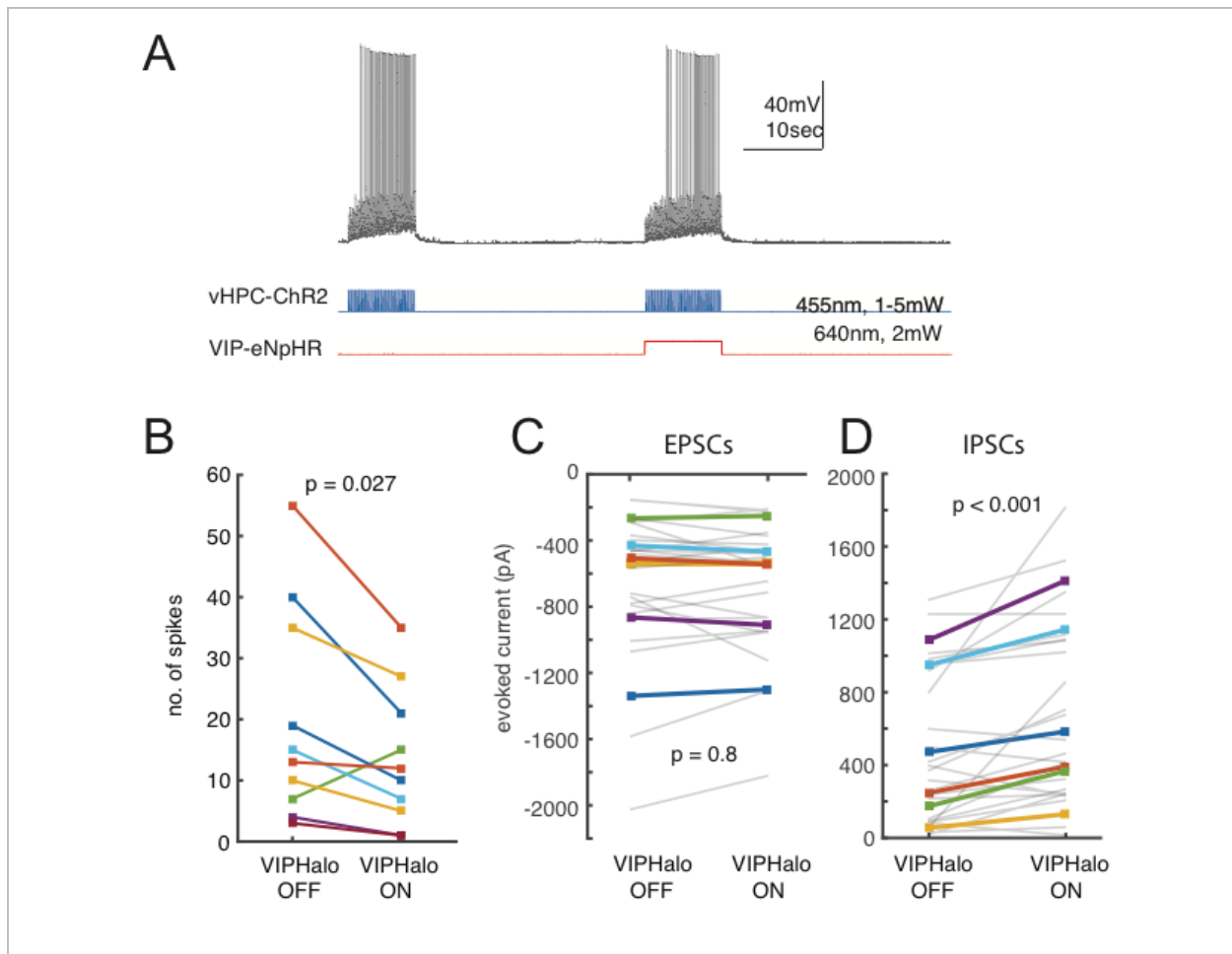
Figure 3.3. VIP interneurons disinhibit prefrontal responses to hippocampal inputs. (A) Experimental design for in vitro patch clamp experiments. We stimulated ChR2 in vHPC terminals at 10Hz +/- 10 sec of concurrent VIP-eNpHR stimulation (constant light, 640nm, 2mW). (B) Inhibiting mPFC VIP interneurons reduced L2/3 pyramidal neuron spiking in response to vHPC terminal stimulation (p = 0.027, n = 10 cells, sign-rank test). (C,D) Inhibiting VIP neurons increased evoked IPSCs (C) but had no effect on evoked EPSCs (D) (p < 0.001 and p = 0.8, respectively, n = 6 cells; ANOVA using cell ID, inhibition, and sweep as factors; $F_{1,38}$ = 13.2). EPSCs and IPSCs were measured by recording peak inward or outward currents in voltage clamp at -70 mV or +10 mV, respectively. Each gray line represents data from a single trace (we recorded three times from each cell), and each colored line represents the average of the three traces from a single cell. The same color indicates the same cell in the left and right panels (different cells were used for panel B and this panel).
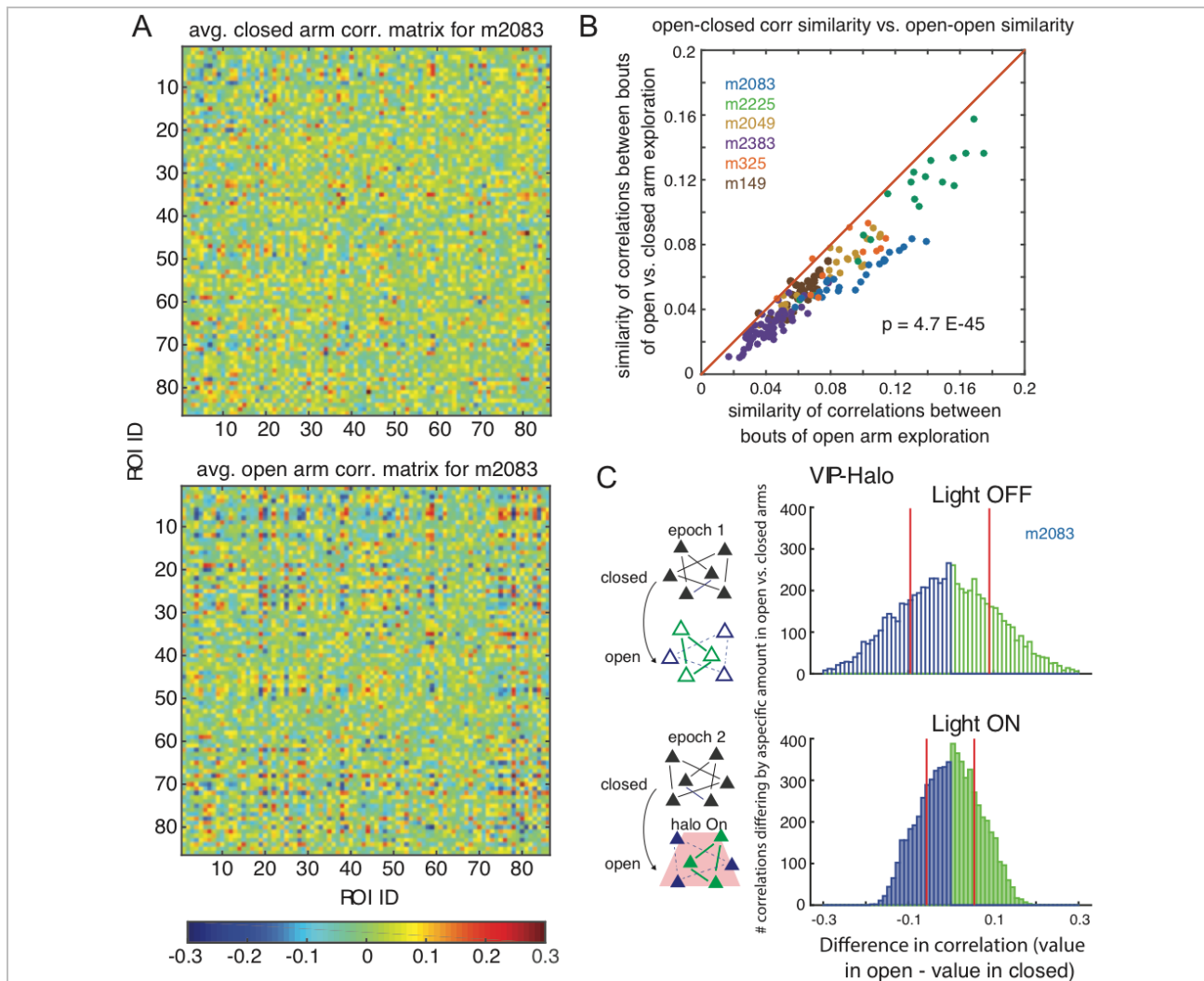
75

Figure 3.4. Inhibiting VIP neurons attenuates anxiety-driven changes in patterns of mPFC microcircuit activity. (A) Averaged correlation matrices representing example patterns of microcircuit activity in the closed vs. open arms. 20 correlation matrices (from one mouse) were averaged for randomly selected times corresponding to closed (top) or open (bottom) arm exploration. (B) Similarity of correlation matrices in open arms to those in the closed arms. For each correlation matrix, based on 2.5 sec of open arm exploration, we computed the similarity between that matrix and other matrices corresponding to exploration of either closed (y-axis) or open (x-axis) arms. Every point falls below the unity line, indicating that all open arm correlation matrices were more similar to other open arm matrices, than to closed arm matrices ($p < 10^{-45}$, paired t-test). Different colors indicate data from different mice (n = 6 mice). (C) The distribution of correlations (from one mouse) which exhibit significant ($p < 0.01$) increases (green) or decreases (blue) between the closed and open arms is shown for the first or second 3 min epoch of EPM exploration (top: first epoch / no VIP interneuron inhibition; bottom: second epoch / VIP interneurons are inhibited in the stim zone). The magnitude of significant changes in correlations between the closed and open arms is reduced during the second epoch, i.e., when VIP interneurons are inhibited. For each epoch, red vertical lines indicate the mean magnitude of significant increases or decreases in correlations.
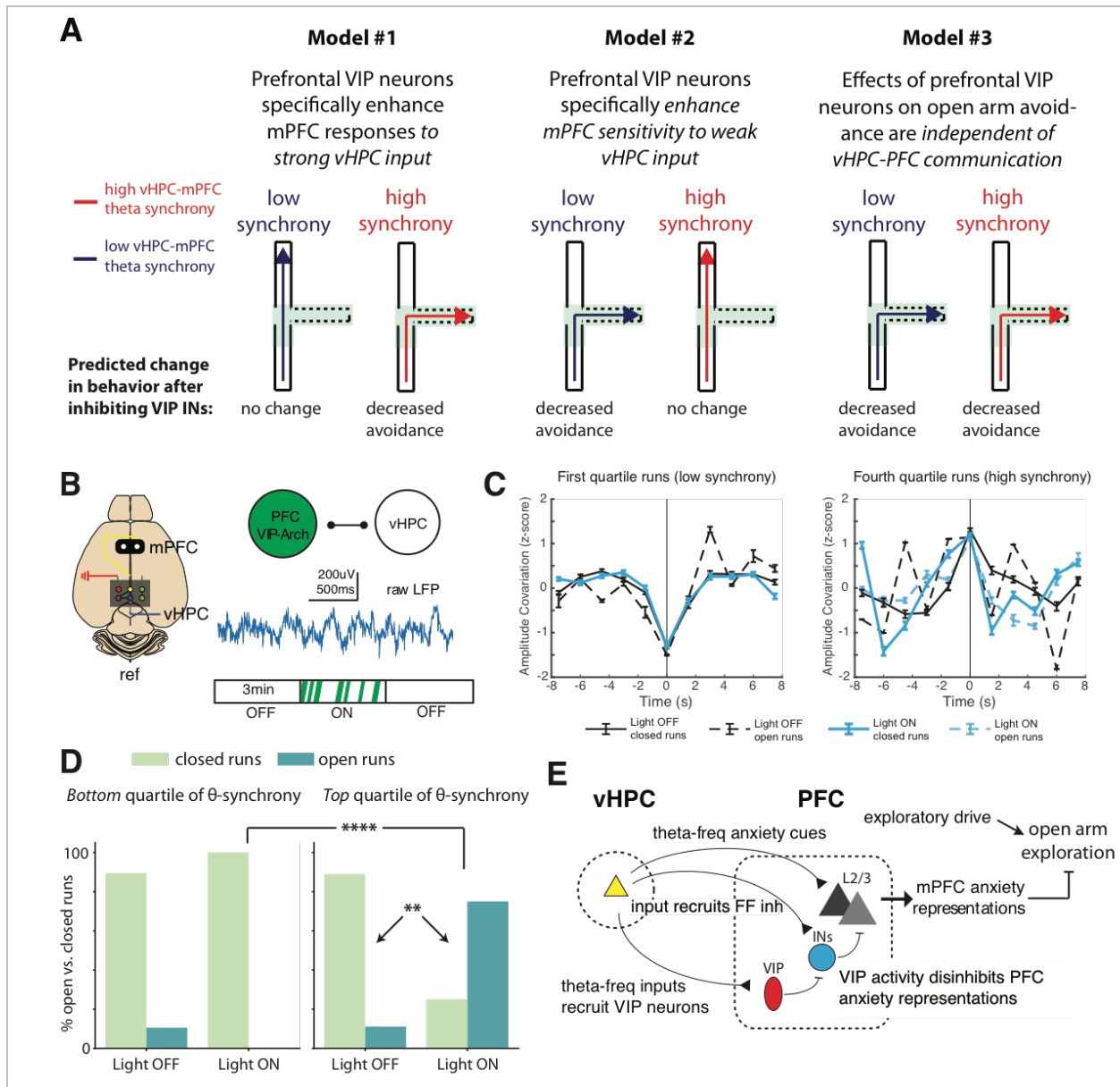
Figure 3.5. Inhibiting prefrontal VIP neurons selectively enhances open arm exploration when hippocampal-prefrontal theta-synchrony is relatively high. (A) Schematic: different models for how the effect of inhibiting VIP interneurons (decreased open arm avoidance) might depend on the current state of the vHPC-mPFC network. Blue and red trajectories represent behavior when vHPC-mPFC theta synchrony is low or high, respectively, corresponding to periods of weak vs. strong vHPC-mPFC communication. Trajectories enter the center compartment of the EPM, then either avoid the open arms (dotted lines) and return to a closed compartment (solid lines), indicating no change in normal avoidance behavior, or explore the open arms, indicating decreased avoidance. (B) Experimental design. Local field potentials were recorded from electrodes in mPFC and vHPC of VIP-Arch mice implanted with bilateral mPFC optical fibers during the real-time EPM optogenetic assay. (C) For mice expressing Arch in

mPFC VIP interneurons (n = 4), we identified runs into the stimulation zone for which the vHPC-mPFC synchrony (amplitude covariation) as mice entered the stim-zone (z-scored relative to the rest of the run, i.e., +/- 7.5 sec from stim-zone entry) was either low (left) or high (right), i.e., in the bottom or top quartile at t=0 (time of stim-zone entry), respectively. Amplitude was calculated from the theta-filtered LFP signal. (D) For runs in each quartile (left: low theta synchrony, right: high theta synchrony), we computed the fraction which either avoided the open arms ("closed" runs, light green bars) or explored the open arms ("open" runs, teal bars). We performed this analysis separately for periods during which no light was delivered ("OFF") and periods during which light (to trigger optogenetic inhibition) was selectively delivered in the stimulation zone ("ON"). When light is ON, the proportion of trials with relatively high synchrony at the time of stim-zone entry which explore the open arms is significantly increased, selectively for high synchrony trials ($\chi2$ test; p = 0.008 for the number of open vs. closed runs during high synchrony trials with light ON vs. OFF; p = 0.0006 for the number of open vs. closed arm runs for high vs. low synchrony trials with light ON). ** p < 0.01, **** p < 0.0001. (E) Schematic: When vHPC-mPFC theta synchrony is high, theta-frequency vHPC input recruits prefrontal VIP interneuron-mediated disinhibition, enhancing prefrontal anxiety representations. (The blue circle represents non-VIP interneurons in mPFC). These prefrontal anxiety representations inhibit open arm exploration. Inhibiting prefrontal VIP interneurons would increased feedforward inhibition, disrupting the ability of vHPC input to drive prefrontal anxiety representations which normally inhibit open arm exploration. The net effect would be to increase open arm exploration during periods when such exploration is normally prevented by hippocampal-prefrontal communication

References

Adhikari, A., Topiwala, M. A., & Gordon, J. A. (2010). Synchronized Activity between the Ventral Hippocampus and the Medial Prefrontal Cortex during Anxiety. *Neuron*, *65*(2), 257–269. https://doi.org/10.1016/j.neuron.2009.12.002

Adhikari, A., Topiwala, M. A., & Gordon, J. A. (2011). Single units in the medial prefrontal cortex with anxiety-related firing patterns are preferentially influenced by ventral hippocampal activity. *Neuron*, *71*(5), 898–910. https://doi.org/10.1016/j.neuron.2011.07.027

Alitto, H. J., & Dan, Y. (2012). Cell-type-specific modulation of neocortical activity by basal forebrain input. *Frontiers in Systems Neuroscience*.

Andreescu, C., Sheu, L. K., Tudorascu, D., Walker, S., & Aizenstein, H. (2014). The ages of anxiety-differences across the lifespan in the default mode network functional connectivity in generalized anxiety disorder. *International Journal of Geriatric Psychiatry*, *29*(7), 704–712. https://doi.org/10.1002/gps.4051

Angoa-Pérez, M., Kane, M. J., Briggs, D. I., Francescutti, D. M., & Kuhn, D. M. (2013). Marble burying and nestlet shredding as tests of repetitive, compulsive-like behaviors in mice. *Journal of Visualized Experiments : JoVE*, (82), 50978. https://doi.org/10.3791/50978

Ayzenshtat, I., Karnani, M. M., Jackson, J., & Yuste, R. (2016). Cortical Control of Spatial Resolution by {VIP} $\mathplus$ Interneurons. *The Journal of Neuroscience*, *36*(45), 11498–11509. https://doi.org/10.1523/jneurosci.1920-16.2016

Bassell, G. J., & Warren, S. T. (2008). *Fragile X syndrome: loss of local {mRNA} regulation alters synaptic development and function.* *60*(2), 201–214. https://doi.org/10.1016/j.neuron.2008.10.004

Batista-Brito, R., Vinck, M., Ferguson, K. A., Laubender, D., Lur, G., Higley, M. J., & Cardin, J. A. (2016). *Developmental Dysfunction of {VIP} Interneurons Impairs Cortical Circuits.* https://doi.org/10.1101/077891

Bourgeron, T. (2015, August 20). From the genetic architecture to synaptic plasticity in autism spectrum disorder. *Nature Reviews Neuroscience*, Vol. 16, pp. 551–563. https://doi.org/10.1038/nrn3992

Bromley, R. L., Mawer, G. E., Briggs, M., & Cheyne, C. (2013). The prevalence of neurodevelopmental disorders in children prenatally exposed to antiepileptic drugs. *Journal of Neurology*. https://doi.org/10.1136/jnnp-2012-304270

Brown, D. A. (2010). Muscarinic acetylcholine receptors {(mAChRs)} in the nervous system: some functions and mechanisms. *J. Mol. Neurosci.*, *41*(3), 340–346. https://doi.org/10.1007/s12031-010-9377-2

Buard, I., Rogers, S. J., Hepburn, S., Kronberg, E., & Rojas, D. C. (2013). Altered oscillation patterns and connectivity during picture naming in autism. *Frontiers in Human Neuroscience*, (NOV). https://doi.org/10.3389/fnhum.2013.00742

Buzsáki, G., Anastassiou, C. A., & Koch, C. (2012, June). The origin of extracellular fields and currents-EEG, ECoG, LFP and spikes. *Nature Reviews Neuroscience*, Vol. 13, pp. 407–420. https://doi.org/10.1038/nrn3241

Calhoon, G. G., & Tye, K. M. (2015). Resolving the neural circuits of anxiety. *Nature Neuroscience*, *18*(10), 1394–1404. https://doi.org/10.1038/nn.4101

Cho, K. K. A., Hoch, R., Lee, A. T., Patel, T., Rubenstein, J. L. R., & Sohal, V. S. (2015). Gamma rhythms link prefrontal interneuron dysfunction with cognitive inflexibility in dlx5/6+/- mice. *Neuron*, *85*(6), 1332–1343. https://doi.org/10.1016/j.neuron.2015.02.019

Christophe, E., Roebuck, A., Staiger, J. F., Lavery, D. J., Charpak, S., & Audinat, E. (2002). Two types of nicotinic receptors mediate an excitation of neocortical layer I interneurons. *J. Neurophysiol.*, *88*(3), 1318–1327.

Ciocchi, S., Passecker, J., Malagon-Vina, H., Mikus, N., & Klausberger, T. (2015). Selective information routing by ventral hippocampal {CA}1 projection neurons. *Science*, *348*(6234), 560–563. https://doi.org/10.1126/science.aaa3245

Coben, R., Mohammad-Rezazadeh, I., & Cannon, R. L. (2014). Using quantitative and analytic EEG methods in the understanding of connectivity in autism spectrum disorders: A theory of mixed over- and under-connectivity. *Frontiers in Human Neuroscience*, *8*(1 FEB). https://doi.org/10.3389/fnhum.2014.00045

Cotney, J., Muhle, R. A., Sanders, S. J., Liu, L., Willsey, A. J., Niu, W., … Noonan, J. P. (2015). The autism-associated chromatin modifier CHD8 regulates other autism risk genes during human neurodevelopment. *Nature Communications*, *6*. https://doi.org/10.1038/ncomms7404

Cui, G., Jun, S. B., Jin, X., Pham, M. D., Vogel, S. S., Lovinger, D. M., & Costa, R. M. (2013). Concurrent activation of striatal direct and indirect pathways during action initiation. *Nature*, *494*(7436), 238–242. https://doi.org/10.1038/nature11846

Dani, J. A., & Bertrand, D. (2007). Nicotinic acetylcholine receptors and nicotinic cholinergic mechanisms of the central nervous system. *Annu. Rev. Pharmacol. Toxicol.* https://doi.org/10.1146/annurev.pharmtox.47.120505.105214

De Rubeis, S., He, X., Goldberg, A. P., Poultney, C. S., Samocha, K., Cicek, A. E., … Buxbaum, J. D. (2014). Synaptic, transcriptional and chromatin genes disrupted in autism. *Nature*, *515*(7526), 209–215. https://doi.org/10.1038/nature13772

Deng, P.-Y. Y., Rotman, Z., Blundon, J. A., Cho, Y., Cui, J., Cavalli, V., … Klyachko, V. A. (2013).

{FMRP} regulates neurotransmitter release and synaptic information transmission by modulating action potential duration via {BK} channels. *Neuron*, *77*(4), 696–711. https://doi.org/10.1016/j.neuron.2012.12.018

Dentici, M. L., Niceta, M., Pantaleoni, F., Barresi, S., Bencivenga, P., Dallapiccola, B., … Tartaglia, M. (2017). Expanding the phenotypic spectrum of truncating POGZ mutations: Association with CNS malformations, skeletal abnormalities, and distinctive facial dysmorphism. *American Journal of Medical Genetics, Part A*, *173*(7), 1965–1969. https://doi.org/10.1002/ajmg.a.38255

Devlin, B., Boone, B. E., Levy, S. E., Lihm, J., Buxbaum, J. D., Wu, Y., … Daly, M. J. (2012, May 10). Patterns and rates of exonic de novo mutations in autism spectrum disorders. *Nature*, Vol. 485, pp. 242–246. https://doi.org/10.1038/nature11011

Do-Monte, F. H., Manzano-Nieves, G., Quinones-Laracuente, K., Ramos-Medina, L., & Quirk, G. J. (2015). Revisiting the Role of Infralimbic Cortex in Fear Extinction with Optogenetics. *Journal of Neuroscience*, *35*(8), 3607–3615. https://doi.org/10.1523/jneurosci.3137-14.2015

Ellwood, I. T., Patel, T., Wadia, V., Lee, A. T., Liptak, A. T., Bender, K. J., & Sohal, V. S. (2017). Tonic or phasic stimulation of dopaminergic projections to prefrontal cortex causes mice to maintain or deviate from previously learned behavioral strategies. *Journal of Neuroscience*, *37*(35), 8315–8329. https://doi.org/10.1523/JNEUROSCI.1221-17.2017

F, D.-B., & Wonnacott, S. (2004). Nicotinic acetylcholine receptors and the regulation of neuronal signalling. *Trends in Pharmacological Sciences*. https://doi.org/10.1016/j.tips.2004.04.006

Fitzgerald, T. W., Gerety, S. S., Jones, W. D., Van Kogelenberg, M., King, D. A., McRae, J., … Hurles, M. E. (2015, March 12). Large-scale discovery of novel genetic causes of developmental disorders. *Nature*, Vol. 519, pp. 223–228. https://doi.org/10.1038/nature14135

Fromer, M., Pocklington, A. J., Kavanagh, D. H., Williams, H. J., Dwyer, S., Gormley, P., … O'Donovan, M. C. (2014). De novo mutations in schizophrenia implicate synaptic networks. *Nature*, *506*(7487), 179–184. https://doi.org/10.1038/nature12929

Fu, Y., Kaneko, M., Tang, Y., Arturo, A.-B., & Stryker, M. P. (2015). A cortical disinhibitory circuit for enhancing adult plasticity. *Elife*, *4*, e05558. https://doi.org/10.7554/eLife.05558

Fu, Y., Tucciarone, J. M., Espinosa, J. S., Sheng, N., Darcy, D. P., Nicoll, R. A., … Stryker, M. P. (2014). A cortical circuit for gain control by behavioral state. *Cell*, *156*(6), 1139–1152. https://doi.org/10.1016/j.cell.2014.01.050

Fukai, R., Hiraki, Y., Yofune, H., Tsurusaki, Y., Nakashima, M., Saitsu, H., … Matsumoto, N. (2015). A case of autism spectrum disorder arising from a de novo missense mutation in POGZ. *Journal of Human Genetics*, *60*(5), 277–279. https://doi.org/10.1038/jhg.2015.13

Garcia-Junco-Clemente, P., Ikrar, T., Tring, E., Xu, X., Ringach, D. L., & Trachtenberg, J. T. (2017). An inhibitory pull{\textendash}push circuit in frontal cortex. *Nature Neuroscience*, *20*(3), 389–392. https://doi.org/10.1038/nn.4483

Gil, Z., Connors, B. W., & Amitai, Y. (1997). Differential regulation of neocortical synapses by neuromodulators and activity. *Neuron*, *19*(3), 679–686. https://doi.org/10.1016/S0896-6273(00)80380-3

Gilissen, C., Hehir-Kwa, J. Y., Thung, D. T., Van De Vorst, M., Van Bon, B. W. M., Willemsen, M. H., … Veltman, J. A. (2014). Genome sequencing identifies major causes of severe intellectual disability. *Nature*, *511*(7509), 344–347. https://doi.org/10.1038/nature13394

Gogolla, N., Takesian, A. E., Feng, G., Fagiolini, M., & Hensch, T. K. (2014). Sensory Integration in Mouse Insular Cortex Reflects GABA Circuit Maturation. *Neuron*, *83*(4), 894–905. https://doi.org/10.1016/j.neuron.2014.06.033

Gotti, C, Moretti, M., Gaimarri, A., & Zanardi, A. (2007). Heterogeneity and complexity of native brain nicotinic receptors. *Biochemical ....* https://doi.org/10.1016/j.bcp.2007.05.023

Gotti, Cecilia, Clementi, F., Fornari, A., Gaimarri, A., Guiducci, S., Manfredi, I., ... Zoli, M. (2009). *Structural and functional diversity of native brain neuronal nicotinic receptors. 78*(7), 703–711. https://doi.org/10.1016/j.bcp.2009.05.024

Guglielmi, L., Servettini, I., Caramia, M., Catacuzzeno, L., Franciolini, F., Maria, D., & Pessia, M. (2015). *Update on the implication of potassium channels in autism: K+ channelautism spectrum disorder. 9.* https://doi.org/10.3389/fncel.2015.00034

Gulsuner, S., Walsh, T., Watts, A. C., Lee, M. K., Thornton, A. M., Casadei, S., ... McClellan, J. M. (2013). XSpatial and temporal mapping of de novo mutations in schizophrenia to a fetal prefrontal cortical network. *Cell, 154*(3). https://doi.org/10.1016/j.cell.2013.06.049

Gunaydin, L., Grosenick, L., Finkelstein, J., Kauvar, I., Fenno, L., Adhikari, A., ... Deisseroth, K. (2014). Natural Neural Projection Dynamics Underlying Social Behavior. *Cell, 157*(7), 1535–1551. https://doi.org/10.1016/j.cell.2014.05.017

Guo, W., Liu, F., Xiao, C., Liu, J., Yu, M., Zhang, Z., ... Zhao, J. (2014). Increased short-range and long-range functional connectivity in first-episode, medication-naive schizophrenia at rest. *Schizophrenia Research, 166*(1–3), 144–150. https://doi.org/10.1016/j.schres.2015.04.034

Han, S., Tai, C., Jones, C. J., Scheuer, T., & Catterall, W. A. (2014). Enhancement of inhibitory neurotransmission by GABAA receptors having α2,3-subunits ameliorates behavioral deficits in a mouse model of autism. *Neuron, 81*(6), 1282–1289. https://doi.org/10.1016/j.neuron.2014.01.016

Han, S., Tai, C., Westenbroek, R. E., Yu, F. H., Cheah, C. S., Potter, G. B., ... Catterall, W. A. (2012). Autistic-like behaviour in Scn1a +- mice and rescue by enhanced GABA-mediated

neurotransmission. *Nature*, *489*(7416), 385–390. https://doi.org/10.1038/nature11356

Hashimoto, R., Nakazawa, T., Tsurusaki, Y., Yasuda, Y., Nagayasu, K., Matsumura, K., … Hashimoto, H. (2016). Whole-exome sequencing and neurite outgrowth analysis in autism spectrum disorder. *Journal of Human Genetics*, *61*(3), 199–206. https://doi.org/10.1038/jhg.2015.141

Hasselmo, M. E., & Sarter, M. (2011). Modes and models of forebrain cholinergic neuromodulation of cognition. *Neuropsychopharmacology*, *36*(1), 52–73. https://doi.org/10.1038/npp.2010.104

Hultman, R., Mague, S. D., Li, Q., Katz, B. M., Michel, N., Lin, L., … Dzirasa, K. (2016). Dysregulation of Prefrontal Cortex-Mediated Slow-Evolving Limbic Dynamics Drives Stress-Induced Emotional Pathology. *Neuron*, *91*(2), 439–452. https://doi.org/10.1016/j.neuron.2016.05.038

Hultman, R., Ulrich, K., Sachs, B. D., Blount, C., Carlson, D. E., Ndubuizu, N., … Dzirasa, K. (2018). Brain-wide Electrical Spatiotemporal Dynamics Encode Depression Vulnerability. *Cell*, *173*(1), 166-180.e14. https://doi.org/10.1016/j.cell.2018.02.012

Hyvärinen, A., & Oja, E. (2000). Independent component analysis: Algorithms and applications. *Neural Networks*, *13*(4–5), 411–430. https://doi.org/10.1016/S0893-6080(00)00026-5

Iossifov, I., O'Roak, B. J., Sanders, S. J., Ronemus, M., Krumm, N., Levy, D., … Wigler, M. (2014). The contribution of de novo coding mutations to autism spectrum disorder. *Nature*, *515*(7526), 216–221. https://doi.org/10.1038/nature13908

Iossifov, I., Ronemus, M., Levy, D., Wang, Z., Hakker, I., Rosenbaum, J., … Wigler, M. (2012). De Novo Gene Disruptions in Children on the Autistic Spectrum. *Neuron*, *74*(2), 285–299. https://doi.org/10.1016/j.neuron.2012.04.009

Jacinto, L. R., Cerqueira, J. J., & Sousa, N. (2016). Patterns of Theta Activity in Limbic Anxiety Circuit Preceding Exploratory Behavior in Approach-Avoidance Conflict. *Frontiers in Behavioral Neuroscience*, *10*. https://doi.org/10.3389/fnbeh.2016.00171

Jung, E. M., Moffat, J. J., Liu, J., Dravid, S. M., Gurumurthy, C. B., & Kim, W. Y. (2017). Arid1b haploinsufficiency disrupts cortical interneuron development and mouse behavior. *Nature Neuroscience*, *20*(12), 1694–1707. https://doi.org/10.1038/s41593-017-0013-0

Just, M. A., Cherkassky, V. L., Keller, T. A., & Minshew, N. J. (2004). Cortical activation and synchronization during sentence comprehension in high-functioning autism: Evidence of underconnectivity. *Brain*, *127*(8), 1811–1821. https://doi.org/10.1093/brain/awh199

Just, M. A., Keller, T. A., Malave, V. L., Kana, R. K., & Varma, S. (2012). Autism as a neural systems disorder: A theory of frontal-posterior underconnectivity. *Neuroscience and Biobehavioral Reviews*, *36*(4), 1292–1313. https://doi.org/10.1016/j.neubiorev.2012.02.007

Kam, J. W. Y., Bolbecker, A. R., O'Donnell, B. F., Hetrick, W. P., & Brenner, C. A. (2013). Resting state EEG power and coherence abnormalities in bipolar disorder and schizophrenia. *Journal of Psychiatric Research*, *47*(12), 1893–1901. https://doi.org/10.1016/j.jpsychires.2013.09.009

Kamigaki, T., & Dan, Y. (2017). Delay activity of specific prefrontal interneuron subtypes modulates memory-guided behavior. *Nature Neuroscience*, *20*(6), 854–863. https://doi.org/10.1038/nn.4554

Kana, R. K., Uddin, L. Q., Kenet, T., Chugani, D., & Müller, R. A. (2014, June 2). Brain connectivity in autism. *Frontiers in Human Neuroscience*, *8*(JUNE). https://doi.org/10.3389/fnhum.2014.00349

Karnani, M. M., Jackson, J., Ayzenshtat, I., Sichani, A., Manoocheri, K., Kim, S., & Yuste, R. (2016). Opening Holes in the Blanket of Inhibition: Localized Lateral Disinhibition by {VIP}

Interneurons. *J Neurosci*, *36*(12), 3471–3480. https://doi.org/10.1523/JNEUROSCI.3646-15.2016

Karvat, G., & Kimchi, T. (2013). Acetylcholine Elevation Relieves Cognitive Rigidity and Social Deficiency in a Mouse Model of Autism. *Neuropsychopharmacology*, *39*(4), 831–840. https://doi.org/10.1038/npp.2013.274

Keehn, B., Wagner, J. B., Tager-Flusberg, H., & Nelson, C. A. (2013). Functional connectivity in the first year of life in infants at-risk for autism: a preliminary near-infrared spectroscopy study. *Frontiers in Human Neuroscience*, *7*. https://doi.org/10.3389/fnhum.2013.00444

Kern, J. K. (2006). The pattern of sensory processing abnormalities in autism. *Autism*, *10*(5), 480–494. https://doi.org/10.1177/1362361306066564

Khoshkhoo, S., Vogt, D., & Sohal, V. S. (2017). Dynamic, Cell-Type-Specific Roles for {GABAergic} Interneurons in a Mouse Model of Optogenetically Inducible Seizures. *Neuron*, *93*(2), 291–298. https://doi.org/10.1016/j.neuron.2016.11.043

Kirkby, L. A., Luongo, F. J., Lee, M. B., Nahum, M., Van Vleet, T. M., Rao, V. R., … Sohal, V. S. (2018). An Amygdala-Hippocampus Subnetwork that Encodes Variation in Human Mood. *Cell*, *175*(6), 1688-1700.e14. https://doi.org/10.1016/j.cell.2018.10.005

Kjaerby, C., Athilingam, J., Robinson, S. E., Iafrati, J., & Sohal, V. S. (2016). Serotonin 1B Receptors Regulate Prefrontal Function by Gating Callosal and Hippocampal Inputs. *Cell Reports*, *17*(11), 2882–2890. https://doi.org/10.1016/j.celrep.2016.11.036

Kjelstrup, K. G., Tuvnes, F. A., Steffenach, H. A., Murison, R., Moser, E. I., & Moser, M. B. (2002). Reduced fear expression after lesions of the ventral hippocampus. *Proceedings of the National Academy of Sciences of the United States of America*, *99*(16), 10825–10830. https://doi.org/10.1073/pnas.152112399

Krumm, N., O'Roak, B. J., Shendure, J., & Eichler, E. E. (2014, February). A de novo convergence of autism genetics and molecular neuroscience. *Trends in Neurosciences*, Vol. 37, pp. 95–105. https://doi.org/10.1016/j.tins.2013.11.005

Lee, A. T., Cunniff, M. M., See, J. Z., Wilke, S. A., Luongo, F. J., Ellwood, I. T., … Sohal, V. S. (2019). VIP Interneurons Contribute to Avoidance Behavior by Regulating Information Flow across Hippocampal-Prefrontal Networks. *Neuron*, *102*(6), 1223-1234.e4. https://doi.org/10.1016/j.neuron.2019.04.001

Lee, S., Kruglikov, I., Huang, Z. J., Fishell, G., & Rudy, B. (2013). A disinhibitory circuit mediates motor integration in the somatosensory cortex. *Nature Neuroscience*. https://doi.org/10.1038/nn.3544

Letzkus, J. J., Wolff, S. B., Meyer, E. M. M., Tovote, P., Courtin, J., Herry, C., & Lüthi, A. (2011). A disinhibitory microcircuit for associative fear learning in the auditory cortex. *Nature*, *480*(7377), 331–335. https://doi.org/10.1038/nature10674

Lopes-dos-Santos, V., Ribeiro, S., & Tort, A. B. L. (2013, November 15). Detecting cell assemblies in large neuronal populations. *Journal of Neuroscience Methods*, Vol. 220, pp. 149–166. https://doi.org/10.1016/j.jneumeth.2013.04.010

Luongo, F., Horn, M., & Sohal, V. S. (2015). *Putative microcircuit-level substrates for attention are disrupted in mouse models of autism.* https://doi.org/10.1016/j.biopsych.2015.04.014

Luongo, F. J., Horn, M. E., & Sohal, V. S. (2016). Putative microcircuit-level substrates for attention are disrupted in mouse models of autism. *Biological Psychiatry*, *79*(8), 667–675. https://doi.org/10.1016/j.biopsych.2015.04.014

M, M. S., Neal, S. J., Lin, Q., Hughes, Z. A., & Smith, D. G. (2013). The {BTBR} Mouse Model of Autism Spectrum Disorders Has Learning and Attentional Impairments and Alterations in

Acetylcholine and Kynurenic Acid in Prefrontal Cortex. *{PLoS} {ONE}*, *8*(4), e62189. https://doi.org/10.1371/journal.pone.0062189

Matsumura, K., Nakazawa, T., Nagayasu, K., Gotoda-Nishimura, N., Kasai, A., Hayata-Takano, A., … Hashimoto, H. (2016). De novo POGZ mutations in sporadic autism disrupt the DNA-binding activity of POGZ. *Journal of Molecular Psychiatry*, *4*(1), 1. https://doi.org/10.1186/s40303-016-0016-x

Mueller, S., Keeser, D., Samson, A. C., Kirsch, V., Blautzik, J., Grothe, M., … Meindl, T. (2013). Convergent Findings of Altered Functional and Structural Brain Connectivity in Individuals with High Functioning Autism: A Multimodal MRI Study. *PLoS ONE*, *8*(6), e67329. https://doi.org/10.1371/journal.pone.0067329

Müller, R.-A., Shih, P., Keehn, B., Deyoe, J. R., Leyden, K. M., & Shukla, D. K. (2011). Underconnected, but How? A Survey of Functional Connectivity MRI Studies in Autism Spectrum Disorders. *Cerebral Cortex*, *21*(10), 2233–2243. https://doi.org/10.1093/cercor/bhq296

Mullins, C., Fishell, G., & Tsien, R. W. (2016, March 16). Unifying Views of Autism Spectrum Disorders: A Consideration of Autoregulatory Feedback Loops. *Neuron*, Vol. 89, pp. 1131–1156. https://doi.org/10.1016/j.neuron.2016.02.017

Nair, A., Treiber, J. M., Shukla, D. K., Shih, P., & Müller, R.-A. (2013). Impaired thalamocortical connectivity in autism spectrum disorder: a study of functional and anatomical connectivity. *Brain*, *136*(6), 1942–1955. https://doi.org/10.1093/brain/awt079

Nelson, S. B., & Valakh, V. (2015, August 19). Excitatory/Inhibitory Balance and Circuit Homeostasis in Autism Spectrum Disorders. *Neuron*, Vol. 87, pp. 684–698. https://doi.org/10.1016/j.neuron.2015.07.033

Nozawa, R. S., Nagao, K., Masuda, H. T., Iwasaki, O., Hirota, T., Nozaki, N., … Obuse, C. (2010). Human POGZ modulates dissociation of HP1α from mitotic chromosome arms through Aurora B activation. *Nature Cell Biology*, *12*(7), 719–727. https://doi.org/10.1038/ncb2075

Padilla-Coreano, N., Bolkan, S. S., Pierce, G. M., Blackman, D. R., Hardin, W. D., Garcia-Garcia, A. L., … Gordon, J. A. (2016). Direct Ventral Hippocampal-Prefrontal Input Is Required for Anxiety-Related Neural Activity and Behavior. *Neuron*, *89*(4), 857–866. https://doi.org/10.1016/j.neuron.2016.01.011

Padilla-Coreano, N., Canetta, S., Mikofsky, R. M., Alway, E., Passecker, J., Myroshnychenko, M. V., … Gordon, J. A. (2019). Hippocampal-Prefrontal Theta Transmission Regulates Avoidance Behavior. *Neuron*. https://doi.org/10.1016/j.neuron.2019.08.006

Padmanabhan, A., Lynn, A., Foran, W., Luna, B., & O'Hearn, K. (2013). Age related changes in striatal resting state functional connectivity in autism. *Frontiers in Human Neuroscience*, *7*. https://doi.org/10.3389/fnhum.2013.00814

Parent, M. A., Wang, L., Su, J., Netoff, T., & Yuan, L. L. (2010). Identification of the hippocampal input to medial prefrontal cortex in vitro. *Cerebral Cortex*, *20*(2), 393–403. https://doi.org/10.1093/cercor/bhp108

Parikh, V., Kozak, R., Martinez, V., & Sarter, M. (2007). Prefrontal acetylcholine release controls cue detection on multiple timescales. *Neuron*.

Perry, E. K., Lee, M. L., CM, M.-R., Court, J. A., Volsen, S. G., Merrit, J., … Wenk, G. L. (2001). Cholinergic activity in autism: abnormalities in the cerebral cortex and basal forebrain. *Am J Psychiatry*, *158*(7), 1058–1066. https://doi.org/10.1176/appi.ajp.158.7.1058

Petreanu, L., Mao, T., Sternson, S. M., & Svoboda, K. (2009). The subcellular organization of neocortical excitatory connections. *Nature*, *457*(7233), 1142–1145.

https://doi.org/10.1038/nature07709

Pfeffer, C. K., Xue, M., He, M., Huang, Z. J., & Scanziani, M. (2013). Inhibition of inhibition in visual cortex: the logic of connections between molecularly distinct interneurons. *Nature Neuroscience.* https://doi.org/10.1038/nn.3446

Pi, H.-J. J., Hangya, B., Kvitsiani, D., Sanders, J. I., Huang, Z. J., & Kepecs, A. (2013). Cortical interneurons that specialize in disinhibitory control. *Nature*, *503*(7477), 521–524. https://doi.org/10.1038/nature12676

Picciotto, M. R., Addy, N. A., Mineur, Y. S., & Brunzell, D. H. (2008). It is not "either/or": activation and desensitization of nicotinic acetylcholine receptors both contribute to behaviors related to nicotine addiction and mood. *Progress in Neurobiology.* https://doi.org/10.1016/j.pneurobio.2007.12.005

Porter, J. T., Cauli, B., Staiger, J. F., Lambolez, B., Rossier, J., & Audinat, E. (1998). *Properties of bipolar {VIPergic} interneurons and their excitation by pyramidal neurons in the rat neocortex.* *10*(12), 3617–3628. https://doi.org/10.1046/j.1460-9568.1998.00367.x

Potter, G. B., Petryniak, M. A., Shevchenko, E., McKinsey, G. L., Ekker, M., & Rubenstein, J. L. R. (2009). Generation of Cre-transgenic mice using Dlx1/Dlx2 enhancers and their characterization in GABAergic interneurons. *Molecular and Cellular Neuroscience*, *40*(2), 167–186. https://doi.org/10.1016/j.mcn.2008.10.003

Redcay, E., Moran, J. M., Mavros, P. L., Tager-Flusberg, H., Gabrieli, J. D. E., & Whitfield-Gabrieli, S. (2013). Intrinsic functional network organization in high-functioning adolescents with autism spectrum disorder. *Frontiers in Human Neuroscience*, (SEP). https://doi.org/10.3389/fnhum.2013.00573

Ronan, J. L., Wu, W., & Crabtree, G. R. (2013, May). From neural development to cognition:

Unexpected roles for chromatin. *Nature Reviews Genetics*, Vol. 14, pp. 347–359. https://doi.org/10.1038/nrg3413

Rubenstein, J. L. R., & Merzenich, M. M. (2003, October). Model of autism: Increased ratio of excitation/inhibition in key neural systems. *Genes, Brain and Behavior*, Vol. 2, pp. 255–267. https://doi.org/10.1034/j.1601-183X.2003.00037.x

Rudy, B., Fishell, G., Lee, S., & Jens, H. (2011). Three groups of interneurons account for nearly 100% of neocortical {GABAergic} neurons. *Devel Neurobio*, *71*(1), 45–61. https://doi.org/10.1002/dneu.20853

Runfeldt, M. J., Sadovsky, A. J., & N, M. J. (2014). *Acetylcholine functionally reorganizes neocortical microcircuits*. *112*(5), 1205–1216. https://doi.org/10.1152/jn.00071.2014

Russo, N., Flanagan, T., Iarocci, G., Berringer, D., Zelazo, P. D., & Burack, J. A. (2007). Deconstructing executive deficits among persons with autism: implications for cognitive neuroscience. *Brain Cogn*, *65*(1), 77–86. https://doi.org/10.1016/j.bandc.2006.04.007

Sanders, S. J., He, X., Willsey, A. J., Ercan-Sencicek, A. G., Samocha, K. E., Cicek, A. E., … State, M. W. (2015). Insights into Autism Spectrum Disorder Genomic Architecture and Biology from 71 Risk Loci. *Neuron*, *87*(6), 1215–1233. https://doi.org/10.1016/j.neuron.2015.09.016

Sarter, M., Parikh, V., & Howe, W. M. (2009). Phasic acetylcholine release and the volume transmission hypothesis: time to move on. *Nature Reviews. Neuroscience*, *10*(5), 383. https://doi.org/10.1038/NM2635

Schneider, T., & Przewłocki, R. (2005). Behavioral alterations in rats prenatally exposed to valproic acid: animal model of autism. *Neuropsychopharmacology*, *30*(1), 80–89. https://doi.org/10.1038/sj.npp.1300518

Selimbeyoglu, A., Kim, C. K., Inoue, M., Lee, S. Y., Hong, A. S. O., Kauvar, I., … Deisseroth, K.

(2017). Modulation of prefrontal cortex excitation/inhibition balance rescues social behavior in CNTNAP2-deficient mice. *Science Translational Medicine*, *9*(401). https://doi.org/10.1126/scitranslmed.aah6733

Shah, A. A., & Treit, D. (2003). Excitotoxic lesions of the medial prefrontal cortex attenuate fear responses in the elevated-plus maze, social interaction and shock probe burying tests. *Brain Research*, *969*(1–2), 183–194. https://doi.org/10.1016/S0006-8993(03)02299-6

Sierra-Mercado, D., Padilla-Coreano, N., & Quirk, G. J. (2010). Dissociable Roles of Prelimbic and Infralimbic Cortices, Ventral Hippocampus, and Basolateral Amygdala in the Expression and Extinction of Conditioned Fear. *Neuropsychopharmacology*, *36*(2), 529–538. https://doi.org/10.1038/npp.2010.184

Sohal, V. S., & Rubenstein, J. L. R. (2019). Excitation-inhibition balance as a framework for investigating mechanisms in neuropsychiatric disorders. *Molecular Psychiatry*, *24*(9), 1248–1257. https://doi.org/10.1038/s41380-019-0426-0

Spellman, T., Rigotti, M., Ahmari, S. E., Fusi, S., Gogos, J. A., & Gordon, J. A. (2015). Hippocampal-prefrontal input supports spatial encoding in working memory. *Nature*, *522*(7556), 309–314. https://doi.org/10.1038/nature14445

Stessman, H. A. F., Willemsen, M. H., Fenckova, M., Penn, O., Hoischen, A., Xiong, B., … Kleefstra, T. (2016). Disruption of POGZ Is Associated with Intellectual Disability and Autism Spectrum Disorders. *American Journal of Human Genetics*, *98*(3), 541–552. https://doi.org/10.1016/j.ajhg.2016.02.004

Suliman, R., Ben-David, E., & Shifman, S. (2014). Chromatin regulators, phenotypic robustness, and autism risk. *Frontiers in Genetics*, *5*(APR). https://doi.org/10.3389/fgene.2014.00081

Tamura, M., Spellman, T. J., Rosen, A. M., Gogos, J. A., & Gordon, J. A. (2017). Hippocampal-

prefrontal theta-gamma coupling during performance of a spatial working memory task. *Nature Communications*, *8*(1). https://doi.org/10.1038/s41467-017-02108-9

Tan, B., Zou, Y., Zhang, Y., Zhang, R., Ou, J., Shen, Y., … Wu, L. (2016). A novel de novo POGZ mutation in a patient with intellectual disability. *Journal of Human Genetics*, *61*(4), 357–359. https://doi.org/10.1038/jhg.2015.156

Toro, R., Konyukh, M., Delorme, R., Leblond, C., Chaste, P., Fauchereau, F., … Bourgeron, T. (2010, August). Key role for gene dosage and synaptic homeostasis in autism spectrum disorders. *Trends in Genetics*, Vol. 26, pp. 363–372. https://doi.org/10.1016/j.tig.2010.05.007

Vinck, M., Oostenveld, R., Van Wingerden, M., Battaglia, F., & Pennartz, C. M. A. (2011). An improved index of phase-synchronization for electrophysiological data in the presence of volume-conduction, noise and sample-size bias. *NeuroImage*, *55*(4), 1548–1565. https://doi.org/10.1016/j.neuroimage.2011.01.055

Wang, X., Xia, M., Lai, Y., Dai, Z., Cao, Q., Cheng, Z., … He, Y. (2014). Disrupted resting-state functional connectivity in minimally treated chronic schizophrenia. *Schizophrenia Research*, *156*(2–3), 150–156. https://doi.org/10.1016/j.schres.2014.03.033

Wang, Y., Wang, J., Jia, Y., Zhong, S., Niu, M., Sun, Y., … Huang, R. (2017). Shared and Specific Intrinsic Functional Connectivity Patterns in Unmedicated Bipolar Disorder and Major Depressive Disorder. *Scientific Reports*, *7*(1). https://doi.org/10.1038/s41598-017-03777-8

White, J., Beck, C. R., Harel, T., Posey, J. E., Jhangiani, S. N., Tang, S., … Sutton, V. R. (2016). POGZ truncating alleles cause syndromic intellectual disability. *Genome Medicine*, *8*(1), 3. https://doi.org/10.1186/s13073-015-0253-0

Willsey, A. J., Sanders, S. J., Li, M., Dong, S., Tebbenkamp, A. T., Muhle, R. A., … State, M. W. (2013). XCoexpression networks implicate human midfetal deep cortical projection neurons

in the pathogenesis of autism. *Cell*, *155*(5), 997. https://doi.org/10.1016/j.cell.2013.10.020

Wondolowski, J., & Dickman, D. (2013, November 21). Emerging links between homeostatic synaptic plasticity and neurological disease. *Frontiers in Cellular Neuroscience*, Vol. 7. https://doi.org/10.3389/fncel.2013.00223

Xing, M., Tadayonnejad, R., MacNamara, A., Ajilore, O., DiGangi, J., Phan, K. L., … Klumpp, H. (2017). Resting-state theta band connectivity and graph analysis in generalized social anxiety disorder. *NeuroImage: Clinical*, *13*, 24–32. https://doi.org/10.1016/j.nicl.2016.11.009

Ye, Y., Cho, M. T., Retterer, K., Alexander, N., Ben-Omran, T., Al-Mureikhi, M., … Chung, W. K. (2015). De novo POGZ mutations are associated with neurodevelopmental disorders and microcephaly . *Molecular Case Studies*, *1*(1), a000455. https://doi.org/10.1101/mcs.a000455

Yizhar, O., Fenno, L. E., Prigge, M., Schneider, F., Davidson, T. J., Ogshea, D. J., … Deisseroth, K. (2011). Neocortical excitation/inhibition balance in information processing and social dysfunction. *Nature*, *477*(7363), 171–178. https://doi.org/10.1038/nature10360

You, X., Norr, M., Murphy, E., Kuschner, E. S., Bal, E., Gaillard, W. D., … Vaidya, C. J. (2013). Atypical modulation of distant functional connectivity by cognitive state in children with Autism Spectrum Disorders. *Frontiers in Human Neuroscience*, (AUG). https://doi.org/10.3389/fnhum.2013.00482

Zeng, K., Kang, J., Ouyang, G., Li, J., Han, J., Wang, Y., … Li, X. (2017). Disrupted brain network in children with autism spectrum disorder. *Scientific Reports*, *7*(1). https://doi.org/10.1038/s41598-017-16440-z

Zhao, S., Ting, J. T., Atallah, H. E., Qiu, L., Tan, J., Gloss, B., … Feng, G. (2011). Cell type-specific channelrhodopsin-2 transgenic mice for optogenetic dissection of neural circuitry function. *Nature Methods*, *8*(9), 745–755. https://doi.org/10.1038/nmeth.1668
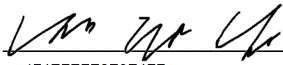
Zhao, W., Tan, J., Zhu, T., Ou, J., Li, Y., Shen, L., … Xia, K. (2019). Rare inherited missense variants of POGZ associate with autism risk and disrupt neuronal development. *Journal of Genetics and Genomics*, *46*(5), 247–257. https://doi.org/10.1016/j.jgg.2019.04.002

Publishing Agreement

It is the policy of the University to encourage the distribution of all theses, dissertations, and manuscripts. Copies of all UCSF theses, dissertations, and manuscripts will be routed to the library via the Graduate Division. The library will make all theses, dissertations, and manuscripts accessible to the public and will preserve these to the best of their abilities, in perpetuity.

Please sign the following statement:

I hereby grant permission to the Graduate Division of the University of California, San Francisco to release copies of my thesis, dissertation, or manuscript to the Campus Library to provide access and preservation, in whole or in part, in perpetuity.

DocuSigned by:

174EFEFE2E9E4FF...

Author Signature

12/18/2019

Date

97